2009

Transfer Properties of the Hair Cell-Afferent Fiber Synapse

Erica C. Keen

ABSTRACT

The perception of sound is initiated in the inner ear by the conversion of vibrational energy into a neural code, a transduction process achieved by the chemical synapses of hair cells in the auditory periphery. Thus, the operation of the hair cell's presynaptic active zone is key to understanding auditory transduction. However, the lack of suitable experimental systems in which to investigate both the presynaptic and postsynaptic aspects of this synapse with high resolution has limited our understanding of its functional characteristics.

This work describes the development of a novel *in vitro* preparation of the amphibian papilla from *Rana catesbeiana* that provides electrical access to the pre- and postsynaptic elements of the hair cell's afferent synapse. The transfer properties of this ribbon-type synapse have been explored with a variety of electrophysiological techniques, including whole-cell recordings, capacitance measurements, and iontophoresis. Glutamate is released from hair cells in response to Ca^{2+} influx through L-type Ca^{2+} channels and is detected by AMPA receptors in postsynaptic fibers. Gradations in the extent of presynaptic stimulation are encoded by a linear increase in the postsynaptic response with respect to the presynaptic Ca^{2+} current, a relation imparted primarily by an increase in the frequency of release events. Both spontaneous and evoked postsynaptic signals are stereotyped in waveform but highly variable in amplitude. Determination of the size of the quantal response provides compelling evidence that the majority of these events are multiquantal. Multiquantal events may originate from individual active zones and do not typically saturate postsynaptic

receptors, thus suggesting that they may have functional significance. The results presented in this study are most consistent with compound exocytosis as the dominant form of transmitter release at individual hair-cell active zones.

CHAPTER ONE

Introduction

Perception of external stimuli by an organism is an ancient problem requiring the detection and transmission of the information relevant for that organism's survival. Perception of sound, in particular, necessitates that sensory receptor cells capture the vibrational energy in auditory stimuli and transmit that information across chemical synapses toward higher processing centers in the brain. To perform this task, these synapses must possess exceptional sensitivity, temporal fidelity, and persistence. Our understanding of the sense of audition therefore depends critically upon elucidating the functional properties of these synapses. On the following pages, I will describe a novel *in vitro* preparation of the amphibian papilla, the primary hearing organ of the bullfrog *Rana catesbeiana*, and its use in the analysis of the transfer properties of the first chemical synapse in the auditory pathway.

Sound propagation in the vertebrate ear

Acoustic stimuli impinge on the tympanum, a broad bandpass filter coupled to the oval window by a series of bones that define the middle ear chamber. The oval window serves as the entry point to the fluid-filled cavity of the inner ear where the transduction of signals by the cellular components of the auditory pathway commences. Encased by an otic capsule composed of bone and cartilage, the inner ear receives complex sounds as fluid displacements and decomposes them into their component frequencies along the

length of a specialized epithelium, resulting in a tonotopic gradient defined by sensitivity to low-frequency sounds at one end and high-frequency sounds at the other. This decomposition is achieved in large part by highly-tuned sensory receptor cells, the hair cells.

The hair cell: sensory receptor and signal transducer

A primary receptor cell in a sensory system must fulfill several requirements in order to successfully process external stimuli. First, it must detect, filter, and sample the relevant information from incoming signals. Second, it must transduce that information into a corresponding change in membrane potential that can traverse the cell from its apical detection organelle toward basolateral regions specialized for signal transmission. Third, it must faithfully transmit the stimulus, now encoded by those potential changes, to the next cellular element in the pathway. In the vertebrate auditory system, the transduction of acoustic stimuli is achieved by a specialized neuroepithelial cell, the hair cell (**Figure 1.1A**). The process of hair-cell transduction involves two successive steps—mechanoelectrical and electrochemical—that are mediated by specialized channels in the apical and basal portions of the cell, respectively.

During mechanoelectrical transduction, the mechanical energy contained in vibrational stimuli is converted to electrical potential changes in the hair-cell membrane. Mechanoelectrical transduction is accomplished by the hair cell's apical cluster of actin-filled stereocilia that constitute a specialized organelle termed the hair bundle. The stereocilia protrude in a graded fashion lengthwise such that the bundle possesses a short edge and a tall edge, and can detect mechanical stimulation in a directionally specific

manner. In non-mammalian vertebrates, a single, true, microtubule-based kinocilium abuts the tall end of the bundle and connects each hair cell to an overlying tectorial membrane, a gelatinous structure composed of extracellular matrix proteins that extends the length of the sensory epithelium. Vibrations of the fluid result in movement of the tectorial membrane, thus deflecting the coupled hair bundles. Adjacent stereocilia are coupled by several lateral connections, the uppermost of which is the tip link, a proteinaceous strand attached to mechanically sensitive transduction channels embedded in the stereociliary membrane (Lumpkin and Hudspeth, 1995). Deflection of stereocilia toward the tall edge of the bundle increases the tension in the tip links, thus biasing transduction channels toward their open states. The ensuing influx of cations, the transduction current, produces a graded, depolarizing potential across the membrane of the hair cell.

During electrochemical transduction, these electrical changes in the hair-cell membrane potential lead to corresponding fluctuations in the release of chemical neurotransmitter in a process known as synaptic transmission. Electrochemical transduction is accomplished by the hair cell's complement of basolateral, voltage-gated Ca^{2+} channels. As a depolarizing receptor potential increases the open probability of these channels, foci of Ca^{2+} influx promote the Ca^{2+}-dependent fusion of neurotransmitter-filled synaptic vesicles with the hair cell's plasma membrane at specialized regions termed active zones. This fusion reaction releases neurotransmitter into the synaptic cleft by a process of exocytosis. Membrane-bound receptors in apposed eighth-nerve afferent fibers detect these molecules, gate ion channels, and thus propagate acoustic signals toward higher-order neurons. The synapses between hair cells and afferent fibers thus

represent physiologically important links between the mechanoelectrical transduction of acoustic stimuli and the electrochemical delivery of that information to the central nervous system.

Chemical synaptic transmission occurs in two major modalities. At phasic synapses, action potentials transiently depolarize the presynaptic membrane to elicit a brief burst of exocytosis and a correspondingly transient postsynaptic response. At tonic synapses, graded changes in membrane potential produce continuously fluctuating rates of neurotransmitter release and thus a constant barrage of postsynaptic signals. Hair-cell synapses fall into this latter class. The hair cell produces graded receptor potentials that increase with sound intensity (Russell and Sellick, 1978). Thus, as the hair cell's membrane potential varies with the extent of acoustic stimulation, the rate of vesicle fusion and neurotransmitter release adjusts correspondingly.

Quantal synaptic transmission and multiquantal release

The quantal theory of synaptic transmission was originally proposed at the neuromuscular junction (del Castillo and Katz, 1954a, 1954b; Katz and Miledi, 1963). Here, the amplitudes of nerve-evoked postsynaptic potentials occurred in integer multiples of the mean amplitude of the spontaneous miniature synaptic potential. Thus, it was suggested that the spontaneous miniature potential represents the basic unit, or quantum, from which the evoked response is composed. Electron-microscopic observation of vesicles within the nerve terminal led to the hypothesis that a spontaneous synaptic potential represents the postsynaptic response to the release of the neurotransmitter contents of a single vesicle—the quantal response. The nerve-evoked

postsynaptic potential then represents the sum of multiple stochastic quantal release events from all sites in a synaptic connection. These anatomical and physiological data formed the basis of the first models of quantal synaptic transmission, in which release was described by a Poisson or binomial process (Martin, 1977; McLachlan, 1978).

From the assumption that neurotransmitter release is quantized and probabilistic, the strength of a synapse can be defined by three parameters: the probability of releasing a quantum at each release site (p), the number of release sites (n), and the size of the postsynaptic response to a single quantum (r) (Katz and Miledi, 1969). Amplitude fluctuations in synaptic responses contain information about p, n, and r that can be extracted by statistical analyses. These quantal parameters depend on both presynaptic and postsynaptic characteristics. Presynaptically, the number of active zones per connection and the release probability per active zone determine the amount of neurotransmitter released. Postsynaptically, the biophysical properties of the receptors, such as their kinetics, affinity for transmitter, and conductance influence the response to transmitter release. Receptor desensitization, in which prolonged exposure to transmitter inactivates receptors, may decrease the extent of the postsynaptic response. Receptor saturation due to a high fractional occupancy may further limit response size.

Synapses were once thought to obey the "one site-one quantum" hypothesis, such that each active zone permits the release of only a single quantum of neurotransmitter (Korn *et al.*, 1994). However, the large amplitude distribution of spontaneous postsynaptic events at many synapses (Liu *et al.*, 1999; Singer *et al.*, 2004; Wu *et al.*, 2007; for a review see Edwards, 2007) suggested that an active zone might release multiple quanta simultaneously. This process, known as multiquantal release (MQR), has

been proposed to occur at several synapses in the central nervous system (Auger *et al.*, 1998; Wadiche and Jahr, 2001; Christie and Jahr, 2006). In most of these studies, though, it has been difficult to determine the size of the quantal response and amplitude histograms of postsynaptic responses have generally failed to display the evenly-spaced peaks that characterize those of the neuromuscular junction. Furthermore, the complicated anatomy of these systems has left most investigators unable to exclude the possibility that single vesicles fuse synchronously at different active zones. Therefore, only indirect evidence is typically used to substantiate the claim of MQR from a single presynaptic active zone.

Three potential mechanisms have been put forth to explain MQR (**Figure 1.2**). Multiple vesicles could fuse simultaneously with the presynaptic membrane in a process termed "coincident fusion." Such synchronous vesicle fusion might be independent, coordinated, or positively cooperative. Next, a vesicle fusing with the presynaptic membrane might transmit a signal to neighboring vesicles, such that a string of vesicle fusions is enabled in a process termed "sequential fusion." Lastly, several vesicles could combine to form a larger vesicle prior to fusing with the presynaptic membrane in a process analogous to the "compound fusion" observed in mast cells. An intriguing related possibility is the exocytotic release of the products of bulk endocytosis (Coggins *et al.*, 2007). If this were the case, vesicular structures of variable volume and neurotransmitter concentration could contribute to synaptic transmission.

Encoding auditory stimuli: synaptic challenges

The phenomenological characteristics of the auditory system—exquisite sensitivity, continuous activity over a large dynamic range, and temporal precision—imply that hair-cell synapses have evolved elaborate mechanisms to transmit acoustic signals to the central nervous system. Sounds may be perceived that deliver energy to the ear at the level of thermal noise (Sivian and White, 1933). Humans can detect sounds with pressures that vary over six orders of magnitude, and frequencies that range from 20 Hz to 20 kHz. Sound localization requires the detection of microsecond differences in the arrival times of signals sent from the two ears (Konishi, 2003). Furthermore, accurate localization persists over a broad range of stimulus amplitudes, suggesting that synaptic signals are effectively compressed into a range appropriate for neuronal processing.

Several characteristics of hair-cell exocytosis provide evidence that their synapses are uniquely specialized for the transfer of auditory signals. Hair cells support exceptionally high rates of continuous transmitter release that approach 500 vesicles per second at each active zone (Parsons *et al.*, 1994). Release persists even in the absence of acoustic stimulation, thus producing continuous "spontaneous" activity in postsynaptic afferent fibers (Sewell, 1984). By poising their resting voltage near the threshold for Ca^{2+} channel activation, hair cells enhance their sensitivity to small stimuli, and may release neurotransmitter in response to membrane-potential changes as small as 100 μV. Furthermore, stimulated exocytosis may be maintained for several hours (Kiang *et al.*, 1965), implying that hair cells possess a large pool of synaptic vesicles and an efficient mechanism for their recruitment and replenishment (for a review see Prescott and

Zenisek, 2005). Temporally precise neurotransmitter release is evidenced by the phase-locking of afferent fiber responses to acoustic stimuli. Phase-locking, the preferential firing of action potentials during a particular segment of an amplitude-modulated stimulus, occurs with near-threshold tones and even at stimulus intensities below those eliciting an increase in firing rate (Rose *et al.*, 1967; Koppl, 1997). Hair-cell exocytosis may drive phase-locking in postsynaptic fibers at rates that approach 9 kHz (Sullivan and Konishi, 1984; Koppl, 1997). Furthermore, afferent fibers in most vertebrate systems are acutely tuned, with Q_{10dB} values that may exceed 20 in some instances (Taberner and Liberman, 2005). This exquisitely sensitive tuning is largely a function of the mechanical properties of the epithelium and the electrical properties of the hair cells, although some frequency selectivity may be intrinsic to the synapse itself (Schnee *et al.*, 2005; Rutherford and Roberts, 2006; Johnson *et al.*, 2008).

Anatomy of the presynaptic active zone

On its basolateral surface, each hair cell forms afferent synapses with distinctive presynaptic specializations (**Figure 1.1B**). The active zone is typical of synapses that release neurotransmitter in response to graded membrane potential changes, including retinal photoreceptors and bipolar neurons, pinealocytes, and electroreceptors (reviewed in Zhai and Bellen, 2000). The distinguishing anatomical feature of these active zones is a submicrometer, osmiophilic presynaptic dense body, or ribbon, which defines the center of the synapse and the site of vesicle fusion. The surface of the ribbon is enveloped by a monolayer of ~35-nm-diameter vesicles tethered to it by short filaments (Lenzi *et al.*,

1999). Thus, the active zone of the hair cell comprises not only the vesicles docked at the membrane, but also a larger pool of vesicles associated with the ribbon.

Although it is the defining structure of the hair-cell active zone, the ribbon is of largely unknown composition and function. Few of its molecular components have been identified, although the self-aggregating protein RIBEYE is a major constituent (Schmitz *et al.*, 2000; Zenisek *et al.*, 2004). CtBP1, the motor protein KIF3A, RIM1, and Piccolo have also been localized to synaptic ribbons (Wang *et al.*, 1997; Muresan *et al.*, 1999; tom Dieck *et al.*, 2005). The ribbon itself is anchored to the presynaptic plasma membrane by Bassoon, a large multidomain protein that interacts with both RIBEYE and the cytoskeleton (tom Dieck *et al.*, 2005). CAST, a cytomatrix-associated protein, is localized with Bassoon at the base of the ribbon (Deguchi-Tawarada *et al.*, 2006). Various roles have been postulated for the ribbon, including those of vesicle immobilization, priming, and trafficking (von Gersdorff, 2001; Trussell, 2002). Although physiological studies of ribbon-deficient mutants suggest that ribbons are required for fast, synchronous release from hair-cell active zones (Khimich *et al.*, 2005), their actual role in the exocytotic process remains obscure.

The precise anatomy of the hair-cell active zone has been best characterized in hair cells of the bullfrog's sacculus. Biophysical and anatomical studies imply that each of 20 active zones in saccular hair cells possesses a cluster of ~90 L-type voltage-gated Ca^{2+} channels and ~40 large-conductance K^+ channels (Roberts *et al.*, 1990). Using the Ca^{2+}-indicator fluo-3 to label synaptic ribbons, simultaneous imaging and electrophysiological studies have confirmed that Ca^{2+} influx occurs at foci that correspond to presynaptic active zones (Issa and Hudspeth, 1994) and that these foci are

the preferential sites of vesicle fusion (Zenisek *et al.*, 2000). However, although fusion events tend to cluster at synaptic ribbons, they may also occur at extraribbon sites both during stimulation and preferentially in its absence (Zenisek, 2008).

Nascent synaptic vesicles are loaded with glutamate by transporters of the VGLUT3 isoform in hair cells (Obholzer *et al.*, 2008). Vesicles are then targeted to fusion sites at the presynaptic membrane by *trans*-membrane complexes of soluble *N*-ethylmaleimide-sensitive factor attachment receptor (SNARE) proteins that consist of a four-helical bundle formed by three helices from SNAREs in the plasma membrane and a fourth helix from a SNARE on the vesicle membrane. Each of the SNARE proteins synaptobrevin, SNAP-25, and syntaxin may occur in different isoforms. Hair cells express synaptobrevin 1, SNAP-25, and syntaxin 1 (Safieddine and Wenthold, 1999). Having docked at the plasma membrane, vesicles next undergo priming, a readying step involving a variety of protein factors (Klenchin and Martin, 2000). Ca^{2+}-dependent vesicle fusion is ultimately effected by a vesicle-associated Ca^{2+} sensor that, upon binding Ca^{2+}, is able to bind phospholipids in the plasma membrane. Synaptotagmins I and II, the major Ca^{2+} sensors at synapses in the central nervous system and neuroendocrine cells, have not been detected at hair-cell synapses (Safieddine and Wenthold, 1999). Instead, hair-cell exocytosis may be realized by the alternative Ca^{2+} sensor otoferlin (Roux *et al.*, 2006). The synapsins, a class of protein involved in the mobilization of synaptic vesicles to the active zone, are also absent from hair-cell synapses (Favre *et al.*, 1986; Safieddine and Wenthold, 1999). The ribbon, by an unknown mechanism, may serve as an alternative means of retaining a large pool of vesicles at the active zone.

Anatomy of the postsynaptic terminal

Innervating afferent fibers from the eighth nerve constitute the first neural elements in the auditory pathway. These fibers terminate on the basolateral surface of hair cells at their active zones to receive glutamatergic signals conveyed across the synaptic cleft.

Ionotropic receptors mediate fast, excitatory transmission at the hair-cell synapse. The postsynaptic membrane apposed to the hair-cell active zone contains a densely packed cluster of low-affinity AMPA receptors composed of co-localized GluR2/3 and GluR4 subunits in the rat cochlea (Reng *et al.*, 1999; Ottersen and Landsend, 1997; Ghosh, 2001). The Ca^{2+}-impermeability and linear voltage properties of GluR2 are dominant in heteromeric GluR2-containing receptors (Burnashev *et al.*, 1992); accordingly, postsynaptic responses at the hair-cell synapse have a low Ca^{2+} permeability, if any (Shimozono *et al.*, 1995; Ruel *et al.*, 2000). The density of AMPA receptors in the postsynaptic membrane is not uniform, but instead decreases in the central region of the terminal beneath the ribbon (Matsubara *et al.*, 1996). In the mammalian cochlea, voltage-gated Na^{+} channels of the Nav1.6 subtype are expressed in the sensory endings immediately below the afferent synapse (Hossain *et al.*, 2005), suggesting that action potentials are generated near the site of synaptic contact. The synaptic structure is loosely ensheathed by supporting cells that express the glutamate-aspartate transporter (GLAST) and glutamine synthetase. These supporting cells may have a function analogous to glial cells in the central nervous system, facilitating the uptake of neurotransmitter from the synaptic cleft to protect hair cells from the excitotoxic effects of elevated extracellular glutamate (Ottersen *et al.*, 1998).

The pattern of afferent innervation differs across species, but is loosely correlated with the frequency bandwidth of a particular endorgan. In the mammalian cochlea, each unbranched afferent fiber forms a single synapse onto a hair cell, thus receiving information from only one active zone. In contrast, non-mammalian afferent fibers in auditory endorgans display different degrees of branching: fibers may innervate multiple active zones in a single presynaptic cell or extend to contact the active zones of several neighboring hair cells. Consistent tonotopic variations are found in these branching patterns: regions sensitive to low-frequency stimuli possess fibers that branch more extensively than those sensitive to high-frequency stimuli.

Presynaptic recordings

A rise in the intracellular concentration of free Ca^{2+} triggers many cellular events, including the fusion of synaptic vesicles with the plasma membrane. Graded synapses, such as those in the hair cell, must minimize the time delay between Ca^{2+} entry and vesicle fusion and maximize the efficiency of fusion events. The efficiency of exocytosis depends upon Ca^{2+}-related parameters: the biophysical properties of the Ca^{2+} channels and Ca^{2+} sensor, the coupling between Ca^{2+} channels and synaptic vesicles, and the extent of the Ca^{2+} cloud formed by a conducting Ca^{2+} channel. These presynaptic parameters have been investigated with a variety of techniques, most notably with capacitance measurements that detect the changes in membrane surface area associated with synaptic vesicle cycling.

Spontaneous and evoked exocytosis from the hair cell depends on Ca^{2+} entry through an atypical class of voltage-gated Ca^{2+} channels: dihydropyridine-sensitive

(L-type) channels with α1D principal subunits (Dou *et al.*, 2004; Kollmar *et al.*, 1997; Platzer *et al.*, 2000; Robertson and Paki, 2002; Keen and Hudspeth, 2006). L-type Ca^{2+} channels in the hair cell activate at relatively negative potentials (~-55 mV), display little inactivation, and have rapid activation and deactivation kinetics (Hudspeth and Lewis, 1988; Koschak *et al.*, 2001). These channel properties allow hair cells to release neurotransmitter readily at low stimulus levels, to follow high-frequency stimulation, and to maintain a relatively constant Ca^{2+} concentration at the active zone during prolonged depolarization. Otoferlin, the putative Ca^{2+} sensor in the hair cell, contains six predicted C2 domains, at least one of which has been demonstrated to bind Ca^{2+} (Roux et al., 2006). Exocytosis has an apparent threshold of 8 μM Ca^{2+} and displays a fifth-order dependence on the Ca^{2+} concentration, suggesting that the Ca^{2+} sensor has a high degree of cooperativity (Beutner *et al.*, 2001).

Hair cells display fast phasic and slower tonic rates of release with different sensitivities to exogenous Ca^{2+} buffers. High concentrations of EGTA strongly inhibit the slower phase, leaving only a rapidly saturating exocytotic response that corresponds to the fusion of ~5-10 vesicles from each active zone at a rate of 1000-2000 vesicles•s^{-1} in mouse hair cells. BAPTA, but not high concentrations of EGTA, can inhibit this fast phase (Moser and Beutner, 2000). Although both chelators have similar equilibrium affinities for Ca^{2+}, BAPTA binds Ca^{2+} approximately 100-fold more rapidly than EGTA. These results then suggest that Ca^{2+} ions exert their effect within a "nanodomain," implying that the vesicle fusion machinery lies within tens of nanometers from the Ca^{2+} channel pore. Pharmacological manipulations of Ca^{2+} channels indeed indicate that hair-cell exocytosis is controlled by a Ca^{2+} nanodomain, such that fusion events are regulated

by the Ca^{2+} influx through one or two closely associated channels (Brandt *et al.*, 2005). Low concentrations of EGTA permit the fusion of several thousand vesicles during sustained depolarization, a number far exceeding that of vesicles both docked and tethered to the ribbon (Parsons *et al.*, 1994; Moser and Beutner, 2000; Eisen *et al.*, 2004). Such extensive exocytosis requires an efficient means of membrane retrieval. In mammalian hair cells, two kinetically distinct modes of endocytosis with different dependencies on intracellular $[Ca^{2+}]$ have time constants of τ = 300 ms and τ = 15 s (Beutner *et al.*, 2001). Two mechanistic modes of endocytosis may also occur. Although some endocytosis is clathrin-mediated, stimulation may also induce the clathrin-independent endocytosis of larger membranous compartments (Lenzi *et al.*, 2002; Jockusch *et al.*, 2005; Coggins *et al.*, 2007).

Fusion events can occur within 100 μs after Ca^{2+} influx at fast central synapses (Sabatini and Regehr, 1996). To achieve such rapid signaling, Ca^{2+} channels within a few tens of nanometers from vesicle fusion sites reduce the Ca^{2+} diffusion time to less than 10 μs (Roberts *et al.*, 1990). Theoretical analysis and modeling suggest that depolarization leads to a free Ca^{2+} concentration of several hundred micromolar within this spatial range near the mouth of an open Ca^{2+} channel, a level well above the threshold for vesicle fusion (Roberts, 1994; Issa and Hudspeth, 1996; Beutner *et al.*, 2001). To temporally and spatially restrict the increase in free Ca^{2+}, hair cells employ millimolar concentrations of mobile Ca^{2+} buffers, such as parvalbumin-3, with fast binding kinetics (Edmonds *et al.*, 2000; Heller *et al.*, 2002; Hackney *et al.*, 2003), thus maintaining a tight relation between neurotransmitter release and hair-cell receptor potential.

Postsynaptic recordings

In response to the presynaptic release of glutamate, postsynaptic AMPA receptors permit a transient influx of cations that generates an excitatory postsynaptic current (EPSC) in afferent fibers. Prior to the studies documented in this thesis, the sole recordings of EPSCs at a hair-cell synapse had been obtained in the immature (postnatal days 7-13) mouse cochlea (Glowatzki and Fuchs, 2002). Multiquantal release (MQR) was suggested to take place at the mammalian hair-cell synapse because of the large coefficient of variation in the amplitude distribution of spontaneous EPSCs (Glowatzki and Fuchs, 2002). However, the necessary evidence to substantiate that claim was lacking: the size of the quantal response had not been established in that system, nor did EPSC amplitude histograms reveal the evenly spaced peaks that strengthened the argument for MQR at the neuromuscular junction. More recently, high-resolution presynaptic capacitance measurements in this system have indicated that multiple release events are indeed coordinated, but to a lesser extent than suggested by the postsynaptic measurements of Glowatzki and Fuchs (Neef *et al.*, 2007).

Furthermore, this experimental system was not ideal for the study of synaptic function in light of the dramatic electrical and morphological changes that hair cells undergo during this developmental period—with the second postnatal week marking the onset of hearing. Immature hair cells generate spontaneous Ca^{2+} action potentials, whereas mature hair cells are generally restricted to graded changes in membrane potential (Kros *et al.*, 1998). Although mature hair cells possess a single ribbon at each active zone, extensive synaptogenesis during the end of the first postnatal week leads to the transient formation of multiribbon active zones (Sobkowicz *et al.*, 1982). Ca^{2+}

channel expression also undergoes large variations during early postnatal development (Beutner and Moser, 2001). Postsynaptic receptor composition changes, with the GluR1 subunit replaced by the Ca^{2+}-impermeable GluR2 subunit (Eybalin *et al.*, 2004). Of most concern, vesicle fusion displays a higher-order dependence on Ca^{2+} in immature hair cells, but the relation approaches linearity with maturation (Beutner and Moser, 2001; Johnson *et al.*, 2005). Given these significant developmental changes, physiological data from synapses in the immature cochlea may not reflect the normal functioning of the mature synapse. A preparation that provides access to the synapse in a mature, hearing animal is a more appropriate system in which to investigate the properties of synaptic transmission in the peripheral auditory system.

The amphibian papilla of *Rana catesbeiana*

Anurans are highly vocal, using acoustic signals to defend territory, secure mates, express emotions, and even distinguish between individuals on the basis of small variations in the spectral or temporal properties of their advertisement calls (Bee and Gerhart, 2002). These animals have therefore evolved a highly specialized inner ear containing two distinct auditory endorgans, the amphibian papilla and basilar papilla, that govern sensitivity to a medium-frequency and a high-frequency range, respectively (Smotherman and Narins, 2000). Detection of airborne vibrations in the frequency range of ~100-1000 Hz is accomplished by the amphibian papilla, the primary auditory receptor organ in the bullfrog. The roughly 600 hair cells of the amphibian papilla are stimulated by the shearing associated with motion of an overlying tectorial membrane coupled to their hair bundles. Unlike the mammalian cochlea, the amphibian papilla lacks the distinction of

inner and outer hair cells, and its hair cells are affixed to the wall of the otic capsule rather than resting on a mechanically tuned basilar membrane. Nevertheless, the amphibian papilla displays several of the hallmarks that functionally define the cochlea and its active, nonlinear behavior: tonotopically arranged hair cells and co-tuned afferent fibers that phase-lock to sinusoidal stimuli at their characteristic frequency (Lewis *et al.*, 1982), spontaneous otoacoustic emissions, distortion product otoacoustic emissions (Meenderink *et al.*, 2005), and two-tone suppression (Ehret *et al.*, 1983). The degree of phase-locking in afferent fibers increases with sound pressure level, saturating at ~20 dB above threshold (Schmitz *et al.*, 1992). Frequency threshold curves from auditory nerve fibers are sharp and similar to curves obtained from mammals at the same characteristic frequency (Feng et al, 1975; Lewis and Leverenz**,** 1983**)**.

In order to study the physiological behavior of hair cell synapses with high resolution, it is essential to have a preparation that preserves functional connections while affording electrical access to them. The amphibian papilla provides a suitable model system.

Overview

To examine the transfer properties of the hair-cell synapse and to ascertain the parameters governing exocytosis at hair-cell active zones, I have developed a novel *in vitro* preparation of the amphibian papilla from the bullfrog that preserves synaptic connections while rendering the pre- and postsynaptic elements accessible for electrophysiological recording. The functional properties of the preparation were investigated in detail with whole-cell recordings from hair cells and afferent nerve fibers.

Hair-cell synapses are shown to be tonically active and to transfer information to postsynaptic terminals linearly with respect to their presynaptic Ca^{2+} currents. This linear relation is primarily determined by an increase in the frequency of postsynaptic events. Spontaneous and evoked release from single active zones is dominated by the highly synchronous release of neurotransmitter equivalent to that contained in several synaptic vesicles. Postsynaptic fibers are not saturated by multiquantal events, indicating that larger events may provide additional information. Finally, compound exocytosis or release of endosomal compartments may underlie the generation of multiquantal postsynaptic responses in this system.

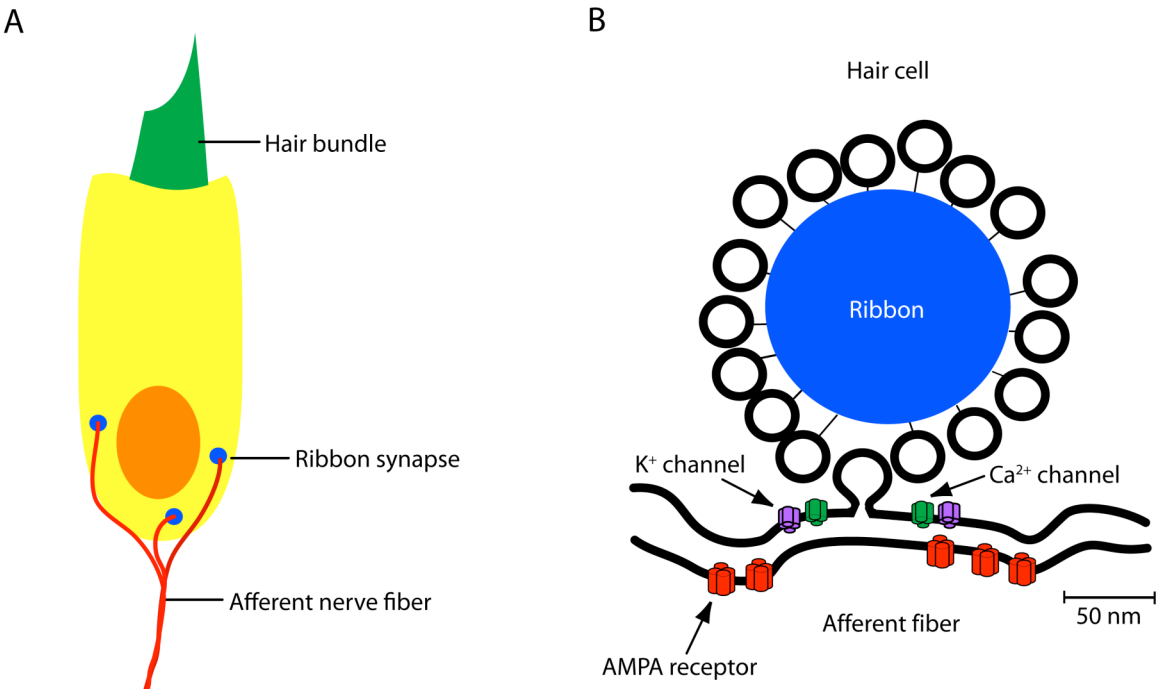
A
Hair bundle
Ribbon synapse
Afferent nerve fiber
B
Hair cell
Ribbon
K+ channel
Ca2+ channel
Afferent fiber
50 nm
AMPA receptor

Figure 1.1

The hair cell and its afferent synapse

(**A**) The hair cell possesses an apical hair bundle where mechanoelectrical transduction occurs. Ribbon synapses on the hair cell's basolateral surface mediate the process of electrochemical transduction, thereby sending signals to postsynaptic afferent nerve fibers. (**B**) A schematic diagram displays the hallmark features of the hair-cell synapse. The active zone is anatomically defined by an electron-dense presynaptic body or ribbon, upon whose surface glutamate-filled synaptic vesicles are tethered. Voltage-gated Ca^{2+} channels and large-conductance K^{+} channels are colocalized at the presynaptic plasma membrane. The apposed postsynaptic membrane of the afferent fiber expresses a high density of ionotropic glutamate receptors of the AMPA subtype.

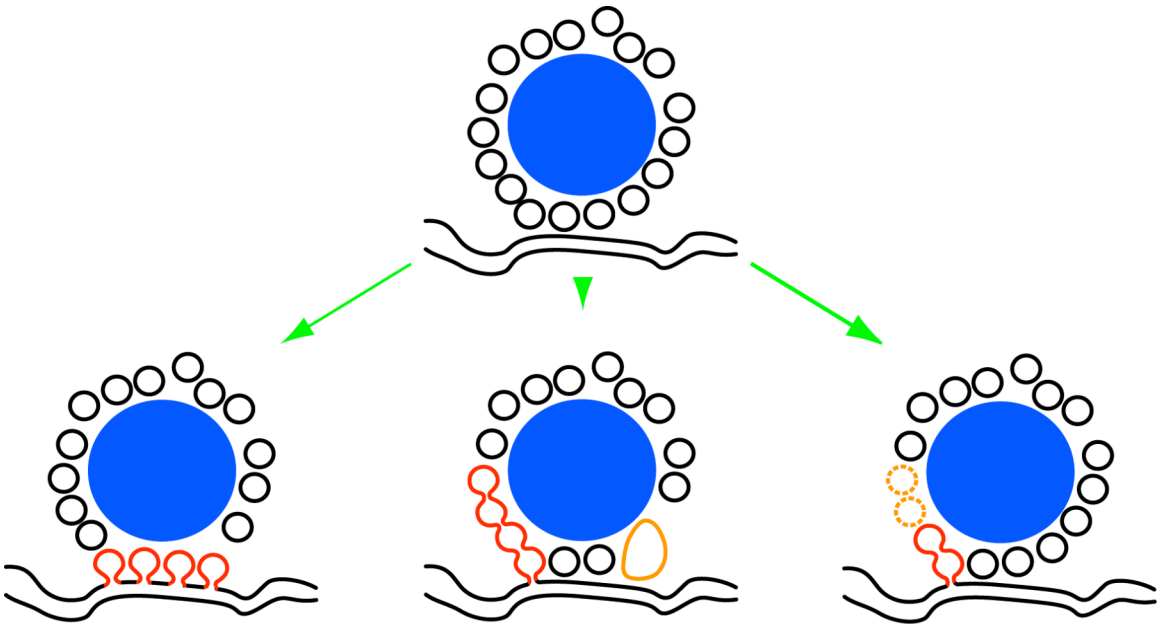
Coincident release
Compound release
Sequential release

Figure 1.2

Modes of multiquantal release

Three potential mechanisms have been proposed to explain multiquantal release from a single active zone. Several vesicles could fuse simultaneously with the presynaptic membrane in a cooperative or coordinated fashion (*Left*). Alternatively, multiple vesicles might prefuse with each other and subsequently undergo fusion with the presynaptic membrane as a compound event (*Middle*). Finally, the fusion of a vesicle with the presynaptic membrane could stimulate adjacent vesicles to fuse sequentially (*Right*).

CHAPTER TWO

On an *in vitro* preparation of the bullfrog's amphibian papilla with exposed afferent synapses

The fusion of synaptic vesicles with the presynaptic membrane leads to release of transmitter into the synaptic cleft. Upon transmitter binding to ionotropic receptor channels in the apposed postsynaptic membrane, a transient influx of extracellular ions ensues. A direct indication of functional transmitter release at a synapse is thus the real-time measurement of current through these channels. In order to investigate the transfer properties of the hair cell's afferent synapse, it was imperative to develop an *in vitro* preparation of an inner ear epithelium that afforded access to postsynaptic fibers for high-resolution electrophysiological recordings. In this chapter, the experimental preparation is described and the anatomical and physiological properties of its synaptic contacts are assessed.

Materials and Methods

Solutions

Isolation and dissection of the amphibian papilla were performed in a perilymph-like solution containing 120 mM NaCl, 2 mM KCl, 2 mM $CaCl_2$, 3 mM D-glucose, 1 mM creatine, 1 mM sodium pyruvate, and 5 mM Hepes at pH 7.30 and 235 mosmol•kg^{-1}. Tetrodotoxin (1 μM) was added to the dissecting and recording solutions to eliminate action-potential generation in nerve fibers. Cyclothiazide (100 μM) was included in

recording solutions as noted to relieve AMPA receptor desensitization. All solutions were bubbled with 100% O_2 for at least 10 minutes prior to experimentation. The internal solution for patch pipettes consisted of 110 mM CsCl, 0.5 mM $MgCl_2$, 2 mM EGTA, 5 mM Na_2ATP, and 10 mM Hepes at pH 7.3 and 230 mosmol•kg^{-1}. All procedures and experiments were performed at a room temperature of 25°.

Dissection procedure

In each experiment, a North American bullfrog (*Rana catesbeiana*) was sedated in cold water, doubly pithed, and decapitated after extinction of the corneal reflex. The lower jaw was removed with scissors to expose the ventral floor of the skull. A number 20 scalpel blade was then used to sever the connection between the middle-ear ossicle, the columella, and the inner ear to minimize mechanical trauma to the epithelium during the dissection.

The otic capsule was opened from its ventral aspect to reveal the inner ear. Once opened, the cavity was kept moist with oxygenated dissecting solution. The dissection continued medially to expose the innervating eighth nerve, which was cut with fine scissors at the brainstem. The posterior wall of the bony otic capsule was subsequently removed, and the semicircular canals were cut to allow removal of the intact inner ear. The entire membranous labyrinth with the eighth nerve was transferred to a dish containing fresh oxygenated dissecting solution.

Removal of the sacculus and its otoconial sac exposed the posterior branch of the eighth nerve that innervates the amphibian papilla, basilar papilla, lagena, and posterior

semicircular canal. The remaining tissues surrounding the amphibian papilla were removed with fine forceps and scissors.

To expose the sensory epithelium of the amphibian papilla, the nerve bundle was severed where it crosses the opening of the cartilaginous cavity. The tectorial membrane was then removed with fine forceps inserted into the mouth of the opened cavity. Importantly, this mechanical abstraction of the tectorial membrane is likely to have rendered the coupled hair bundles nonfunctional. A single cut was made to the cartilaginous roof of the papilla at its rostral end. This permitted reflection of the roof from the sensory epithelium by gently folding it back from the lateral edge of the papilla.

To expose afferent nerve terminals for recording, the papilla was placed atop a 125-μm-diameter tungsten wire affixed at its ends to the bottom of a recording chamber. The tissue was positioned such that the wire paralleled the tonotopic axis of the epithelium. The lateral aspect of the papilla, containing the entry point of the nerve bundle, was immobilized with fine pins at three positions on one side of the wire, thus constraining the epithelium to lie directly above the wire. In most experiments, the control solution was replaced with a zero-Ca^{2+}/EGTA perilymph during the splitting process. The cationic depletion of this solution seemed to facilitate the dissolution of cell-cell adhesions. Finally, a fourth pin on the opposite side of the wire was used to press upon the opened cartilaginous roof **(Figure 2.1A)**. The resulting stress often split the epithelium along its tonotopic axis in the mid- to high-frequency range, thus exposing afferent fibers at their terminations on hair cells (**Figure 2.1B**).

Labeling of afferent nerve fibers

The innervation pattern of the amphibian papilla and the fine structure of its afferent fiber terminals were examined with three techniques.

Immunocytochemistry

Dissected papillae were incubated in phosphate-buffered saline containing 4% formaldehyde (Electron Microscopy Science, Hatfield, PA) for one hour at 4˚ C. The fixed papillae were washed three times in phosphate-buffered saline and then incubated in phosphate-buffered saline supplemented with 5% normal goat serum (Gibco, Invitrogen) to reduce the non-specific binding of primary antibodies.

Afferent nerve fibers were immunolabeled with 3A10 monoclonal antibodies (Sigma) that recognize neurofilament-associated proteins (1:20 dilution). Hair cells were immunolabeled with an antiserum directed against the Ca^{2+} buffer parvalbumin 3 at a dilution of 1:20,000. Afferent fiber Na^{+} channels were immunolabeled with SP19 monoclonal antibodies (Sigma) that recognize a highly conserved sequence of the α subunit of the rat type I voltage-gated Na^{+} channel at a dilution of 1:100. Myelin was immunolabeled with an antiserum directed against the S100 protein (Sigma) at a concentration of 1:100. Papillae were incubated with primary antibodies in phosphate-buffered saline and 1% normal goat serum overnight at 4˚ C. Following three washes in phosphate-buffered saline, papillae were incubated with fluorophore-conjugated secondary antibodies (1:200 dilution) in phosphate-buffered saline supplemented with 1% normal goat serum (Molecular Probes, Invitrogen) for two hours at room temperature.

Images were acquired with a laser-scanning confocal microscope (LSM 510, Zeiss) interfaced to an upright microscope (Axioskop 2, Zeiss) and processing was performed with Zeiss proprietary (AIM) software.

Retrograde labeling with lipophilic dye

Dissected papillae were fixed at room temperature for 15 minutes in phosphate-buffered saline containing 4% formaldehyde and then washed three times in phosphate-buffered saline. The papillar nerve was cut close to its point of exit from the epithelium. A fine tungsten wire was then used to apply crystals of the lipophilic tracer 1,1'-dioctadecyl-3,3,3',3'-tetramethylindocarbocyanine perchlorate [diIC_{18}(3)] to the severed end of the nerve bundle. Papillae were stored in darkness overnight at room temperature to permit diffusion of the dye to nerve terminals.

Whole-cell fiber labeling

50 μM Alexa hydrazide 488 was added to the internal solution of pipettes used for recording afferent fiber activity. Establishment of the whole-cell configuration permitted diffusion of the dye from the pipette into the attached fiber, thus labeling its fine terminations onto hair cells.

Images were acquired from live preparations with an upright microscope (Axioskop 2, Zeiss) equipped with laser-scanning confocal microscopy (LSM-510, Zeiss) and processed with the included software.

Electron microscopy of afferent synapses

Amphibian papillae were isolated as previously described. To avoid tissue deterioration, however, the otic capsule was perfused during the dissection with a primary fixative

solution containing 200 mM glutaraldehyde (Electron Microscopy Sciences, Hatfield, PA), 400 mM formaldehyde (Electron Microscopy Sciences, Hatfield, PA), 70 mM sodium cacodylate, and 1 mM $CaCl_2$. The isolated papillae were incubated in the primary fixative for 20 hours at room temperature and subsequently washed twice in 70 mM sodium cacodylate and 1 mM $CaCl_2$. Papillae were postfixed in a solution containing 50 mM OsO_4, 10 mM K^+ ferrocyanide, 70 mM sodium cacodylate, and 1 mM $CaCl_2$ for two hours at 4° C. After washing with 10 mM sodium cacodylate and then with distilled water, papillae were dehydrated by sequential ten-minute immersions in 50%, 70%, 80%, and 95% ethanol at room temperature. *En bloc* staining of the papilla was achieved by immersion in 0.4% uranyl acetate in 95% ethanol for one hour at room temperature. The stained tissue was fully dehydrated by immersion in 100% ethanol for two hours and then in propylene oxide for two hours, both at room temperature. To facilitate embedding, the tissue was placed in a 50% resin mixture in propylene oxide for twenty-four hours and then in 100% resin mixture for a subsequent twenty-four hours with rotatory stirring. The resin mixture was composed of 1.09 g ml^{-1} EMbed-812 resin, 1.01 g ml^{-1} dodecenyl succinic anhydride (DDSA), 1.25 g ml^{-1} nadic methyl anhydride (NMA), and 1% 2,4,6-tri(dimethylaminomethyl)phenol (DMP-30). The immersed specimen was transferred to a silicone mold and the sample was cured under vacuum for 48 hours at 50° C.

The specimen was sectioned at a thickness of 70 nm on a diamond knife (Ultra 45 degree, Diatome) with an ultramicrotome (Ultracut-E, Reichert-Jung). After collection onto copper grids, the sections were stained for 2 minutes with 50% saturated aqueous uranyl acetate in 50% acetone and then for 1.5 minutes with Sato's lead stain (Sato,

1967). Transmission electron micrographs were obtained with a Tecnai G2-12 Biotwin electron microscope (FEI, Hillsboro, Oregon) equipped with a digital camera (XR60, Advanced Microscopy Techniques Corp.).

Electrophysiological recordings

Hair cell and afferent fiber recordings were obtained with whole-cell, tight-seal pipettes. Recording pipettes were pulled from borosilicate tubing (1.5 mm outer diameter, 1.17 mm inner diameter; Sutter Instruments) with a horizontal puller (Model P-80/PC, Sutter Instruments). The tips of pipettes for recording from hair cells and afferent fibers were fire-polished to resistances of 2-4 MΩ and 6-10 MΩ, respectively. To facilitate a perpendicular approach to fiber terminals, afferent fiber pipettes were subsequently bent with a custom-made microforge. The internal solution for pipettes consisted of 110 mM KCl or CsCl, 0.5 mM $MgCl_2$, 2 mM EGTA, 5 mM Na_2ATP, and 10 mM Hepes at pH 7.3 and 230 mosmol•kg^{-1}.

Cells were visualized by differential-interference-contrast microscopy on an upright microscope (Axioscope 2, Zeiss) with a X63 water-immersion objective lens, X5 optical magnification, and X2 digital magnification. Whole-cell voltage-clamp recordings were performed using Axopatch 200B amplifiers (Axon Instruments, Union City, CA). Voltage and current responses were recorded under current-clamp and voltage-clamp modes, respectively. EPSCs were measured in afferent fibers maintained at -74 or -94 mV. *Post hoc* correction for the 4-mV tip potential yielded holding potentials of -70 or -90 mV as indicated.

Stimuli were generated and data acquired with programs written in LabVIEW (National Instruments, Austin, TX). Data were sampled at 50-μs intervals and low-pass filtered at 8 kHz with an eight-pole Bessel filter (Wavetek 852, Indianapolis, IN).

Data analysis

Data were analyzed with Excel 2003 (Microsoft Corp., Redmond, WA), Minianalysis (Synaptosoft, Jaejin Software, Leonia, NJ), and Mathematica (Wolfram Research, Champaign, IL). Averaged values are reported as means ± standard deviations unless otherwise specified.

Results

The *in vitro* preparation

With proper positioning and adequate immobilization of the amphibian papilla atop the tungsten wire, the epithelium could be split in the majority of dissections. This cleavage of the epithelium exposed the unmyelinated terminals of afferent fibers on the basolateral surfaces of hair cells **(Figure 2.1B**). Splitting occurred most readily just medio-caudal to the papillar nerve, in the region expected to contain hair cells and fibers with best frequencies of 400-800 Hz **(**Simmons *et al.*, 1992**)**. The healthiest preparations were those in which the splitting was achieved without repositioning of the fastening pins; more extensive damage was observed when the epithelium was initially resistant to tearing and was further manipulated during the dissection. Due to the mechanical trauma inherent in such a preparation, experiments were performed only with papillae from behaviorally healthy frogs.

Microscopy revealed the health of the preparation: damaged papillae displayed swollen hair cells with splayed hair bundles and swollen or retracted afferent fibers, whereas viable papillae displayed plump hair cells with compact hair bundles and fibers extending from their basolateral aspects **(Figure 2.1B)**. Residual supporting cell membranes often spread across the plane of cleavage, obscuring the path for recording electrodes. Addition of DNase or flow directed onto the tissue with a low-resistance pipette did little to remove this elastic barrier, but rather tended to produce severe hair-cell damage. Therefore, cells selected for electrical recordings were those that appeared healthy by the above criteria and lacked any membranous covering by supporting cells. Most fibers were recorded in the whole-cell configuration with pipettes at the point where their terminals merged to form a calyx-like structure below the base of the hair cell. Because of this geometry, postsynaptic recordings were likely to include the activity of several presynaptic active zones from a single hair cell.

Innervation of the *in vitro* preparation

The amphibian papilla displays a tonotopic gradient in its afferent fiber distribution: fibers in the rostral, low-frequency region are of larger diameter and branch more extensively than those in the caudal, high-frequency zone (Lewis *et al*., 1982; Lewis and Leverens, 1983; Simmons *et al*., 1992). This tonotopic difference was confirmed by immunohistochemical analysis of the innervation in rostral *versus* caudal regions of the papilla. In the medio-caudal region of interest, afferent fibers extended through the basement membrane and branched sparsely to terminate on only one or a few closely spaced hair cells (**Figure 2.2A**). Immunohistochemical analysis of voltage-gated Na^+

channel and myelin expression revealed prominent staining that commenced only after these fibers extended across the basement membrane of the epithelium (**Figure 2.2B,C**). No staining was evident at the synaptic contacts between hair cells and afferent fibers in whole-mount preparations.

Despite disturbances to the epithelial structure, synaptic connections were preserved in the preparation. The fine projections of an individual fiber onto a hair cell were better delineated by the sparse staining achieved with $DiIC_{18}(3)$ and by dialysis of 50 μM Alexa hydrazide included in the patch pipette **(Figure 2.3)**. A prominent feature of many fibers in the mid- to high-frequency range of the papilla is a calyx-like structure that surrounds the basolateral surface of a hair cell and from which extend finer projections that form synaptic contacts onto hair-cell active zones. Fibers displayed an average of 6 terminations onto hair cells in the region of experimentation and these terminals rarely extended above the level of the nucleus. Afferent terminals ranged in diameter from 0.8 μm to 2 μm.

Synaptic ultrastructure

The ultrastructure of presynaptic active zones in the mid- to high-frequency region of the amphibian papilla was investigated by electron microscopy. Each hair-cell active zone displayed presynaptic and postsynaptic densities, a population of docked vesicles, and a characteristic ~150-nm-diameter presynaptic dense body enveloped by tethered synaptic vesicles **(Figure 2.4)**. Rarely, active zones were observed to contain two closely spaced dense bodies opposed to a single postsynaptic density (**Figure 2.4C**). Membrane-bounded compartments larger than synaptic vesicles were often observed near the dense

body just beyond the region of tethered vesicles (**Figure 2.4D**). Numerous mitochondria, smooth endoplasmic reticulum, and clathrin-coated vesicles characterized the cytoplasmic environment immediately adjacent to the active zone. No efferent terminals were found in the examined region of the papilla.

Properties of afferent fibers

Recordings from afferent fibers were obtained in the whole-cell configuration in split preparations of the amphibian papilla. Fiber resting potentials ranged from -50 mV to -75 mV in standard perilymph. When fibers were severed from their central projections, whole-cell capacitances were 1-5 pF. The input resistance of afferent fibers recorded with the KCl pipette solution was ~250 MΩ. When fibers were instead dialyzed with the CsCl solution, their input resistance increased. For 10 afferent fibers recorded with CsCl, the average input resistance was 517±16 MΩ. Furthermore, current-voltage relations revealed a slowly activating outward current in fibers recorded with the K^+-based solution (**Figure 2.5A**). This current was eliminated in the presence of Cs^+, leaving a linear current-voltage relation with a lower slope signifying a higher membrane resistance (**Figure 2.5B**). Therefore, all subsequent fiber recordings were obtained with the CsCl pipette solution to improve voltage-clamp control.

When fibers were recorded in the current-clamp configuration in the absence of tetrodotoxin, spontaneous spiking was occasionally observed. In nonspiking fibers, action potentials could be elicited by depolarization. Fibers displayed different behaviors upon current injection. Some fibers exhibited a high-frequency train of action potentials that persisted for the duration of the depolarization with little or no adaptation in

frequency (**Figure 2.6A**). Others displayed phasic spiking, firing a few action potentials limited to the initial few seconds of the depolarizing stimulus (**Figure 2.6B**). In most recordings, action potentials were small in amplitude (5-10 mV) and required a large depolarization of the afferent terminal (to approximately -40 mV), suggesting that voltage-gated Na^+ channels were not in close proximity to the recording pipette.

Properties of spontaneous EPSCs

Voltage-clamp recordings were obtained from afferent fibers near their terminations on the basolateral surfaces of hair cells. Establishment of the whole-cell configuration was apparent from the appearance of spontaneous EPSCs, which occurred at rates of 4-130 s^{-1}. The rate of EPSCs in a given recording was rarely constant: in some fibers, the rate showed small fluctuations, but in others bursts of EPSCs appeared at irregular intervals (**Figure 2.7A**).

The large amplitude range of spontaneous EPSCs in the amphibian papilla was striking: EPSC amplitudes varied over an order of magnitude in most recordings (**Figure 2.7B**). The amplitude of spontaneous EPSCs from seven fibers held at a membrane potential of -90 mV averaged -129±24 pA and the coefficient of variation was 0.35**.** During periods of increased frequency, EPSCs amplitudes tended to converge toward a common value in some fibers (**Figure 2.7C**). In fibers that displayed a high tonic rate of EPSCs, the average amplitude of EPSCs was constant for the duration of the recording, implying that hair cells can release large quantities of neurotransmitter without fatigue. Despite occupying a range of amplitudes, the interevent interval histograms of spontaneous EPSCs during period of relatively constant frequency were exponentially

distributed (**Figure 2.8**), suggesting that release events are governed by a single Poisson process.

The waveforms of EPSCs were predominantly monophasic, displaying fast rise times and slower exponential decays without inflections (**Figure 2.9A**). For 3,944 spontaneous EPSCs in three fibers held at -70 mV, the mean 10%-90% rise time was 0.37±0.28 ms, and the mean decay time constant was 0.59±0.19 ms. A small fraction of events possessed complex rise or decay phases and were typically large (**Figure 2.9B**). The smallest rise and decay times were observed for the smallest events; however, these values were not appreciably greater for large events (**Figure 2.9C**).

Properties of postsynaptic receptors

The small rise times and exponential decays of EPSCs accorded with the kinetics of currents mediated by glutamate receptors of the AMPA type in the auditory system (Glowatzki and Fuchs, 2002).

To investigate the voltage sensitivity of the postsynaptic responses, spontaneous EPSCs were recorded while a fiber was maintained at holding potentials from -100 mV to +50 mV. The kinetics and amplitudes of EPSCs were voltage-dependent; responses slowed at more positive potentials and reversed sign near 0 mV, as expected for the nonselective cation current mediated by AMPA receptors (**Figure 2.10A**). To assess the quality of the voltage clamp in recordings, fibers were therefore routinely depolarized to 0 mV. Recordings that showed persistent EPSCs at 0 mV were excluded from analysis. Application of 6-cyano-7-nitroquinoxaline-2,3-dione (CNQX), an antagonist of AMPA and kainate receptors, completely and reversibly blocked EPSCs (**Figure 2.10C**).

Application of 50 μM D(-)-2-Amino-5-phosphonopentanoic acid (D-AP5), an antagonist of NMDA receptors, had no effect on EPSC amplitude or frequency (data not shown). Picrotoxin, a GABA(A) receptor antagonist, likewise failed to alter postsynaptic signals (data not shown). Cyclothiazide, an agent that reduces the desensitization of AMPA receptors, doubled the decay time constant of EPSCs (**Figure 2.10B**). These results indicate that EPSCs at the amphibian papilla's afferent synapse are mediated by ionotropic glutamate receptors of the AMPA subtype.

Discussion

An *in vitro* preparation for investigating hair-cell synapses

Despite considerable interest in auditory ribbon-type synapses, the inaccessibility of afferent fibers for whole-cell recording has impeded detailed analysis of their physiological properties. With this novel *in vitro* preparation, one may record postsynaptic signals in the whole-cell configuration from unmyelinated fibers at their terminations onto hair cells. This preparation therefore provides an opportunity to explore parameters that functionally define the synapse, such as quantal size, presynaptic regulation of vesicle fusion, and postsynaptic responsiveness to transmitter release.

The split preparation of the bullfrog's amphibian papilla has particular advantages for studying synaptic function in the auditory periphery. Derived from a poikilotherm, the papillar preparation is significantly more stable than one from the mammalian cochlea: a healthy papilla may remain viable for up to one hour *in vitro*, providing the experimenter with the ability to test the effects of pharmacological agents that require extended incubation times. Furthermore, the preparation is obtained from adult, hearing

animals, permitting characterization of mature auditory synapses. The papilla possesses a well-characterized tonotopic array of hair cells and corresponding afferent fibers (Lewis *et al.*, 1982; Megela, 1984, Smotherman and Narins, 1999). At their calyx-like coalescence beneath hair cells, afferent fibers have diameters of 2-5 μm, considerably larger than those in the mammalian cochlea. In the caudal region of investigation, hair cells lack efferent innervation (Flock and Flock, 1966). Finally, the splitting of the tissue often fortuitously severs afferent fibers from both the basement membrane and peripheral hair-cell contacts, ensuring that recordings capture inputs from only a single presynaptic cell.

Anatomy of synapses in the *in vitro* preparation

In the region of experimentation, a hair cell receives one to two afferent fibers, each of which forms approximately six synaptic contacts that coalesce immediately beneath the hair cell's basolateral surface. These fibers do not appear to express voltage-gated Na^+ channels until they penetrate the basement membrane several millimeters from the afferent synapse, an expression pattern consistent with the small amplitude of afferent-fiber action potentials and the resistance to spiking upon fiber depolarization in whole-cell recordings. Furthermore, outside-out patches obtained from fibers at their coalescence point do not display measurable Na^+ currents (Henrique von Gersdorff, personal communication). Thus, passively propagating analog signals from several active zones are likely to be integrated by an afferent fiber prior to action-potential generation. This innervation pattern and coding strategy contrast with those of the mammalian cochlea, in which a hair cell receives multiple afferent fibers, each of which

contacts a single active zone (Liberman, 1980) and expresses Nav1.6 Na^+ channels in its ending directly beneath the hair-cell synapse (Hossain *et al.*, 2005). The lower frequency bandwidth of the amphibian papilla relative to that of the cochlea may be a partial rationale for the apparent differences in innervation and expression patterns in the two systems. If less stringent temporal precision is required, the papilla may be more permissive of the temporal jitter associated with the use of postsynaptic potentials, rather than action potentials, for signal coincidence detection.

Electron-microscopic analysis demonstrates that the active zones in amphibian papilla hair cells possess the ultrastructural characteristics common to ribbon-type synapses. This *in vitro* preparation is therefore a valuable system in which to explore the physiological hallmarks of exocytosis at these synapses.

Physiological properties of synapses in the *in vitro* preparation

In a single-compartmental model, the response of a cell to an influx of current will depend on its passive membrane properties: its membrane resistance will determine the change in voltage elicited by a given current, and its resistance together with capacitance will low-pass filter that response with a time constant $\tau = RC$. The relatively low resting input resistance (~250 MΩ) of fibers in the amphibian papilla should facilitate a rapid rate of change in membrane potential after the opening of postsynaptic receptors, thus aiding in the discrimination of closely timed synaptic inputs and the coincident detection of signals from several active zones (Trussell, 1997). However, a low input resistance also reduces a cell's sensitivity to small inputs. The large amplitude of spontaneous

EPSCs in this system might represent a way to overcome this limitation by providing sufficient currents to elicit the requisite changes in voltage.

Amphibian papilla fibers are shown here to have distinct responses to depolarizing current injections: both rapidly adapting and slowly adapting fibers were observed. In concordance with these observations, papillar fibers display diverse spike adaptation rates when presented with a tone at their best excitatory frequency: although some exhibit tonic firing for the duration of the tone, others have a highly phasic response concentrated at the onset of the stimulus (Megela and Capranica, 1981; Megela, 1984). The variation in spiking behavior in this system may therefore reflect intrinsic properties of the postsynaptic element in addition to the depletion of presynaptic vesicle pools suggested in other systems (Spassova *et al.*, 2004; Goutman and Glowatzki, 2007).

Spontaneous EPSCs in the amphibian papilla are mediated by ionotropic, AMPA-type glutamate receptors that undergo fast desensitization. The sensitivity to cyclothiazide suggests that afferent fibers express the 'flip' isoform of the GluR gene, as AMPA receptor channels possessing 'flip' subunits show a marked sensitivity to cyclothiazide (Partin *et al.*, 1994). Fast desensitization is potentially advantageous in a system that releases high concentrations of transmitter for extended durations and for which temporal precision is imperative. Although massive exocytosis might prolong the timecourse of glutamate in the synaptic cleft, receptor desensitization acts to narrow the temporal window of the postsynaptic response, safeguarding downstream coincidence detection while permitting the hair cell to maximize its sensitivity with high rates of vesicle fusion.

The broad distribution of spontaneous EPSC amplitudes found in the amphibian papilla has also been observed in the immature rat cochlea (Glowatzki and Fuchs, 2002). In the neonatal cochlea, however, the EPSC amplitude distribution is highly skewed, with a mode at its left-most edge suggested to represent single-vesicle events. In contrast, the EPSC amplitude distribution in the adult amphibian papilla is more Gaussian, with a mode at -100 to -200pA, well above the smallest EPSCs as well as the background noise in the recording. If we assume that smaller events reflect single-vesicle fusions, the predominant mode of release in this system appears to be the nearly simultaneous exocytosis of the transmitter corresponding to that contained in several synaptic vesicles.

If exocytotic events are stochastic and each vesicle is independent, EPSCs generated by the fusion of multiple vesicles should have slower rise times than those generated by the fusion of a single vesicle. Although the fastest kinetics was observed for the smallest events, there was a negligible difference in waveform between small and large EPSCs. If multiple presynaptic release events were desynchronized, one might expect to observe inflections on the rising or falling phase of larger EPSCs. Although such inflection points were observed in a small fraction of events, most displayed exceedingly fast, monophasic waveforms that were independent of their amplitudes. These results therefore strongly suggest that the transmitter corresponding to several synaptic vesicles is released from hair cells with a high degree of temporal precision and that this mode is dominant during spontaneous activity *in vitro*.

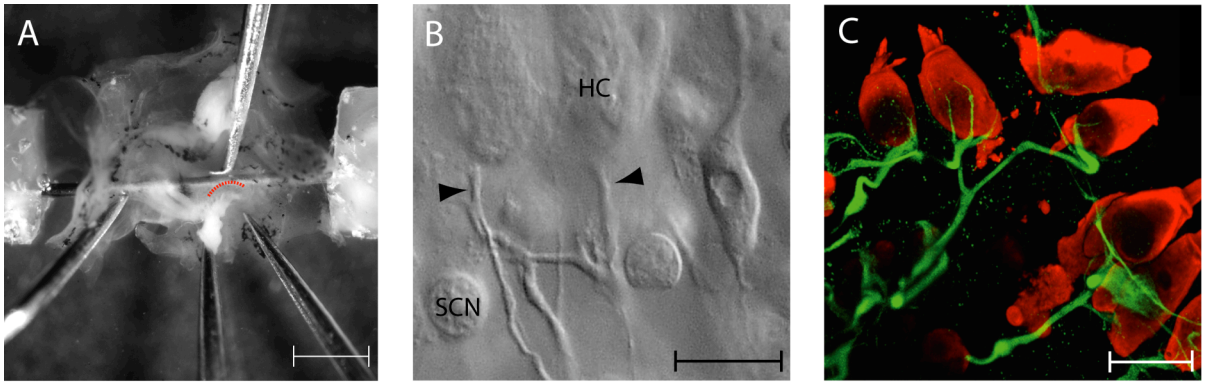
A
B
HC
SCN
C

Figure 2.1

in vitro preparation of the amphibian papilla from *Rana catesbeiana*

(**A**) A micrograph taken through a dissection microscope displays the amphibian papilla positioned above the tungsten wire used to split the epithelium along its tonotopic axis. Pins anchored to a sheet of magnetic plastic are used to apply the opposing forces required to expose hair cell-afferent fiber synapses. The dashed line delineates the region of the papilla in which synapses were typically exposed. (**B**) A DIC image shows the preservation of synapses in the split preparation. Arrowheads denote the sites of whole-cell patch-clamp recordings from afferent fibers. HC, hair cell; SCN, supporting cell nucleus. (**C**) A confocal image of the split preparation reveals the fine terminations of afferent fibers (green) onto the basolateral surfaces of hair cells (red). Hair cells are labeled with an antiserum against parvalbumin 3 and afferent fibers with antibodies directed against neurofilament proteins. Scale bars: (**A**) 500 μm; (**B**), 20 μm; (**C**), 20 μm.

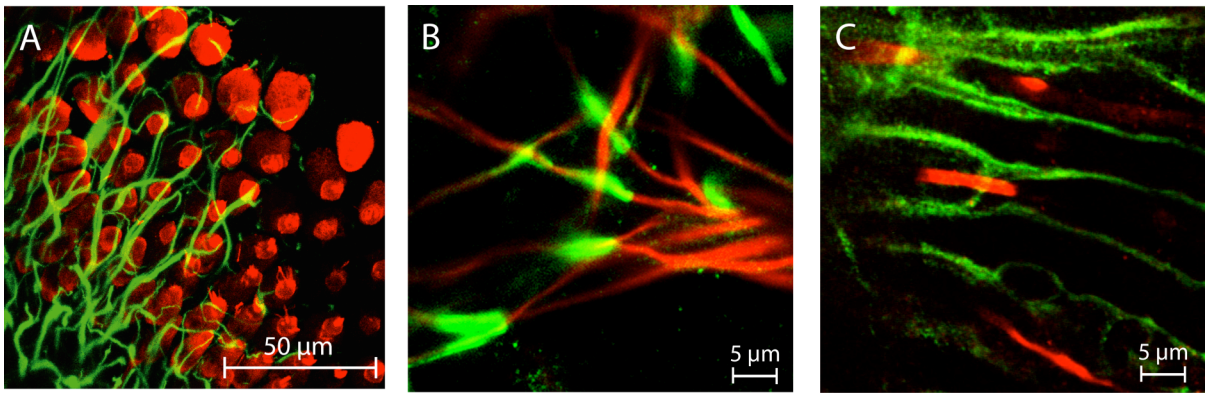
A
50 µm
B
5 µm
C
5 µm

Figure 2.2

Afferent fibers in the amphibian papilla

(**A**) Afferent fibers in the region of experimentation branch sparsely to contact one to two hair cells in the intact epithelium. Hair cells are labeled with an antiserum against parvalbumin 3 (red) and afferent fibers with antibodies directed against neurofilament proteins (green). (**B**) Voltage-gated Na^+ channels (green) are expressed at discrete locations along afferent fibers (red) below the basement membrane. (**C**) Afferent fibers (red) express myelin basic protein (green) along their lengths. Staining commences only after the fibers have penetrated the basement membrane. The image in panel **A** is a flattened confocal z-stack; panels **B** and **C** display single confocal sections.

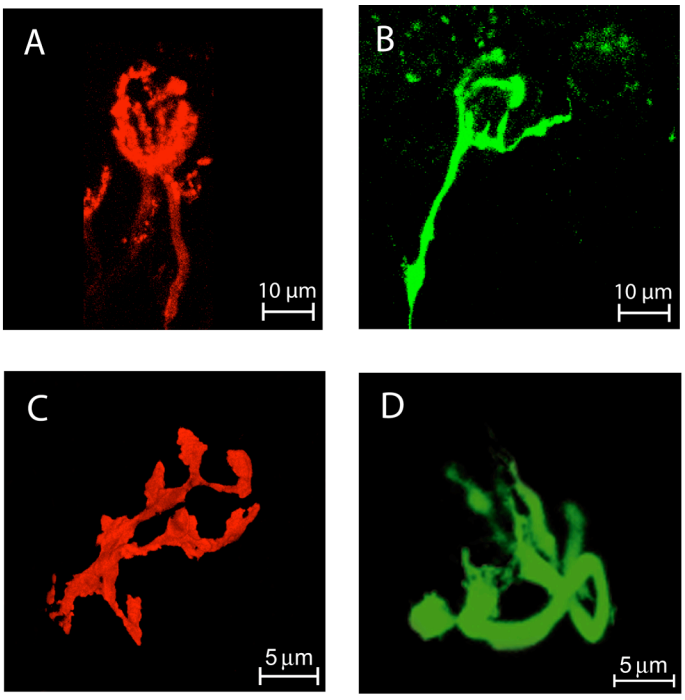
A
10 µm
B
10 µm
C
5 µm
D
5 µm

Figure 2.3

Fine structure of afferent nerve terminals

(**A**) An afferent fiber labeled with $DiIC_{18}(3)$ forms a calyceal-like connection onto a single hair cell. (**B)** An afferent fiber dialyzed with 50 μM Alexa 488 hydrazide dye in the whole-cell pipette projects several fine extensions onto the basolateral surface of a hair cell. Strong labeling was obtained after several minutes of whole-cell recording, and permitted imaging in live preparations. (**C, D**) Higher-magnification views of two fibers labeled with $DiIC_{18}(3)$ and Alexa 488, respectively, reveal the complexity of the synaptic contacts. In the medio-caudal region of physiological recordings, each fiber typically encircled the base of a single hair cell and extended finer apical fingers. All images shown are compressed confocal z-stacks.

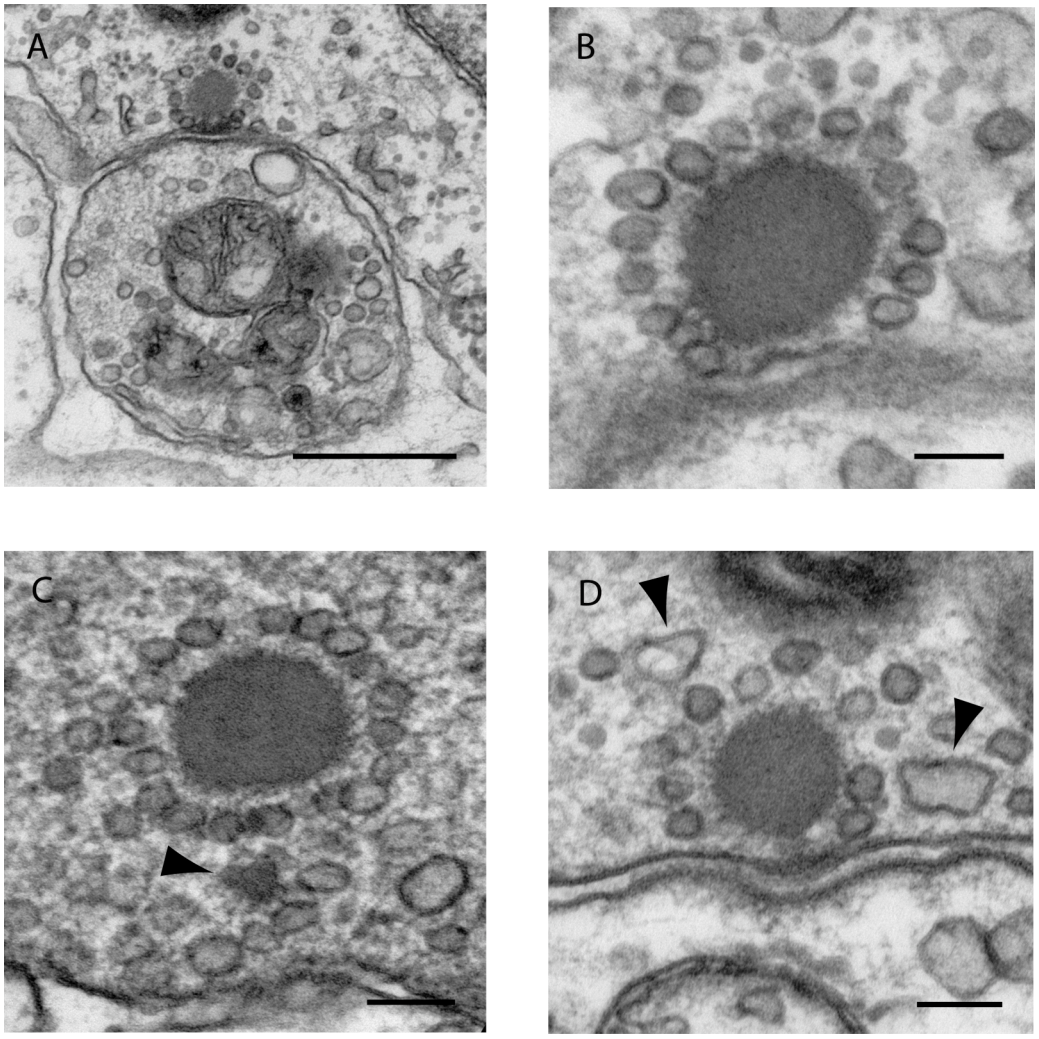
A
B
C
D

Figure 2.4

Synaptic ultrastructure

(**A**) An electron micrograph from a conventionally fixed preparation displays a well-preserved synaptic connection. A presynaptic dense body or ribbon covered with synaptic vesicles is closely apposed to an afferent fiber. (**B**) A higher-magnification view of a hair cell's active zone shows the characteristic 150-nm diameter presynaptic dense body or ribbon that anatomically defines the site of exocytosis. Synaptic vesicles are tethered to the surface of the ribbon at high density. (**C**) In rare instances, two synaptic bodies were observed at a single active zone. The arrowhead denotes a portion of the second synaptic body. (**D**) Membrane-bounded compartments of various shapes and sizes exceeding those of synaptic vesicles were often seen in the region of the presynaptic active zone. The arrowheads indicate two such structures. Scale bars: (**A**), 500 nm; (**B), (C), (D**), 100 nm.

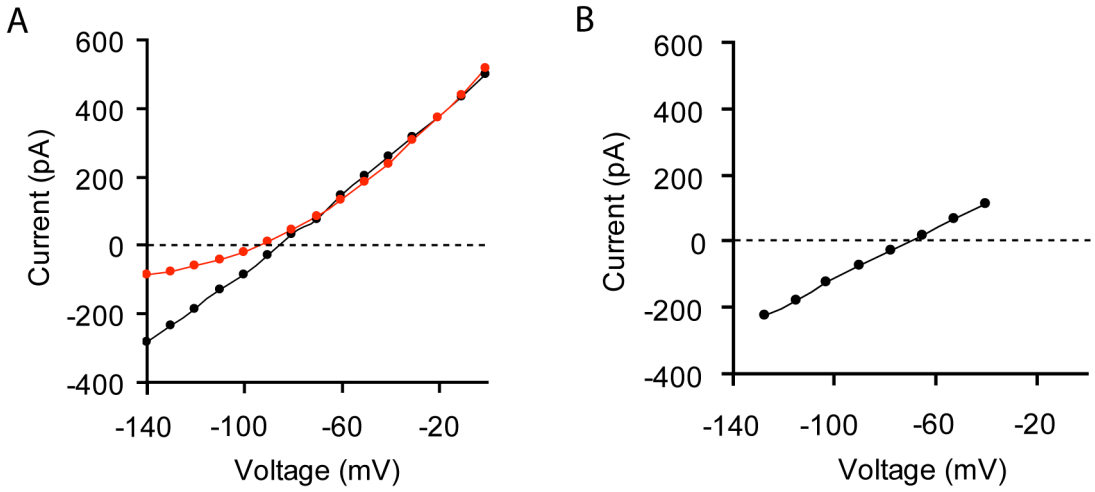
A
600
400
200
0
-200
-400
Current (pA)
-140
-100
-60
-20
Voltage (mV)
B
600
400
200
0
-200
-400
Current (pA)
-140
-100
-60
-20
Voltage (mV)

Figure 2.5

Current-voltage relation in afferent fibers

(**A**) An afferent fiber recorded with a KCl-based internal solution displays a linear current-voltage relation 1 ms after the voltage step (black), but a nonlinear relation at 20 ms (red). This fiber had an input resistance of 150 MΩ. (**B**) Another afferent fiber recorded with a CsCl-based solution exhibits an ohmic current-voltage relation across the same range of holding potentials throughout the duration of the stimulus. This fiber had an input resistance of 250 MΩ.

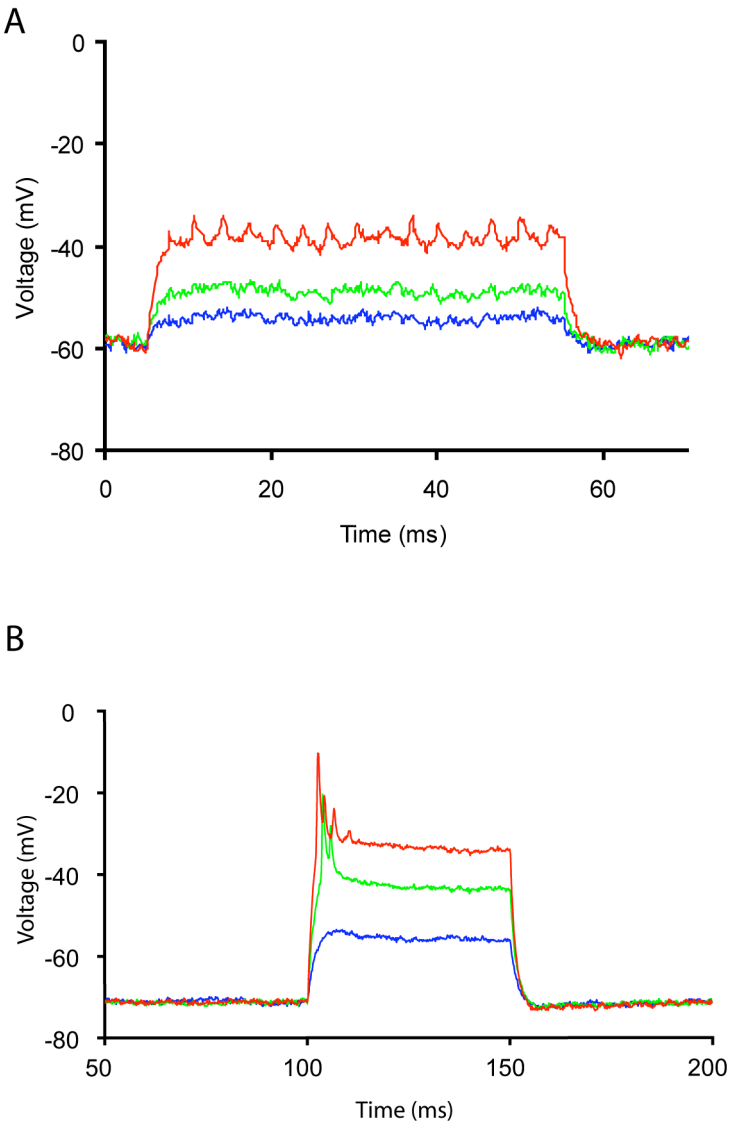
A
0
-20
-40
-60
-80
Voltage (mV)
0
20
40
60
Time (ms)
B
0
-20
-40
-60
-80
Voltage (mV)
50
100
150
200
Time (ms)

Figure 2.6

Spiking behavior of afferent fibers

(**A**) Depolarization of an afferent fiber to -40 mV leads to a steady rate of action-potential generation. Injected current amplitudes were 50 pA (blue), 100 pA (green), and 200 pA (red). (**B**) Depolarization of another afferent fiber results in phasic spiking behavior. Injected current amplitudes were 100 pA (blue), 200 pA (green), and 300 pA (red). Note also the small amplitude of the evoked action potentials. Recordings were performed in the whole-cell, current-clamp mode in the absence of tetrodotoxin.

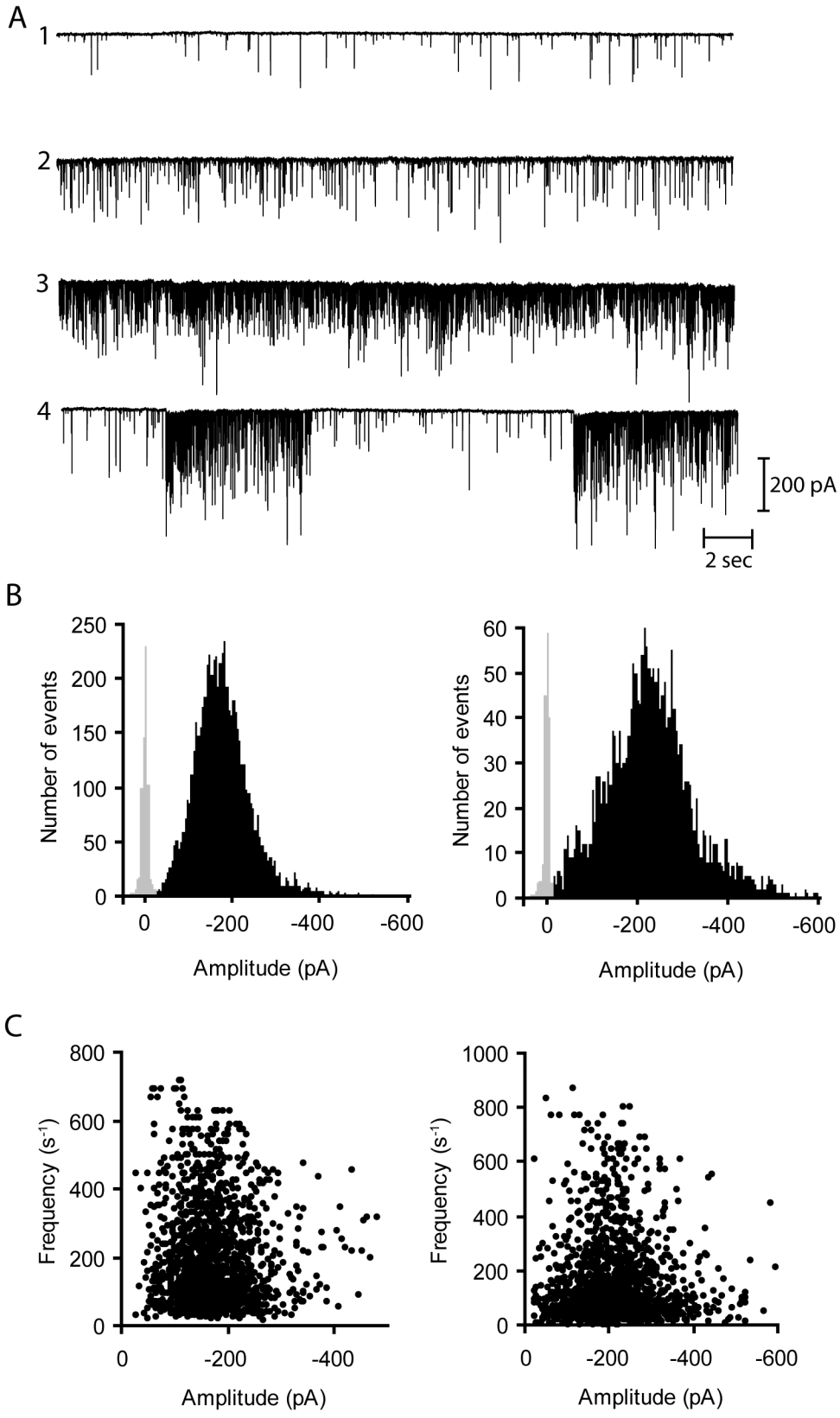
A
1
2
3
4
200 pA
2 sec
B
Number of events
250
200
150
100
50
0
0
-200
-400
-600
Amplitude (pA)
Number of events
60
50
40
30
20
10
0
0
-200
-400
-600
Amplitude (pA)
C
Frequency (s-1)
800
600
400
200
0
0
-200
-400
Amplitude (pA)
Frequency (s-1)
1000
800
600
400
200
0
0
-200
-400
-600
Amplitude (pA)

Figure 2.7

Amplitude and frequency of spontaneous EPSCs

(**A**) Spontaneous EPSCs recorded from four afferent fibers vary widely in amplitude and timing. The average frequency at which EPSCs occurred during the displayed recordings was (from top to bottom) 6 s^{-1}, 14 s^{-1}, 102 s^{-1}, and 47 s^{-1}. (**B**) The amplitude distributions of spontaneous EPSCs (black) recorded in fibers **3** (left) and **4** (right) extend over more than one order of magnitude, but display a Gaussian profile. Analysis of 6,116 events in fiber **3** showed a mean amplitude of -178±65 pA. Analysis of 2,124 events in fiber **4** gave a mean amplitude of -237±98 pA. The scaled distributions of noise amplitudes are shown in gray. (**C**) The relation between EPSC amplitude and instantaneous frequency for fibers **3** (left) and **4** (right) reveal that high-frequency events are more tightly distributed in amplitude and are not among the smallest or the largest of those recorded in a given fiber.

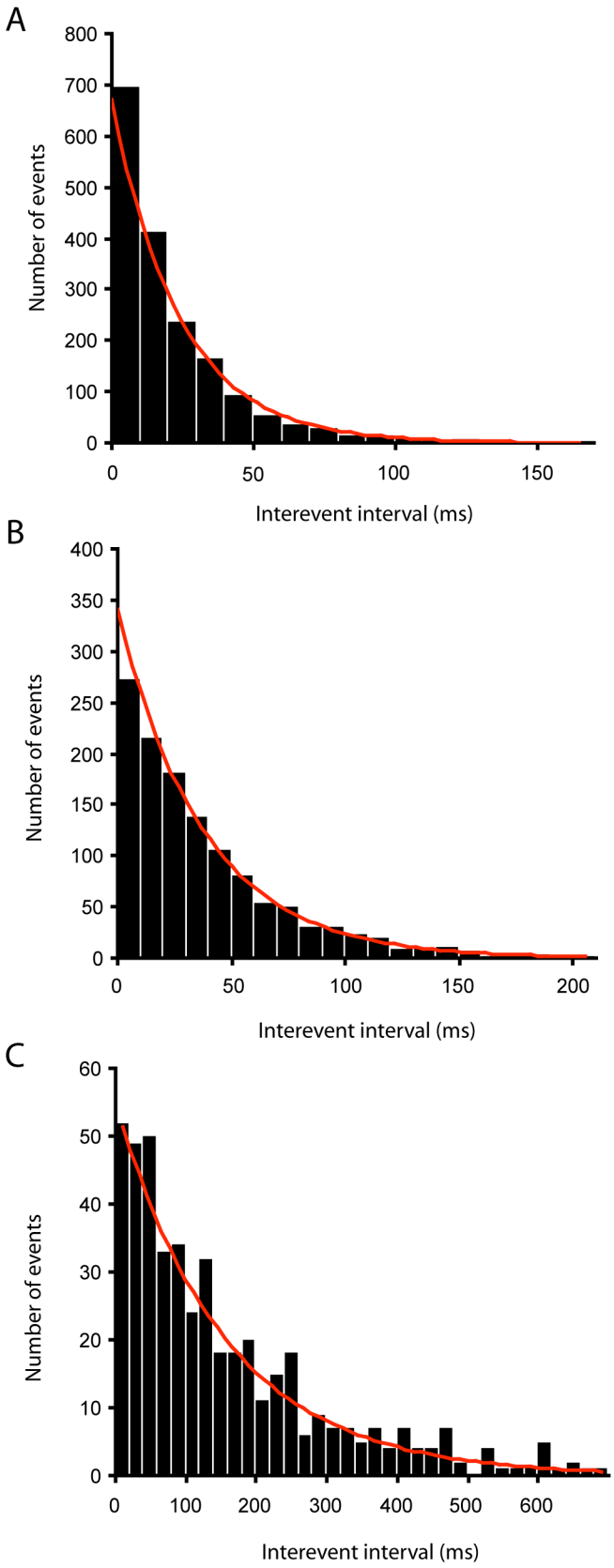
A
800
700
600
500
400
300
200
100
0
Number of events
0
50
100
150
Interevent interval (ms)
B
400
350
300
250
200
150
100
50
0
Number of events
0
50
100
150
200
Interevent interval (ms)
C
60
50
40
30
20
10
0
Number of events
0
100
200
300
400
500
600
Interevent interval (ms)

Figure 2.8

Interevent interval histograms

Interevent interval histograms were generated from spontaneous EPSCs during periods of relatively constant frequency (bin width 10 ms). The histograms were well fit with single exponential functions. For the three afferent fiber recordings shown here, τ = 21 ms (**A**), τ = 38 ms (**B**), and τ = 62 ms (**C**).

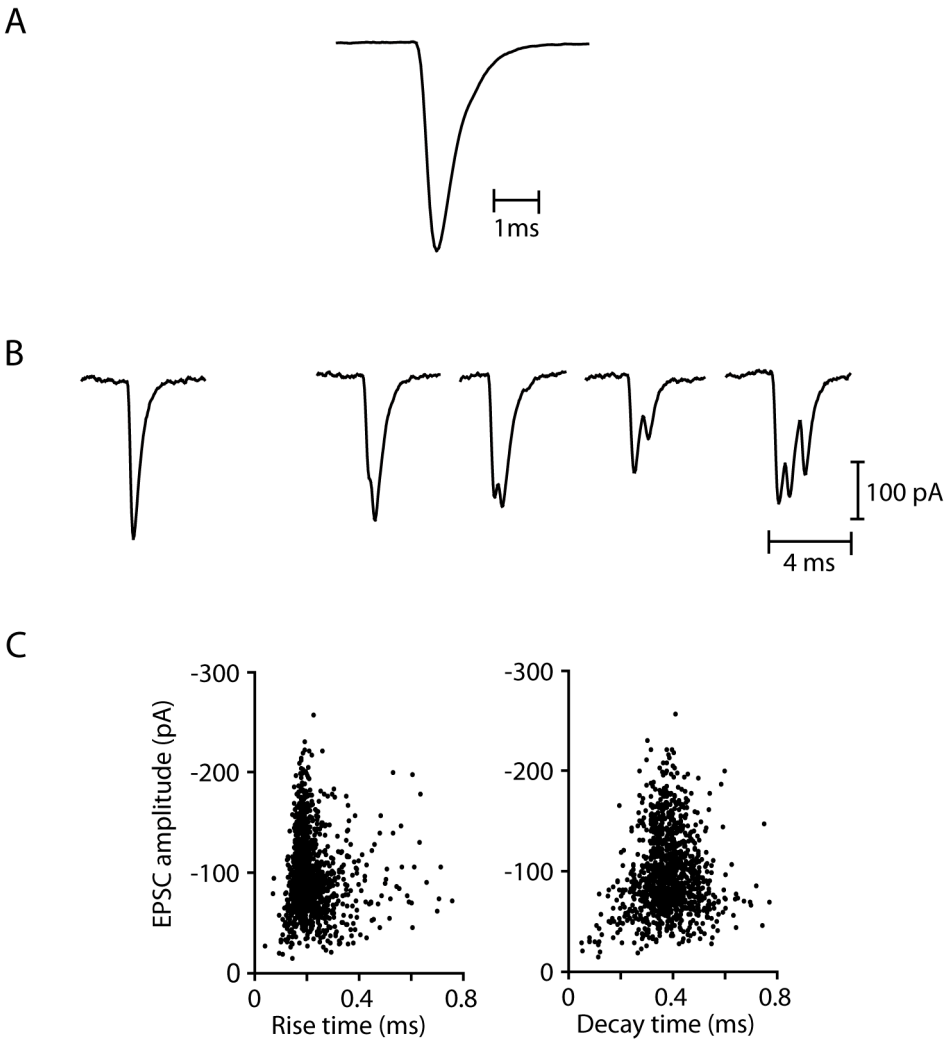
A
1ms
B
100 pA
4 ms
C
EPSC amplitude (pA)
-300
-200
-100
0
0
0.4
0.8
Rise time (ms)
Decay time (ms)

Figure 2.9

Kinetics of spontaneous EPSCs

(**A**) A representative spontaneous EPSC displays a monophasic waveform, with a fast rise and slower exponential decay. (**B**) Although most EPSCs are monophasic (*Left*), a small subset of EPSCs displays more complex waveforms suggestive of multivesicular release slightly dispersed in time (*Right*). (**C**) The 10%-90% rise times (*Left*) and time constants of decay (*Right*) for EPSCs from a representative afferent fiber recording display tight distributions, suggesting that multiple release events are highly synchronized.

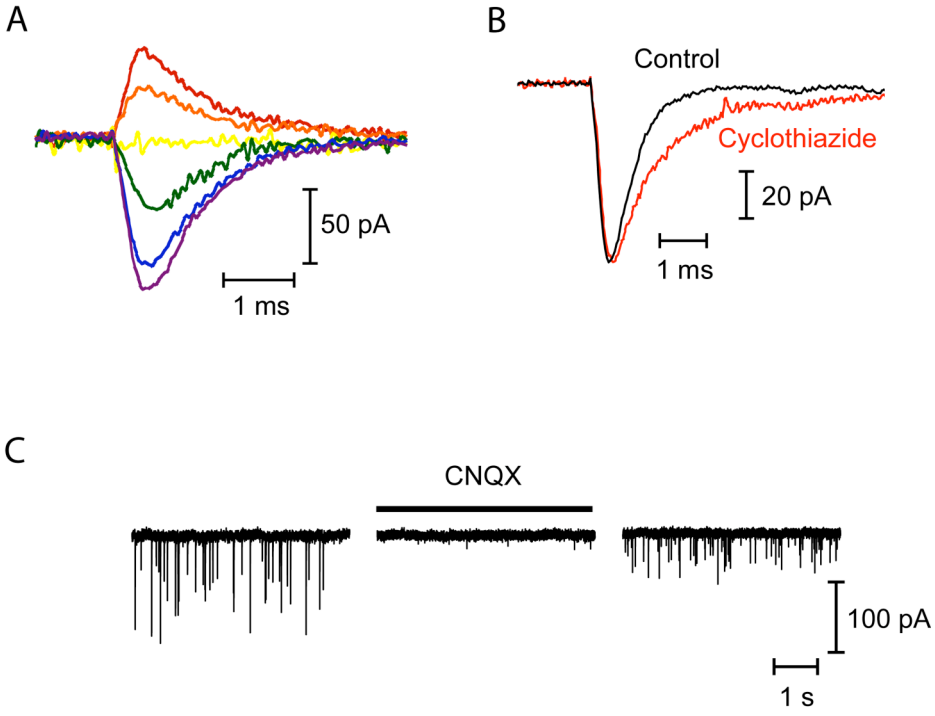
A
50 pA
1 ms
B
Control
Cyclothiazide
20 pA
1 ms
C
CNQX
100 pA
1 s

Figure 2.10

Properties of postsynaptic receptors

(**A**) As the postsynaptic potential was varied, averaged EPSCs reversed sign near 0 mV and slowed at more positive potentials. From top to bottom, the holding potentials were +50 mV, +30 mV, 0 mV, -20 mV, -70 mV, and -100 mV. (**B**) Addition of 100 μM cyclothiazide doubled the average decay time of spontaneous EPSCs, increasing the time constant from 0.65±0.13 ms (n=91) to 1.25±0.27 ms (n=38). (**C**) 10 μM 6-cyano-7-nitroquinoxaline-2,3-dione (CNQX), an antagonist of AMPA and kainate receptors, reversibly blocked spontaneous EPSCs.

CHAPTER THREE

On the input-output function at a hair-cell synapse

In the previous chapter, an *in vitro* preparation that preserves and exposes functional afferent synapses was described. In order to investigate more directly the transfer characteristics of this synapse, it was desirable to simultaneously control both presynaptic and postsynaptic voltages. In this chapter, the results of paired recordings from hair cells and afferent fibers are shown and the input-output function of the synapse is assessed.

Materials and Methods

In vitro preparation of the bullfrog's amphibian papilla

Isolation, dissection, and splitting of the amphibian papilla were performed as described in Chapter Two. To facilitate access of the recording pipettes to both hair cells and afferent terminals, excess cartilage and connective tissue were removed from either end of the papilla prior to its immobilization in the recording chamber. 1 μM tetrodotoxin was included in the perilymph to block voltage-gated Na^+ channels during all afferent fiber recordings.

Electrophysiological recordings

Recordings were performed at room temperature (~23°) with borosilicate pipettes prepared as described in Chapter Two. During paired recordings, afferent fiber terminals were held at a potential of -70 mV and hair cells at a potential of -80 mV between

stimulus presentations. Holding potentials were corrected *post hoc* for a 4-mV junction potential, but not for the uncompensated series resistance. Because the Ca^{2+} current did not exceed 300 pA in all hair-cell recordings, the voltage error was at most 2 mV.

Data analysis

Data were analyzed with Minianalysis (Synaptosoft; Jaejin Software, Leonia, NJ), Excel (Microsoft), and Mathematica (Wolfram Research, Champaign, IL). The presynaptic Ca^{2+} current was defined as the peak amplitude of the leak-subtracted Ca^{2+} current during the presentation of the 100-ms test potential. The total charge transferred with each evoked postsynaptic current was calculated by integrating the change in the postsynaptic current during the presentation of the 100-ms hair-cell depolarization. The average postsynaptic current was determined by dividing this total charge by the duration of the stimulus. The amplitudes of individual, evoked EPSCs were determined using a deconvolution algorithm developed by Daniel Andor (The Rockefeller University).

Results

Paired recordings

Simultaneous whole-cell recordings were obtained from hair cells and afferent fibers to determine the relation between presynaptic parameters and the postsynaptic response. A whole-cell recording was first obtained from an afferent fiber near its termination on the basolateral surface of a hair cell. Spontaneous EPSCs were acquired from this fiber prior to attaining a whole-cell recording from the innervated hair cell. The addition of fluorescent dye in the patch pipette permitted anatomical analysis of the innervating fiber.

In five of six paired recordings, the fiber contacted solely the voltage-clamped hair cell. This result was confirmed physiologically by the near extinction of postsynaptic currents when the hair cell was hyperpolarized to a potential of -80 mV.

Evoked EPSCs

The relationship between presynaptic voltage and postsynaptic response was examined by stepping each hair cell to potentials between -70 mV and +10 mV from a holding potential of -80 mV. EPSCs were evoked by hair-cell depolarization and persisted for the duration of each test stimulus (**Figure 3.1**). With increasing presynaptic depolarization, the latency to the first evoked EPSC decreased (**Figure 3.2**). The rate of release during the stimulus presentation varied among fibers: EPSCs in some experiments displayed adaptive changes during large presynaptic depolarizations, and in others showed an increase in rate suggestive of a progressive accumulation of Ca^{2+} at the presynaptic active zone (**Figure 3.3**). The evoked EPSCs of some cell pairs were superimposed, precluding comparative analysis of the amplitude and kinetics of spontaneous and evoked currents from such fibers. In three of the paired recordings, however, individual EPSCs were discernible during maximal presynaptic depolarization. The kinetic parameters of evoked EPSCs in these experiments did not differ from those of spontaneous EPSCs recorded in the same fiber. Furthermore, the largest evoked EPSCs were no larger than those of the largest spontaneous EPSCs recorded from the same fiber.

Relation between presynaptic voltage and postsynaptic response

The temporal pattern, amplitudes, and frequency of evoked EPSCs varied as a function of the presynaptic potential. The latency between stimulus onset and the first evoked EPSC decreased with larger depolarizations (**Figure 3.2**). For stimuli that evoked near-maximal Ca^{2+} currents, the postsynaptic response often persisted after the termination of the pulse and the presynaptic Ca^{2+} current (**Figure 3.1**).

During small presynaptic depolarizations, evoked EPSCs were infrequent and had consistently small amplitudes. During larger depolarizations, evoked EPSCs occurred at a higher rate and displayed a broad distribution of amplitudes, encompassing the full range of sizes observed in spontaneous EPSCs recorded from the same fiber. However, above a voltage threshold that was several millivolts more positive than the activation level of the presynaptic Ca^{2+} current, the average EPSC amplitude remained relatively constant (**Figure 3.4A**). Above this level, the increase in the total postsynaptic response was determined primarily by an increase in the frequency of evoked EPSCs (**Figure 3.4B**).

When the innervated hair cell was held at -80 mV outside of the depolarizing stimulus, small, infrequent EPSCs were observed. The mean amplitude of these events was uniformly smaller than those recorded during spontaneous activity in the same fiber (**Figure 3.5**). The amplitude distribution of EPSCs during hair-cell hyperpolarization to -80 mV could be well fit by a Gaussian function with a mean value of -61.3±13 pA for a postsynaptic potential of -90 mV.

Relation between presynaptic Ca^{2+} influx and postsynaptic response

Depolarizing voltage pulses activated an inward current in the hair cell and evoked EPSCs in the afferent fiber (**Figure 3.6**). The presynaptic inward current revealed with a Cs^{+}-based internal solution was noninactivating and nifedipine-sensitive, which, together with its current-voltage relation, signified Ca^{2+} influx through L-type Ca^{2+} channels (Rodriguez-Contreras and Yamoah, 2001; Schnee and Ricci, 2003).

As a measure of the postsynaptic response, the evoked postsynaptic current was integrated and the result was divided by the duration of the depolarizing stimulus. This average postsynaptic current was presumably proportional to the number of glutamate receptors that bound the released transmitter, and in turn to the number of synaptic vesicles that liberated their contents. The average postsynaptic current depended on the hair cell's membrane potential and mirrored the steep voltage dependence of the presynaptic Ca^{2+} current (**Figure 3.7**). The Ca^{2+} current activated near -55 mV and was maximal at -20 mV; similarly, the postsynaptic current displayed an activation threshold between -55 mV and -50 mV and peaked at -20 mV to -10 mV.

At the presynaptic active zones of hair cells, the local Ca^{2+} concentration is expected to be directly proportional to the Ca^{2+} current (Roberts, 1994). To determine the dependence of exocytosis on Ca^{2+}, the average amplitude of the postsynaptic current—effectively the convolution of the frequencies and amplitudes of the evoked EPSCs—was plotted against the presynaptic Ca^{2+} current at each test potential. Both signals varied between cell pairs, perhaps as a consequence of the heterogeneous properties of amphibian papilla hair cells and differences in the number of postsynaptic receptors or

active zones involved. Nevertheless, the data from four cell pairs were well approximated by linear fits over a range of presynaptic potentials that corresponds to physiological levels of stimulation (**Figure 3.8**). The relation tended to deviate from linearity at either end. In most instances, the postsynaptic response vanished at potentials more negative than -55 mV, despite the persistence of a small Ca^{2+} current. At more depolarized voltages, the postsynaptic response tended to saturate although the presynaptic Ca^{2+} current increased further.

The average postsynaptic response closely followed the extent of presynaptic Ca^{2+} influx, so it was of interest to determine whether this linear relation was achieved primarily by an increase in the amplitude or the frequency of evoked EPSCs. Importantly, the average amplitudes of EPSCs were fairly constant in response to stimuli that elicited presynaptic Ca^{2+} currents during hair-cell depolarization (**Figure 3.9A**). In contrast, the frequency of evoked EPSCs increased dramatically, and in a linear fashion, with an increase in presynaptic Ca^{2+} influx (**Figure 3.9B**). The linearity of the synaptic transfer function is therefore dominated by an increase in the rate of fusion events, rather than an increase in the size of those events.

Discussion

Synaptic delay

The rate-limiting step in synaptic transmission is likely to be dominated by the time needed to trigger vesicle fusion (Sabatini and Regehr, 1999): neurotransmitter release from a fusing vesicle, neurotransmitter diffusion across the synaptic cleft, and postsynaptic receptor activation occur with time constants well under 1 ms (Clements *et*

al., 1992; Clements, 1996; Eccles and Jaeger, 1958). In the experiments described above, the latency to the first evoked EPSC was correlated with the degree of presynaptic depolarization (**Figure 3.2**). Interestingly, this delay often exceeded several milliseconds, despite the rapid activation of the presynaptic Ca^{2+} current, suggesting that an accumulation of Ca^{2+} was required to elicit exocytosis. In a system thought to demonstrate rapid responsiveness *in vivo*, such a synaptic delay *in vitro* is surprising. Several potential differences between the *in vivo* and *in vitro* preparations could account for this discrepancy. Dialysis of the hair cell during whole-cell recording may have depleted proteins essential for exocytosis; however, the rapidity with which EPSCs were evoked with larger hair-cell depolarizations suggests that this was not the case. The introduction of an exogenous Ca^{2+} buffer may have altered the spatiotemporal profile of Ca^{2+} entering the cytoplasm through voltage-gated channels; however, the 2 mM EGTA included in the whole-cell pipette is believed to be much less efficient at Ca^{2+} capture than the endogenous buffering system in hair cells (Roberts, 1993) and vesicles are expected to lie well within the focal spire of Ca^{2+} generated by voltage-gated Ca^{2+} channel influx (Roberts, 1994). Alternatively, and perhaps most likely, the local cytoplasmic Ca^{2+} concentration at the active zone was reduced to an unphysiologically low level between stimuli by the intervening hyperpolarization. Tonic spontaneous activity in auditory afferent fibers *in vivo* suggests that the hair cell's resting potential is sufficiently positive for Ca^{2+}-current activation and thus spontaneous transmitter release (Robertson and Paki, 2002; Taberner and Liberman, 2005). Voltage-clamping the hair cell to –80 mV, then, should dramatically decrease the resting Ca^{2+} concentration at active zones, perhaps reducing the steady-state occupancy of the Ca^{2+} sensor and thus the

probability of vesicle fusion. Notably, secretion in mast cells has been shown to depend upon a threshold elevation of intracellular Ca^{2+}, such that the delay in Ca^{2+} rise is closely matched to the delay in the initiation of secretion (Kim *et al.*, 1997). Translocation of synaptic vesicles to the active zone has also been shown to depend upon intracellular Ca^{2+} (Koenig *et al.*, 1993). It is therefore also possible that vesicle docking sites were transiently depleted due to hair-cell hyperpolarization and required significant Ca^{2+} influx to be replenished. Further experiments exploring the effect of various presynaptic holding potentials prior to depolarization may clarify the mechanism underlying the observed latency.

Relation between presynaptic stimulation and EPSC amplitude

Infrequent, small EPSCs were detected when the presynaptic hair cell was held at -80 mV (**Figure 3.5**). Although L-type Ca^{2+} channels activate near -60 mV, brief channel openings have been recorded at -80 mV in single-channel recordings from chicken hair cells (Zampini *et al.*, 2006). The few EPSCs observed during hair-cell hyperpolarization therefore likely represent vesicle fusions due to low-probability openings of L-type Ca^{2+} channels.

The relation between the presynaptic voltage and Ca^{2+} current and the average amplitude of evoked EPSCs suggests that the size of a postsynaptic event depends upon intracellular Ca^{2+}, but either saturates or becomes independent of the level of presynaptic stimulation above a relatively negative potential. This saturation threshold lies only several millivolts above that required for activation of the Ca^{2+} current, implying a highly cooperative dependence on Ca^{2+}. Although the mechanism that determines EPSC

amplitude remains obscure, this nonlinear behavior is reminiscent of the Ca^{2+} dependence displayed by the proteins involved in membrane fusion reactions such as exocytosis.

Linear relation between Ca^{2+} influx and hair-cell exocytosis

Exocytosis has a higher-order dependence on the presynaptic Ca^{2+} concentration (Dodge and Rahamimoff, 1967), a macroscopic observation taken to reflect a kinetic model involving the sequential and cooperative binding of multiple Ca^{2+} ions to a sensor required to activate an irreversible fusion reaction. Flash photolysis of caged Ca^{2+} in mouse inner hair cells provides evidence for five cooperative Ca^{2+}-binding steps for each exocytic event (Beutner *et al*., 2001). However, the hair-cell afferent synapse evidently operates in a linear regime under our experimental conditions. Such a relationship has also been observed for the ribbon synapses of rod photoreceptors (Thoreson *et al*., 2004) and since this study has been confirmed for mammalian hair-cell synapses as well (Goutman and Glowatzki, 2007). In several auditory receptor organs, presynaptic vesicle fusion has also been shown to depend linearly on the presynaptic Ca^{2+} current (Johnson *et al*., 2005; Schnee *et al*., 2005; Brandt *et al*., 2005). The demonstration that this linear relation extends across the synapse to the postsynaptic current implies that postsynaptic receptors faithfully transmit the information conveyed by hair-cell exocytosis. The fidelity of these receptors is further examined in Chapter Four.

The linearity of the synaptic transfer function is in agreement with the proposal that exocytosis at the hair-cell synapse depends upon a Ca^{2+} nanodomain, such that fusion-competent vesicles sense Ca^{2+} influx from only one or a few closely associated channels (Brandt *et al*., 2005). In this scenario, a linear increase in exocytosis is

expected with presynaptic depolarization, as this manipulation primarily increases the number of open Ca^{2+} channels rather than their single-channel conductances. The Ca^{2+} nanodomain model agrees well with the observation that the linear relation between presynaptic Ca^{2+} current and postsynaptic response is dominated by the change in the frequency of evoked EPSCs (**Figure 3.4, 3.9**): as the open probability of Ca^{2+} channels increases with hair-cell depolarization, the number of exocytotic events increases accordingly. These results also accord with those obtained from the hair-cell synapse in goldfish. In that system, acoustic stimulation promoted an increase in the size of the readily releasable pool of vesicles rather than an increase in vesicle release probability (Furukawa *et al.*, 1978).

For finely graded intensity discrimination over a large dynamic range of sound stimuli, the most efficient encoding method is a linear translation of presynaptic Ca^{2+} influx into exocytosis. In order for this high-fidelity transmission to be received without distortion, the postsynaptic receptors must similarly perform a linear transformation of neurotransmitter concentration into postsynaptic current. The observed linear relation between presynaptic Ca^{2+} influx and postsynaptic current suggests that this is indeed the operational mode of the synapse within a physiological range of depolarizations. This encoding strategy may allow the hair-cell afferent synapse to be sensitive to low-amplitude stimuli, finely discriminate intensity differences, and transfer complex waveforms rapidly with minimal distortion.

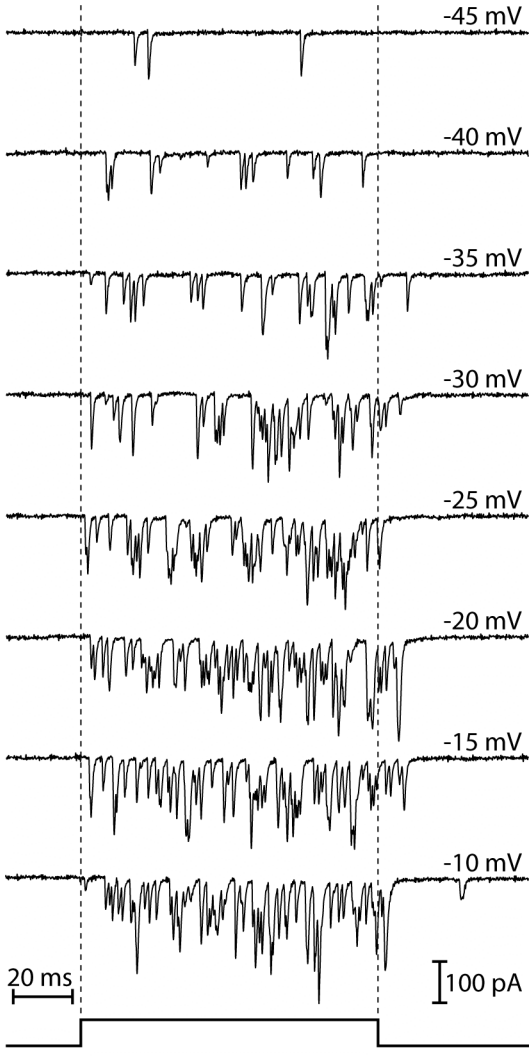
-45 mV
-40 mV
-35 mV
-30 mV
-25 mV
-20 mV
-15 mV
-10 mV
20 ms
100 pA

Figure 3.1

Evoked EPSCs

In a simultaneous voltage-clamp experiment, the hair cell was confronted with a series of 100-ms depolarizations whose timing is displayed at the bottom of the figure. Discrete evoked EPSCs became superimposed during larger depolarizations. For depolarizations that evoked near-maximal hair-cell Ca^{2+} currents, the latency between stimulus onset and the first response decreased, and evoked EPSCs tended to persist after the termination of the pulse and the presynaptic Ca^{2+} current.

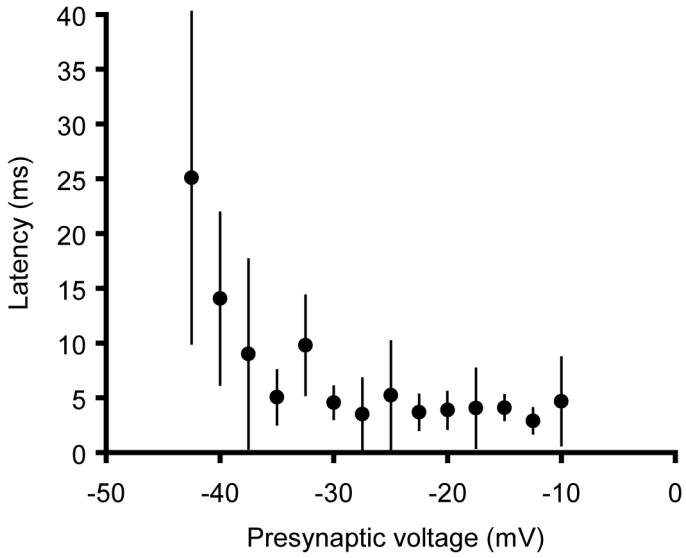
40
35
30
25
20
15
10
5
0
Latency (ms)
-50
-40
-30
-20
-10
0
Presynaptic voltage (mV)

Figure 3.2

Latency to the first evoked EPSC

The delay between hair-cell depolarization and the postsynaptic response decreases with stimulus intensity. Data shown are presented as means with standard errors of the means for three paired recordings.

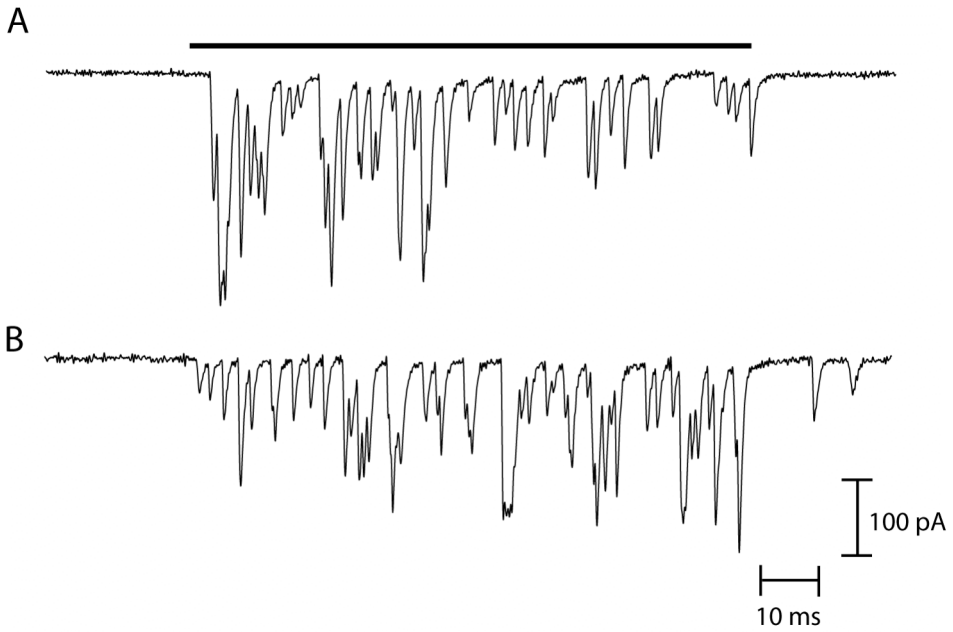
A
B
100 pA
10 ms

Figure 3.3

Patterns of exocytosis during large-amplitude stimuli

In paired recordings, evoked EPSCs displayed different temporal patterns in response to presynaptic depolarizations that elicited near-maximal hair-cell Ca^{2+} currents. During a 100-ms stimulus to -30 mV, the afferent fiber in panel **A** displayed adaptation. The same stimulus delivered to another hair cell whose afferent fiber recording is shown in panel **B** exhibited a gradual increase in the amplitude of EPSCs during hair-cell depolarization. Note that several exocytotic events also persisted after the termination of the pulse. The timing of the presynaptic stimuli is denoted by the black bar.

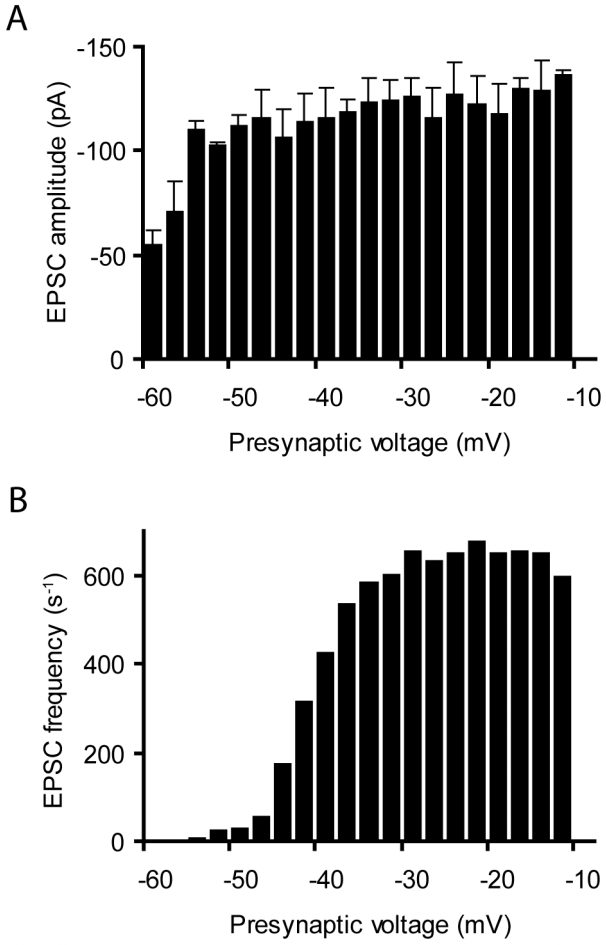
A
-150
-100
-50
0
EPSC amplitude (pA)
-60
-50
-40
-30
-20
-10
Presynaptic voltage (mV)
B
600
400
200
0
EPSC frequency (s-1)
-60
-50
-40
-30
-20
-10
Presynaptic voltage (mV)

Figure 3.4

Relation between the presynaptic voltage and evoked EPSCs

(**A**) The average amplitude of evoked EPSCs increased with small-amplitude stimuli, but was fairly constant during larger depolarizations. (**B**) The frequency of evoked EPSCs increased steeply with depolarization to ~-30 mV, but did not change significantly during larger depolarizations. The data shown are averages of two trials of 100-ms depolarizations from -60 mV to -12.5 mV each delivered to two hair cells. In these two experiments, individual evoked EPSCs were detectable in the afferent fiber during stimulus presentation. Error bars denote the standard errors of the mean for the four trials.

A

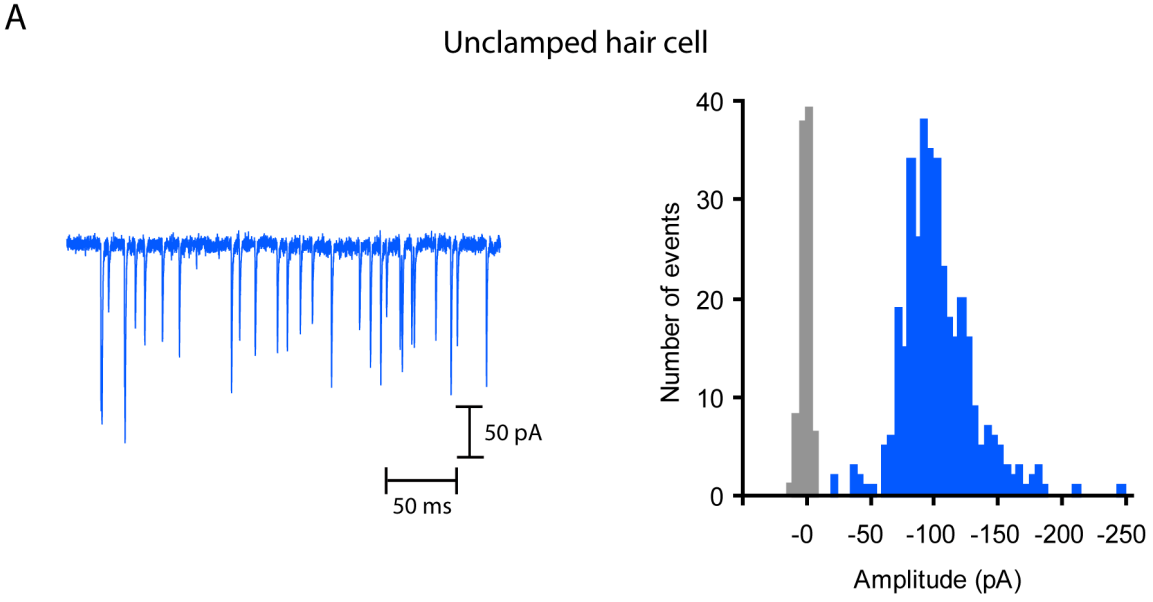
Unclamped hair cell
50 pA
50 ms
Number of events
40
30
20
10
0
-0
-50
-100
-150
-200
-250
Amplitude (pA)

B

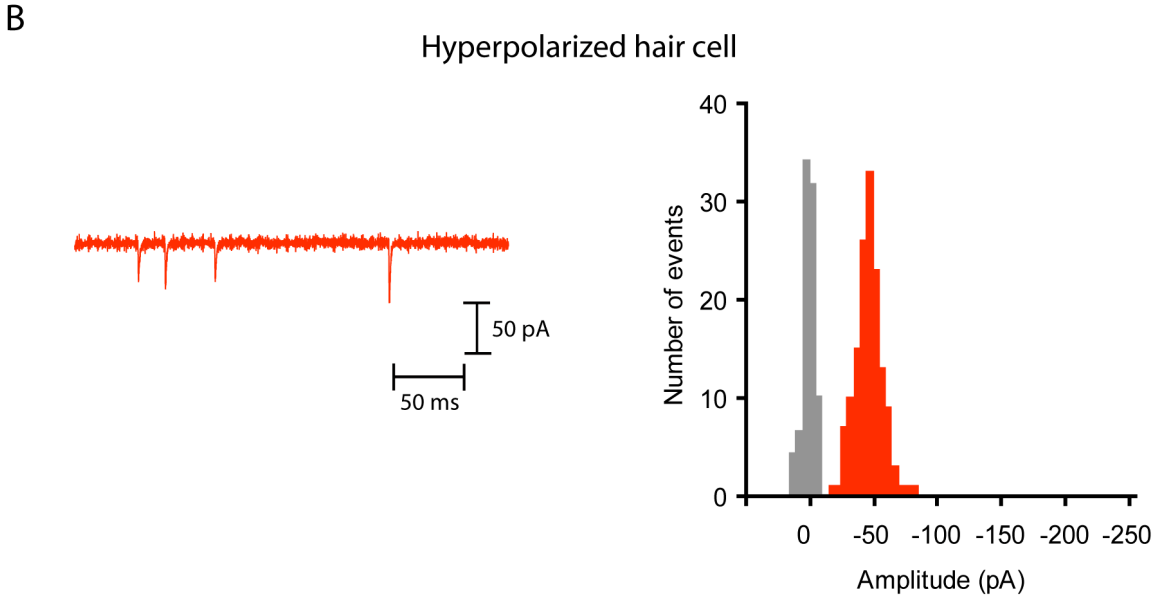
Hyperpolarized hair cell
50 pA
50 ms
Number of events
40
30
20
10
0
0
-50
-100
-150
-200
-250
Amplitude (pA)

Figure 3.5

Effect of hair-cell hyperpolarization on EPSC amplitude

(**A**) Spontaneous EPSCs recorded from an afferent fiber in contact with an unclamped hair cell have a large range of amplitudes. The amplitude distribution of spontaneous EPSCs (*Right*) from the recording (*Left*) has a mean value of -99±30 pA at a fiber holding potential of -70 mV (n=363). (**B**) Voltage-clamping the presynaptic hair cell to -80 mV eliminates all large events and reduces the frequency of events recorded from the same fiber (*Left*). The amplitude distribution of EPSCs during hair-cell hyperpolarization (*Right*) fell to an average of -46±13 pA (n=145). For both histograms, EPSCs were binned at 10-pA intervals. The noise amplitude distributions (gray) are scaled to the maximum of the EPSC distributions.

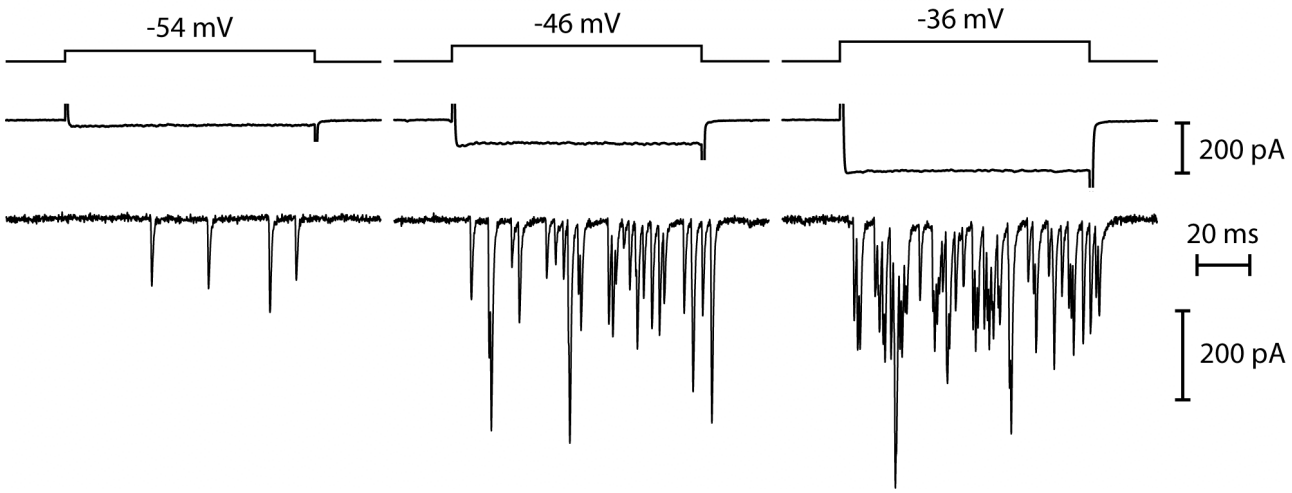
-54 mV
-46 mV
-36 mV
200 pA
20 ms
200 pA

Figure 3.6

Hair-cell depolarization elicits presynaptic Ca^{2+} currents and evoked EPSCs

Recordings during a simultaneous voltage-clamp experiment of a hair cell and its innervating afferent fiber depict presynaptic Ca^{2+} currents (middle traces) and evoked EPSCs (bottom traces) evoked by 100-ms hair-cell depolarizations to the indicated potentials (top traces). The hair cell was held at a potential of -80 mV when not experiencing the depolarizing stimuli.

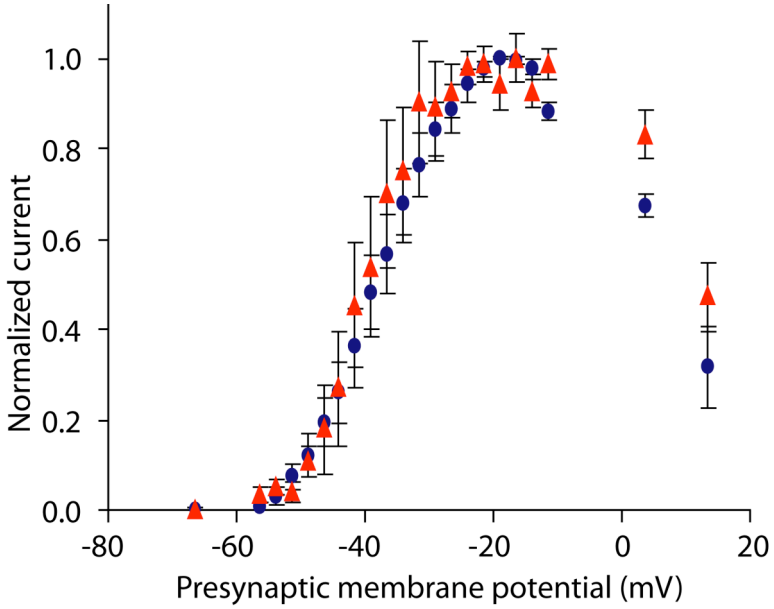
Normalized current
1.0
0.8
0.6
0.4
0.2
0.0
-80
-60
-40
-20
0
20
Presynaptic membrane potential (mV)

Figure 3.7

Voltage dependence of the presynaptic Ca^{2+} current and the postsynaptic current

Both the presynaptic Ca^{2+} current (circles) and the postsynaptic current (triangles) display a sigmoidal dependence on the hair-cell test potential. Data are presented as normalized means ± standard errors of the means for four experiments.

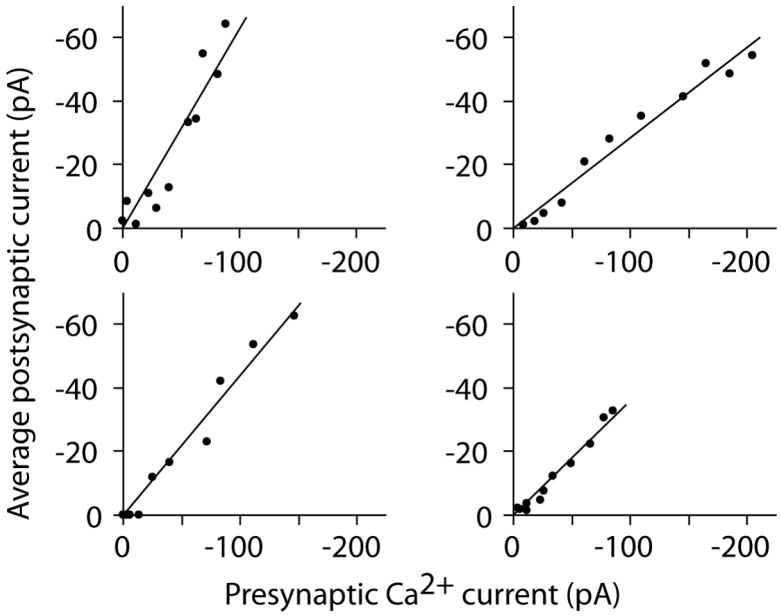
Average postsynaptic current (pA)
-60
-40
-20
0
0
-100
-200
Presynaptic Ca2+ current (pA)

Figure 3.8

Linearity of the synaptic transfer function

In each of four paired recordings, the dependence of the postsynaptic current on the presynaptic Ca^{2+} current is approximately linear over a physiologically relevant range of hair-cell membrane potentials, here -56 mV to -31 mV. Clockwise from the upper left, the linear regression coefficients (r^2) are 0.88, 0.97, 097, and 0.95.

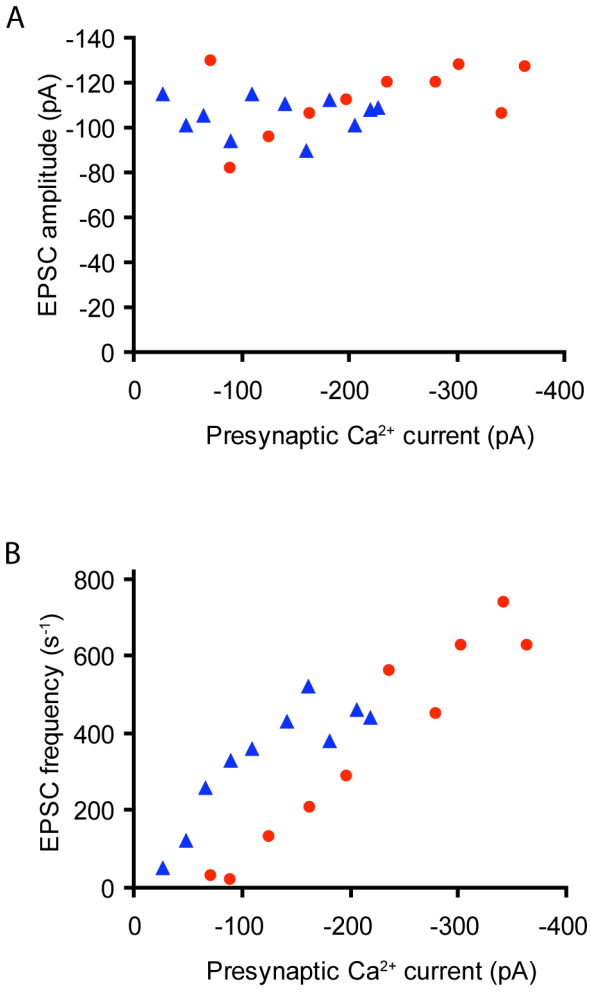
A
-140
-120
-100
-80
-60
-40
-20
0
EPSC amplitude (pA)
0
-100
-200
-300
-400
Presynaptic Ca2+ current (pA)
B
800
600
400
200
0
EPSC frequency (s-1)
0
-100
-200
-300
-400
Presynaptic Ca2+ current (pA)

Figure 3.9

Relation between the presynaptic Ca^{2+} current and evoked EPSCs

(**A**) The average amplitude of evoked EPSCs during hair-cell depolarization increased only slightly with an increase in presynaptic Ca^{2+} influx. (**B**) The frequency of evoked EPSCs increased in a linear fashion with the presynaptic Ca^{2+} current during hair-cell depolarization. The data shown are single trials of 100-ms depolarizations from -56 mV to -31 mV delivered to two hair cells in separate paired recordings. In these two experiments, individual evoked EPSCs were detectable in the afferent fiber during stimulus presentation.

CHAPTER FOUR

On multiquantal release at a hair-cell synapse

EPSCs at the synapses of sensory receptors and of some central-nervous-system neurons include large events thought to represent the synchronous release of neurotransmitter from several vesicles in a process known as multiquantal release. However, determination of the unitary or quantal size underlying such putatively multiquantal events has proven difficult. The unfavorable anatomical complexity in the central nervous system has generally prevented precise determination of the quantum. In this chapter, the magnitude of the quantal response at this sensory synapse is established, providing compelling evidence that the majority of spontaneous and evoked EPSCs are in fact multiquantal. Multiquantal EPSCs can originate from a single presynaptic active zone and do not saturate postsynaptic receptors, thus permitting the transfer of information encoded in large exocytotic events. Release of Ca^{2+} from internal stores, a potential mechanism for synchronizing the fusion of multiple synaptic vesicles, appears to be neither necessary nor sufficient to generate multiquantal events at this synapse.

Materials and Methods

In vitro preparation of the bullfrog's amphibian papilla

The isolation, dissection, and splitting of the amphibian papilla were performed as described in Chapter Two.

Electrophysiological recordings

Afferent fiber whole-cell recordings were performed with borosilicate pipettes manufactured and filled as described in Chapter Two. For iontophoresis, borosilicate capillary glass with filaments (1.2 mm outer diameter, 0.68 mm inner diameter, World Precision Instruments, Sarasota, Fl) was pulled in a horizontal puller (Model P-80/PC, Sutter Instrument Co.) to resistances of 80-100 MΩ when filled with standard internal solution. Electrodes for the presynaptic delivery of Ca^{2+} were filled with 0.5 M $CaCl_2$ at pH 7.0. Electrodes for the postsynaptic application of glutamate were filled with 0.2 M Na^{+}glutamate and 10 mM NaCl at pH 9.0. Iontophoretic currents were delivered with an Axoclamp-2A amplifier (Axon Instruments, Union City, CA). Evoked EPSCs were recorded in voltage-clamp mode with an Axopatch 200B amplifier (Axon Instruments, Union City, CA). Both stimulating and evoked currents were sampled at 20 kHz, low-pass filtered at 8 kHz, and recorded with a computer running LabVIEW.

For Ca^{2+} iontophoresis, papillae were placed in Ca^{2+}-free perilymph with 100 μM EGTA. For glutamate iontophoresis, papillae were maintained in control perilymph. Holding currents of ~2 nA were applied to minimize diffusion of the agonist from the pipette tip prior to stimulus delivery. The holding current was empirically determined as the minimal current required to prevent hair-cell exocytosis for Ca^{2+} iontophoresis or a change in baseline postsynaptic current for glutamate iontophoresis. For ejection, pulses of positive current and negative current were applied to the Ca^{2+}- and glutamate-filled pipettes, respectively.

Data analysis

Data were analyzed with Minianalysis (Synaptosoft; Jaejin Software, Leonia, NJ), Excel (Microsoft), and Mathematica (Wolfram Research, Champaign, IL).

Results

EPSC kinetics as a function of amplitude

As described in Chapter Two, spontaneous EPSCs are of widely varying magnitude, yet most possess smooth onset and decay phases (**Figure 2.9**). If larger events arise from the superposition of multiple quantal events, they might be expected to display broadening owing to slight differences in the times at which their constituent vesicles undergo exocytosis (Wall and Usowicz, 1998). In fact, however, the temporal characteristics of EPSCs were independent of their amplitudes (**Figure 4.1**). Putatively multiquantal EPSCs at the hair cell's afferent synapse therefore reveal no substructure indicative of independent but nearly coincident vesicle fusions.

Ca^{2+} iontophoresis

Because afferent fibers in the amphibian papilla form multiple terminal branches onto hair cells, recordings customarily sampled release events from several presynaptic active zones. Thus, large EPSCs could in principle represent the simultaneous fusion of vesicles at distinct synaptic ribbons within a hair cell. To determine whether large events could originate from a single active zone, the preparation was bathed in a zero-Ca^{2+} solution to silence spontaneous activity and Ca^{2+} was applied iontophoretically with a Ca^{2+}-filled pipette. Iontophoretic applications of Ca^{2+} were highly localized to a region

near the pipette tip (**Figure 4.2A**). Within the range of stimulation intensities, the amplitude of the ejection current was linearly related to the Ca^{2+} concentration as measured with a fluorescent indicator (**Figure 4.2B**).

Iontophoretic pulses of Ca^{2+} were sufficient to evoke EPSCs with amplitudes as large as spontaneous EPSCs recorded from the same fiber in control solution (**Figure 4.3**). Similar results were observed in three afferent fiber recordings. Using empirically determined values for the transference number and diffusion coefficient of Ca^{2+} (Keenan *et al*., 1945; Tinevez *et al*., 2007), it was estimated that these stimuli presented the active zone with a maximal concentration of ~200 μM Ca^{2+}. Under conditions of minimal stimulation consisting of small, brief iontophoretic currents, uniformly large EPSCs were evoked (**Figure 4.4**). The amplitude distribution of events evoked with this minimal stimulus was compact, with a mean value of -155±27 pA, yielding a coefficient of variation of 18%. In contrast, the amplitude distribution of spontaneous EPSCs recorded from the same fiber in control solution was somewhat broader, with a mean value of -132±48 pA and a coefficient of variation of 36%. In another experiment, a similar result was observed with minimal iontophoretic stimuli: the evoked EPSC amplitude distribution had a mean value of -180±34 pA with a coefficient of variation of 18%, although the spontaneous EPSC amplitude distribution had a mean value of -143±54 pA with a coefficient of variation of 38%. Thus, in two experiments, presentations of brief, localized pulses of Ca^{2+} were sufficient to elicit large, tightly distributed EPSCs. These results suggest that large EPSCs arise from a single active zone and that large, spontaneous events originate from single synaptic ribbons. Furthermore, under

conditions of minimal stimulation that afford only brief exposure to Ca^{2+} and elicit but a single EPSC, large release events may occur preferentially.

Glutamate iontophoresis

Variations in EPSC amplitude may originate from presynaptic differences in the extent of neurotransmitter release or from postsynaptic fluctuations in the number and properties of receptors. Focal application of an agonist to individual postsynaptic sites has been used to determine whether such variability arises from presynaptic or postsynaptic mechanisms (McAllister and Stevens, 2000). Therefore, I used iontophoretic pulses of glutamate to examine the properties of the postsynaptic response to neurotransmitter. Control experiments determined that iontophoresis of glutamate was highly spatially constrained: the postsynaptic response fell rapidly with displacement of the stimulating pipette from the postsynaptic terminal and the spatial scale of the decay paralleled that of a fluorescent glutamate-like compound (**Figure 4.5**) (Murnick *et al.*, 2002). Glutamate iontophoresis should therefore be sufficiently restricted to activate a single postsynaptic cluster of receptors.

To estimate how much of the variability in EPSC amplitudes could be attributed to postsynaptic receptors, the variance of the postsynaptic response to fixed concentrations of iontophoresed glutamate was examined. Although spontaneous EPSCs displayed a broad range of amplitude (**Figure 4.6A**), evoked postsynaptic responses displayed little variation in amplitude at three different levels of stimulation (**Figure 4.6B**). For the experiment described in Figure 4.6, the coefficient of variation was 6% at a stimulus strength that evoked a -50 pA response, 3% for a stimulus strength that evoked

a -150 pA response, and 2% for a stimulus strength that evoked a -325 pA response. The variability in the postsynaptic response to a fixed concentration of glutamate was far less than that observed for spontaneous EPSCs in the same fiber (**Figure 4.6A, C**). These results argue that variations in cleft glutamate concentration are largely responsible for the observed variation in spontaneous EPSC amplitudes.

A fundamental question in synaptic physiology is whether postsynaptic receptors are saturated by the neurotransmitter released from a single vesicle; if this is the case, multiquantal release fails to convey any information beyond that of a single-vesicle fusion event. To test this directly, increasing concentrations of glutamate were iontophoretically applied to postsynaptic terminals. The peak amplitude of the evoked postsynaptic response increased with that of the stimulus until it reached a plateau (**Figure 4.7A,B**). For the fiber described in **Figure 4.7,** the response saturated at -291±12 pA. Importantly, this current amplitude was nearly 2-fold larger than the largest spontaneous EPSCs recorded in the same fiber (**Figure 4.7C**). The maximal evoked postsynaptic current was similar for two other fiber recordings. For three fibers, the maximal current amplitude was -302±18 pA. These data indicate that, under normal physiological conditions, postsynaptic receptors are not saturated by presynaptic exocytosis. For the range of spontaneous EPSCs typically observed in control recordings, approximately linear summation of the postsynaptic current is expected.

Effect of extracellular Mg^{2+}

In an effort to reveal quantal components in the putatively multiquantal events, I attempted to reduce the influx of Ca^{2+}, the presumed trigger for exocytosis, by increasing

the extracellular concentration of Mg^{2+}. At the neuromuscular junction, the effects of Ca^{2+} and Mg^{2+} are mutually antagonistic: increasing Mg^{2+} reduces the efficacy of synaptic transmission, but responsiveness may be rescued by a compensatory increase in Ca^{2+}. Increased Mg^{2+} in the presence of normal Ca^{2+} lowers the probability of transmitter release and may thus reveal underlying quantal events (Castillo and Engbaek, 1954; Castillo and Katz, 1954). The addition of 12 mM or 25 mM Mg^{2+} decreased the mean amplitude of spontaneous EPSCs in four experiments (**Figure 4.8A**). However, Mg^{2+} had no significant effect on the coefficient of variation of the EPSC amplitude or the rate of EPSC occurrence (**Figure 4.8B,C**). To determine whether the drop in EPSC amplitude was due to a decrease in presynaptic release or postsynaptic sensitivity, the postsynaptic response to iontophoresed glutamate was recorded in the absence and presence of 25 mM Mg^{2+}. High extracellular Mg^{2+} reduced the amplitude of the evoked postsynaptic response (**Figure 4.8D**) to an extent comparable to that of the spontaneous EPSCs (**Figure 4.8A**). These results suggest that the principle effect of increased extracellular Mg^{2+} in this system is an inhibition of postsynaptic receptor responsiveness, rather than a decrease in presynaptic release probability. Interestingly, Mg^{2+} has been shown to decrease the sensitivity of the postsynaptic terminal and to have no effect on the frequency of spontaneous discharge at the neuromuscular junction as well as several central synapses (Ault *et al*., 1980; Castillo and Engbaek, 1954; Castillo and Katz, 1954).

Effect of hair-cell hyperpolarization

In a separate attempt to demonstrate quantal components underlying release events, spontaneous EPSCs were compared before and after lowering the membrane potential of

the hair cell from its resting level of about -50 mV to -80 mV. Hyperpolarizing a hair cell reduced the frequency of EPSCs and selectively eliminated large events (**Figure 4.9**). The EPSC amplitude during hyperpolarization of 6 hair cells fell to a mean value of -56±16 pA for a fiber holding potential of -90 mV. In the 5 recordings with sufficient events for analysis, the coefficient of variation (CV) averaged 0.29, a value similar to that obtained for miniature EPSCs at both the neuromuscular junction and central synapses (Del Castillo and Katz, 1954; Forti *et al.*, 1997; Crowley *et al.*, 2007). To determine the corresponding value for the postsynaptic charge transfer, the integrals of EPSCs recorded during hair-cell hyperpolarization were calculated. Because the waveforms of EPSCs do not vary with amplitude, the charge-transfer distribution displayed a similar Gaussian profile with a mean value of -50.2±2.8 fC.

Presynaptic capacitance measurements

During exocytosis, incorporation of vesicular membrane into the plasma membrane transiently increases the capacitance of secretory cells (Neher and Marty, 1982; Angleson and Betz, 1997). Thus, the change in membrane capacitance upon presynaptic stimulation is a useful metric for the extent of synaptic vesicle fusion. In collaboration with Genglin Li (The Vollum Institute, Oregon Health & Science Univ.), I estimated the rate of vesicle fusion during exocytosis by depolarizing a hair cell from a potential of -90 mV to -30 mV and measuring the change in membrane capacitance. The presynaptic Ca^{2+} current, which had characteristics of L-type Ca^{2+} currents, was recorded simultaneously.

At the holding potential of -90 mV, 15 hair cells from the bullfrog's amphibian papilla displayed an average capacitance of 11.6±1.5 pF. A 500-ms depolarization increased their capacitance by 99±39 fF. Because neither the series resistance nor the membrane resistance changed after the depolarization, the capacitance measurement was devoid of conductance artifacts (**Figure 4.10A**). The capacitance change increased monotonically for hair-cell depolarizations ranging from 10 ms to 1000 ms (**Figure 4.10B**). Because the capacitance returned to its baseline value with an exponential time constant of approximately 11 s (data not shown), capacitance measurements made within 500 ms of the depolarizing pulse should not be significantly contaminated by membrane retrieval.

Paired pre- and postsynaptic recordings

Simultaneous recordings from a hair cell and its innervating fiber permitted correlation of the rate of vesicle fusion, as manifested by a change in the presynaptic capacitance, with the rate of transmitter release, as measured by an evoked postsynaptic current. All paired recordings were performed by Genglin Li at The Vollum Institute.

Presynaptic depolarizations that produced robust capacitance changes also resulted in large postsynaptic responses with highly overlapping events (**Figure 4.11A**). Therefore, the cumulative postsynaptic charge transfer, or integral of the postsynaptic current, was used as the measure of the postsynaptic response. During a sustained depolarization, the postsynaptic charge transfer first rose briskly, then continued to increase at a lower, linear rate (**Figure 4.11B**). Averaged over 11 recordings, the kinetics of the postsynaptic response accorded with that of the average presynaptic capacitance

increase in six hair cells. These results are consistent with exocytosis from a readily releasable pool of vesicles followed by a reserve pool (Moser and Beutner, 2000; Spassova et al., 2004; Johnson et al., 2005; Schnee et al., 2005; Rutherford and Roberts, 2008). This close agreement between postsynaptic charge transfer and capacitance increases suggests that neither desensitization nor saturation of AMPA receptors occurs to a significant degree at this synapse.

The postsynaptic charge transfer increased concomitantly with the presynaptic capacitance (**Figure 4.11C**); the relation was approximately linear. For a total of 22 depolarizations in 7 cell pairs, the slope of the relation was -1.01 ± 0.07 $kC \cdot F^{-1}$. As discussed below, this value can be used to obtain an independent estimate of the quantal response.

Electron microscopy and the capacitance of a single vesicle

To estimate the capacitance change expected from fusion of a single synaptic vesicle, electron microscopy was conducted on hair cells in the region of the amphibian papilla from which the physiological results originated. At 23 ribbon-type active zones, A. James Hudspeth measured the dimensions of 119 vesicles whose perimeters were bounded completely by trilaminar membrane, and which therefore lay largely or entirely within the 70-nm sections. The geometric mean of the greatest and least diameters, measured at the center of the trilaminar structure, was 37.6±4.5 nm; the arithmetic mean was 37.8±4.5 nm. The amplitude distribution was well fit by a Gaussian function with a mean value of 40.3 nm (**Figure 4.12**). Assuming a standard specific membrane capacitance of 10 $mF \cdot m^{-2}$ we obtain a best estimate of the single-vesicle capacitance of 45.0±10.6 aF.

Emergence of putatively quantal events

In control solution, EPSCs of approximately -50 pA were rarely observed; rather, amplitude distributions were normally distributed around a modal amplitude two to three times as large as that of EPSCs recorded during hair-cell hyperpolarization (**Figure 4.13A1**). Certain experimental manipulations, however, led to the emergence of a distinct secondary peak with a modal amplitude of approximately -50 pA.

The combination of BayK 8644, an activator of L-type Ca^{2+} channels, and a reduction in the extracellular Ca^{2+} concentration produced a secondary peak in the amplitude histogram (**Figure 4.13A2**). A secondary peak emerged in the histogram of another fiber after ~20 minutes of recording (**Figure 4.13B**). When a third preparation was placed in a nominally zero-Ca^{2+} solution and provided with low levels of Ca^{2+} by iontophoresis, a small secondary peak in the amplitude histogram again became apparent (**Figure 4.13C**). Importantly, the kinetics of events in the secondary peaks was similar to, or faster than, those of the events in the larger, primary peaks; small events, therefore, are not likely to represent large EPSCs recorded from a distant synapse. Furthermore, the modal amplitude of the secondary peak in each of the experiments was roughly -50 pA, the size of the putatively quantal response.

Effect of Ca^{2+} channel inhibition

Release of neurotransmitter from the hair cell depends on Ca^{2+} influx through L-type, voltage-gated channels in the plasma membrane (Robertson and Paki, 2002; Keen and Hudspeth, 2006). To examine the effect of reducing the number of functional Ca^{2+}

channels on the amplitude and frequency of spontaneous EPSCs, nifedipine or Cd^{2+} was used to block the channels. Although both reagents caused a precipitous decline in the frequency of spontaneous EPSCs within one minute, the average amplitude of those EPSCs was reduced to a lesser extent and occasionally unchanged (**Figure 4.14**). In fact, only after several minutes in a reduced-Ca^{2+} state do the amplitudes of infrequent spontaneous EPSCs approach the quantal size of -50 pA (data not shown).

If large EPSCs represent the simultaneous fusion of independent vesicles in response to the synchronous openings of multiple Ca^{2+} channels, a reduction in release probability should lead to a corresponding decrease in EPSC amplitude (Fatt and Katz, 1952; del Castillo and Katz, 1954b). However, these results suggest that a mechanism incorporating cooperativity between vesicles fusing in a coincident, sequential, or compound manner underlies the generation of large EPSCs. Experimental evidence in favor of compound (homotypic) fusion of synaptic vesicles is discussed in Chapter Five.

Anomalous kinetic behavior of EPSCs

Although most spontaneous events possessed fast kinetics that were independent of amplitude, uncharacteristically slow EPSCs were also observed in several recordings when the presynaptic Ca^{2+} influx was reduced. Inhibition of Ca^{2+} channels with nifedipine sometimes led to the appearance of small EPSCs with distinctly slower rise times than those in control solution (**Figure 4.15A-C**). Similar results were observed in another preparation when placed in a nominally Ca^{2+}-free solution (**Figure 4.15D, E**). Large, fast events thus appear to be more sensitive to a reduction in extracellular Ca^{2+} influx than slow events in these recordings. Similar changes in the kinetics of

postsynaptic signals have also been observed in the cerebellum upon removal of extracellular Ca^{2+} (Llano *et al*., 2000). The emergence of slow EPSCs under conditions that deplete the active-zone Ca^{2+} concentration may be the postsynaptic representation of protracted glutamate release through slowly opening fusion pores, as intracellular Ca^{2+} has been shown to regulate the rate of pore expansion (Pawlu *et al*., 2004; Scepek *et al*., 1998).

Effect of manipulating Ca^{2+} stores

The predominance of putatively multiquantal EPSCs suggested that a Ca^{2+} signal more expansive than that arising from a plasma-membrane Ca^{2+} channel might be required to synchronize the fusion of multiple vesicles. Ca^{2+} released from internal stores through high-conductance, cooperatively gating channels (Marx *et al*., 1998; Marx *et al*., 2001) could hypothetically coordinate the fusion of several vesicles and thus underlie the generation of large multiquantal events, as has been indicated at several central synapses (Llano *et al*., 2000; Sharma *et al*., 2008). To test whether store Ca^{2+} is involved in exocytosis at the hair-cell synapse, I employed pharmacological agents meant either to reduce or enhance the efflux of Ca^{2+} from stores. Ryanodine, an inhibitor of receptors that regulate store Ca^{2+} release, neither eliminated large EPSCs nor significantly reduced their frequency (**Figure 4.16A, B**). To test whether Ca^{2+} from internal stores could elicit exocytosis independent of extracellular Ca^{2+} influx, preparations were placed in a zero-Ca^{2+}/EGTA solution and then challenged with agents that induce Ca^{2+} efflux from internal stores (Mahmoud and Fewtrell, 2001; Yoshida and Plant, 1992). In six experiments in which the remaining free Ca^{2+} concentration was estimated to be less than

100 nM, store Ca^{2+}-releasing agents failed to restore exocytosis (**Figure 4.16C**). These results suggest that Ca^{2+} from internal stores is neither necessary nor sufficient for the generation of putatively multiquantal EPSCs at this synapse.

Discussion

The unitary charge transfer

The large variation in the amplitudes of EPSCs at the synapses of the central nervous system and sensory organs suggests that neurotransmitter can be released in amounts corresponding to multiple quanta. However, because it is difficult to determine the response owing to transmitter release from a single vesicle—the unitary or quantal event —it is usually impossible to ascertain how many vesicles contribute to a multiquantal response. Under ordinary recording conditions, amplitude histograms of spontaneous EPSCs at hair-cell synapses show no substructure indicative of independently fusing vesicles. However, the effects of hyperpolarization (**Figure 4.9**) and of alterations in the extent of presynaptic Ca^{2+} influx (**Figure 4.13**) suggest that these synapses can release transmitter in smaller quantities that yield postsynaptic events about -50 fC in charge or -55 pA in amplitude; such events may represent the response to single-vesicle fusion events. The paired recordings (performed by Genglin Li using the system developed and characterized in Chapter Two), which relate the postsynaptic response to the presynaptic capacitance change, buttress this conclusion by providing an independent estimate of the unitary charge transfer.

The mean postsynaptic charge transfer q associated with the release of transmitter from a single fused vesicle generates a corresponding increase in the presynaptic

membrane's capacitance by an amount c. If depolarization of a hair cell causes an increase C in the presynaptic membrane capacitance and evokes a postsynaptic response with a total charge transfer Q, then

$$\frac{q}{c} = \left(\frac{P}{R}\right)\frac{Q}{C} \text{ or } q = \left(\frac{\pi d^2 \mathsf{C} P}{R}\right)\frac{Q}{C}.$$

Here P is the probability that a fusion event occurs at a presynaptic active zone and can be sensed by the postsynaptic receptors and R is the innervation ratio of afferent fibers per stimulated hair cell. The fusion of a single vesicle increases the presynaptic capacitance by an amount $c = \pi d^2 \mathsf{C}$, in which d is the diameter of a vesicle and C is the specific capacitance of the vesicle membrane; our electron-microscopic results suggest that c = 45-50 aF. If $P = R = 1$, then the value of Q/C = -1.01 kC·F^{-1} adduced from our physiological measurements implies that q = -50 fC, a value in good agreement with that obtained from histograms of the postsynaptic charge transfer during hair-cell hyperpolarization (-50.2±2.8 fC).

This analysis relies upon three important assumptions. First, most synaptic vesicles are released at presynaptic active zones, so that $P \approx 1$. For hair cells isolated from the bullfrog's sacculus, though, some ectopic exocytosis may take place (Zenisek *et al.*, 2003; Lenzi et al., 2002). If this also occurs in hair cells of the amphibian papilla, the value of P might be less than unity. It is also possible that some afferent fibers are torn from hair cells during the dissection, again with the consequence of a lower value for P. The second assumption is that each depolarized hair cell contacts only the single afferent fiber involved in a simultaneous recording, so that the innervation ratio $R \approx 1$. Several

lines of evidence support the contention that each afferent fiber receives input from but a single hair cell; in particular, holding the hair cell in a paired recording at a potential of -80 mV nearly abolishes postsynaptic activity. It is less certain, however, that each hair cell synapses with only a single afferent fiber; if this is not the case, R might exceed unity. Finally, the specific capacitance of the synaptic-vesicle membrane is assumed to be similar to that for other biological membranes, so that $C \approx 10\ \mathrm{mF \cdot m^{-2}}$ (Fettiplace et al., 1971). However, because each vesicle contains a high density of transmembrane proteins (Takamori *et al.*, 2006), the true value of C might be smaller. Remarkably enough, the uncertainties associated with these assumptions make contributions in the same direction to the estimate of q: the consequence would be that some of the measured change in presynaptic capacitance would not be associated with a postsynaptic response. As a result, the true value of q—and thus the amplitude of the unitary postsynaptic current—could only be *larger* than suggested by our calculation. Therefore, the actual value of q is unlikely to be *smaller* than we calculate, eliminating the greatest problem in most estimates of the magnitude of unitary events: that quantal events are so small that they are buried in the noise of a recording.

Two further reservations deserve mention. First, no correction was made in the estimate of the vesicle diameter d for distortion produced by electron-microscopic preparation. In some instances, fixation, dehydration, and embedding inflict a shrinkage artifact of roughly 20% (Tatsuoka and Reese, 1989). However, recent high pressure-quick frozen cryo-electron microscopy, a technique in which no such artifact is expected, reports a brain synaptic vesicle diameter of 33 nm (Takamori *et al.*, 2006). Second, the release of transmitter by a kiss-and-run mechanism might artifactually lower the estimate

of the capacitance increase associated with a postsynaptic response. However, optical measurements from isolated bipolar cells suggest that release usually involves the complete fusion of vesicles with the presynaptic membrane (Zenisek *et al.*, 2002).

Number of AMPA receptors activated by one vesicle fusion

The estimate of about -55 pA for the unitary response is reasonable in the light of other information about the ribbon synapses of hair cells. At the -90 mV holding potential of afferent fibers, this quantal size corresponds to a postsynaptic conductance of about 600 pS. If each AMPA receptor at the ribbon synapse in the bullfrog's amphibian papilla has a conductance of about 20 pS (Parks, 2000; Sahara and Takahashi, 2001), the unitary response involves the gating of approximately 30 receptors. The largest putatively multiquantal responses, with magnitudes near -300 pA, would correspond to the activation of about 150 receptors. Freeze-fracture electron microscopy indicates that the postsynaptic membrane of afferent synapses in the mammalian cochlea is studded with large intramembrane particles thought to be AMPA receptors at a density of 3000 μm^{-2} (Saito, 1990). The afferent terminals at the ribbon synapse of the sacculus, another receptor organ of the bullfrog's internal ear, display particles of a similar density (Jacobs and Hudspeth, 1990). In the region of the amphibian papilla under investigation, the postsynaptic membrane specialization at each ribbon synapse is about 150 nm across and 250 nm in length (Simmons *et al.*, 1995; Keen and Hudspeth, 2006). If the membrane at this synapse holds AMPA receptors at the density observed by freeze-fracture electron microscopy, there are about 110 such receptors directly opposing each presynaptic active

zone. The agreement between this value and that obtained for the maximal receptor activation provides further support for our estimate of the unitary response.

Nonsaturation and variability in the postsynaptic response

Because the number of glutamate molecules in a synaptic vesicle exceeds the number of postsynaptic receptors and because the volume of the synaptic cleft is small, it has been thought that the glutamate released from a single vesicle tends to saturate postsynaptic receptors (Burger *et al.*, 1989; Clements *et al.*, 1992). But if multiquantal release is to transfer any information above that conveyed by the release from single vesicles, postsynaptic receptors must not be saturated by physiological levels of neurotransmitter release. Focal stimulation experiments in other systems have shown that AMPA receptors may not be saturated during normal synaptic transmission (Liu *et al.*, 1999; McAllister and Stevens, 2000). The results of similar experiments at the hair-cell synapse demonstrate that postsynaptic receptors are generally far from saturation and that they reliably report the concentration of neurotransmitter with which they are presented (**Figure 4.6, 4.7**). Therefore, the postsynaptic fiber may faithfully encode any information represented by the size of presynaptic exocytotic events.

Multiquantal EPSCs from a single active zone

Because afferent fibers in the amphibian papilla form several synapses onto a single hair cell, large EPSCs could in principle represent the simultaneous fusion of single vesicles at different synaptic ribbon sites. However, the results of Ca^{2+} iontophoresis experiments demonstrate that large EPSCs may arise from a putative single active zone (**Figure 4.3,**

4.4). Furthermore, statistical arguments suggest that the probability of independent vesicles fusing simultaneously at the rates observed in this system is exceedingly low—on the order of 10^{-160} (courtesy of Daniel Andor). Rather, some degree of cooperativity between vesicles at a single active zone is required to produce the multiquantal EPSCs observed at this synapse.

Multiquantal EPSCs independent of internal Ca^{2+} stores

The direct involvement of internal stores in transmitter release is unresolved, although several studies suggest that presynaptic Ca^{2+}-induced Ca^{2+} release (CICR) can modulate neurotransmitter release. Ca^{2+} from internal stores has been implicated in the generation of multiquantal events at central synapses in the absence of external Ca^{2+} (Llano *et al.*, 2000) and has been thought to play a role in spontaneous and evoked release at several ribbon synapses (Kennedy and Meech, 2002; Krizaj *et al.*, 1999; Suryanarayanan and Slaughter, 2006). Furthermore, mammalian hair cells express ryanodine receptors near their presynaptic active zones (Beurg *et al.*, 2005). Amplification of the Ca^{2+} signal from plasma-membrane channels by the tightly-coupled release of store Ca^{2+} seems advantageous for a system that seeks to enhance its sensitivity to small stimuli. I cannot exclude the possibility that store Ca^{2+} contributes to the steady-state level of Ca^{2+} at the active zone, thus enhancing the probability of vesicle fusion events. Although unlikely, I also cannot rule out the possibility that Ca^{2+} stores emptied rapidly in the absence of external Ca^{2+}, thus rendering the Ca^{2+} ionophore ineffective. However, the results presented here suggest that Ca^{2+} from internal stores is neither required for the generation of multiquantal events nor sufficient to elicit exocytosis at the hair-cell synapse.

Coincident, compound, and sequential exocytosis

The results described in this chapter demonstrate the occurrence in afferent fibers of unitary events about -55 pA in amplitude. Whether recorded as spontaneous EPSCs or as components of evoked EPSCs, larger postsynaptic signals should therefore represent the summation of several such unitary events. The usual response of about -130 pA implies the release of transmitter equivalent to two or three quanta; the largest events, about -300 pA in magnitude, correspond to the synchronous exocytosis of five or six quanta. Because no temporal substructure has been detected in the waveforms of large events, we do not have evidence that they arise from independent vesicle fusions. Thus, we cannot distinguish among three candidate mechanisms for the production of large signals: highly synchronous, perhaps cooperative fusion at distinct docking sites; compound fusion, in which several vesicles prefuse with each other prior to undergoing exocytosis at a single site; and sequential fusion, in which exocytosis by one docked vesicle initiates the rapid, piggyback fusion of several additional ones on the ribbon's surface (**Figure 1.2**). It is also formally possible that the amount of transmitter contained in a single vesicle is variable, perhaps subject to endogenous regulation (Wu *et al.*, 2007). If this were the situation at the hair-cell synapse, large EPSCs could arise from effectively multiquantal, but nonetheless univesicular, fusion events.

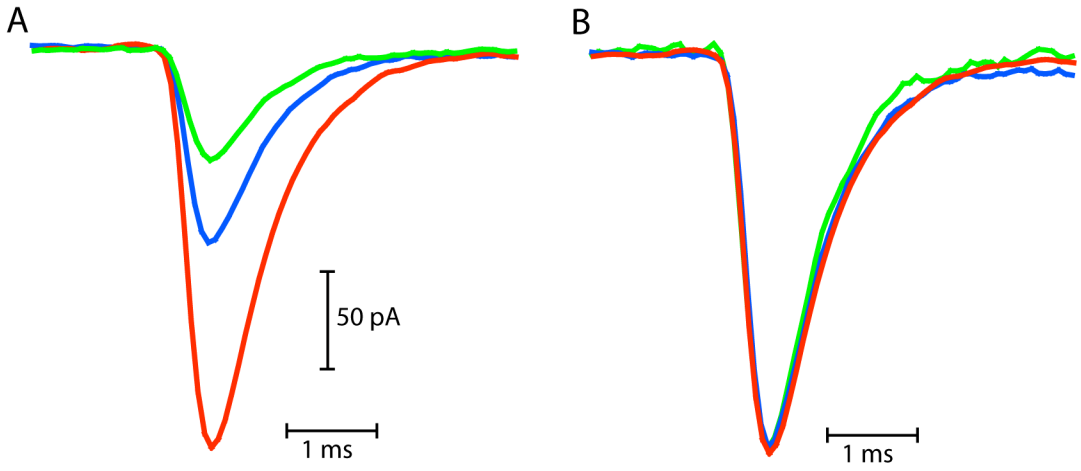
A
50 pA
1 ms
B
1 ms

Figure 4.1

Amplitude-independent kinetics of spontaneous EPSCs

(**A**) Averages of 20 EPSCs with amplitudes of -50 ± 3 pA (green), -100 ± 3 pA (blue), and -200 ± 3 pA (red) show that events of these different size classes possess smooth rise and decay phases. (**B**) Normalization of the three groups of EPSCs in **A** reveals that they display similar kinetics. Traces in panels **A** and **B** are from the same postsynaptic recording, during which the afferent fiber was held at -90 mV. A single-exponential fit to the decay phase of the -100 pA group yielded a decay time constant of 0.57 ms.

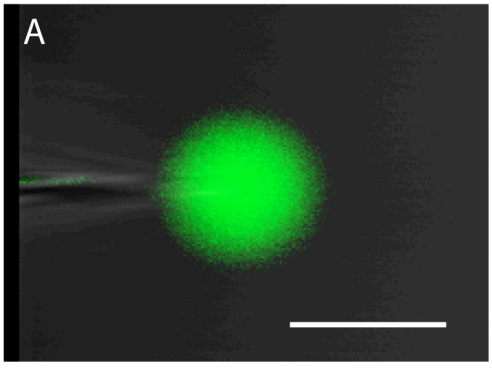
A

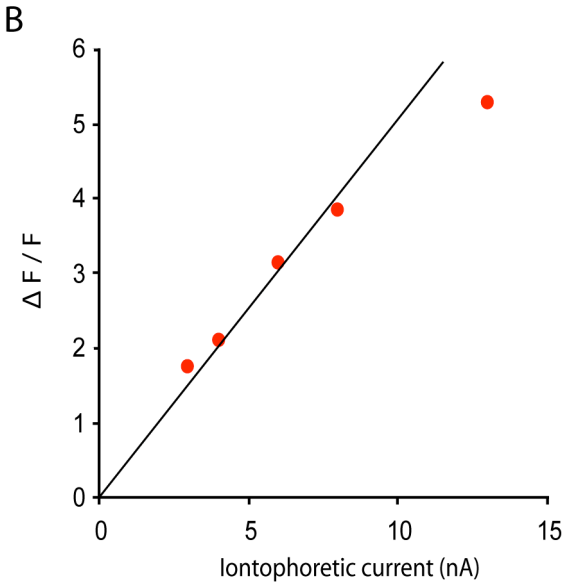
B
6
5
4
3
2
1
0
Δ F / F
0
5
10
15
Iontophoretic current (nA)

Figure 4.2

Spatially localized iontophoresis of Ca^{2+}

(**A**) A compressed confocal z-stack displays the extent of Ca^{2+} diffusion from the iontophoretic pipette during the application of a constant 3-nA ejection current. The pipette was filled with 0.5 mM $CaCl_2$ and the bath solution contained 0 Ca^{2+}/100 μM EGTA and 90 μM fluo-3. Note the spherical symmetry of the signal, which demonstrates that bulk fluid flow does not occur during iontophoretic stimulation. Scale bar: 5 μm. (**B**) A linear relation between ejection current and fluo-3 signal is observed over the range of stimuli used in physiological experiments. The change in fluorescence was calculated by subtracting the baseline fluorescence from the average peak fluorescence during the ejection period.

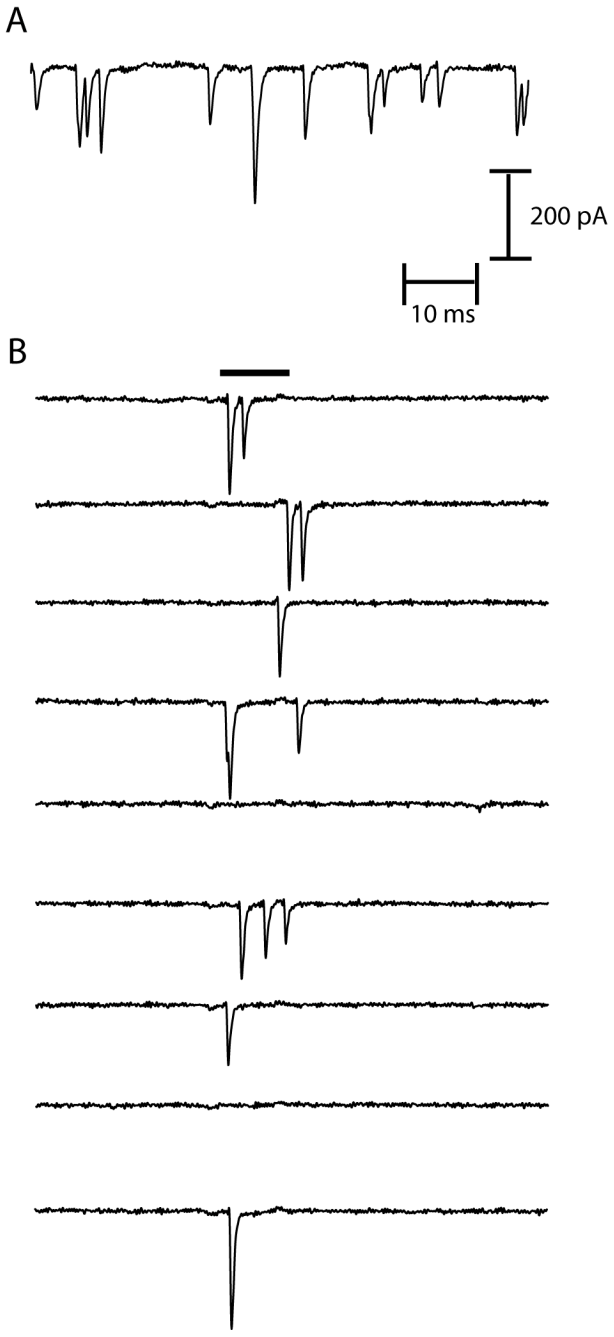
A
200 pA
10 ms
B

Figure 4.3

Large EPSCs from a single presynaptic active zone

(**A**) Under control recording conditions, spontaneous EPSCs in an afferent fiber display a wide range of amplitudes. (**B**) When the preparation is bathed in a zero-Ca^{2+} solution, spontaneous events are suppressed. A 10-ms iontophoretic pulse of Ca^{2+} (black bar) onto a putative single active zone elicits EPSCs as large as those recorded from the same fiber in control solution. A 3-nA ejection current was applied from a holding current of -2 nA. Presentations of Ca^{2+} were separated by a 1-second rest period. Failures to evoke EPSCs occurred for 33% of the iontophoretic stimuli in this experiment.

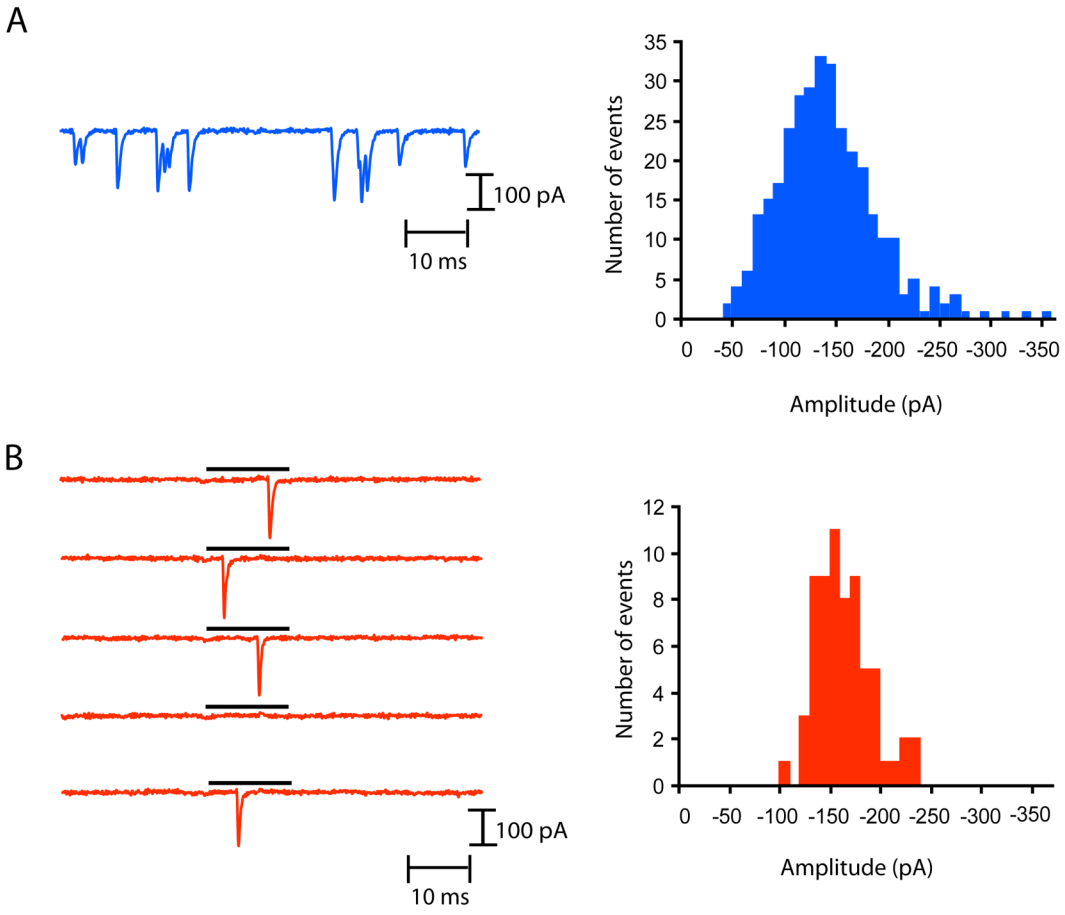
A
100 pA
10 ms
Number of events
35
30
25
20
15
10
5
0
0 -50 -100 -150 -200 -250 -300 -350
Amplitude (pA)
B
100 pA
10 ms
Number of events
12
10
8
6
4
2
0
0 -50 -100 -150 -200 -250 -300 -350
Amplitude (pA)

Figure 4.4

Large EPSCs elicited selectively with minimal iontophoretic stimulation

(**A**) Under control recording conditions, spontaneous EPSCs in an afferent fiber display a wide range of amplitudes (*Left*). The amplitude distribution of 323 spontaneous EPSCs (*Right*) has a mean value of -132±48 pA and a coefficient of variation of 36%. (**B**) When the preparation is bathed in a zero-Ca^{2+} solution, spontaneous events are suppressed (*Left*). Multiple trials of a 10-ms, 3-nA iontophoretic pulse of Ca^{2+} (black bar) onto a putative single active zone elicit single EPSCs of relatively constant amplitude. The amplitude distribution of 66 evoked EPSCs (*Right*) has a mean value of -155±27 pA and a coefficient of variation of 18%. Data were taken from 80 stimulus presentations; the rate of failure to elicit EPSCs was 18% in this experiment. An estimated Ca^{2+} concentration of 200 μM was delivered at the peak of the iontophoretic pulse.

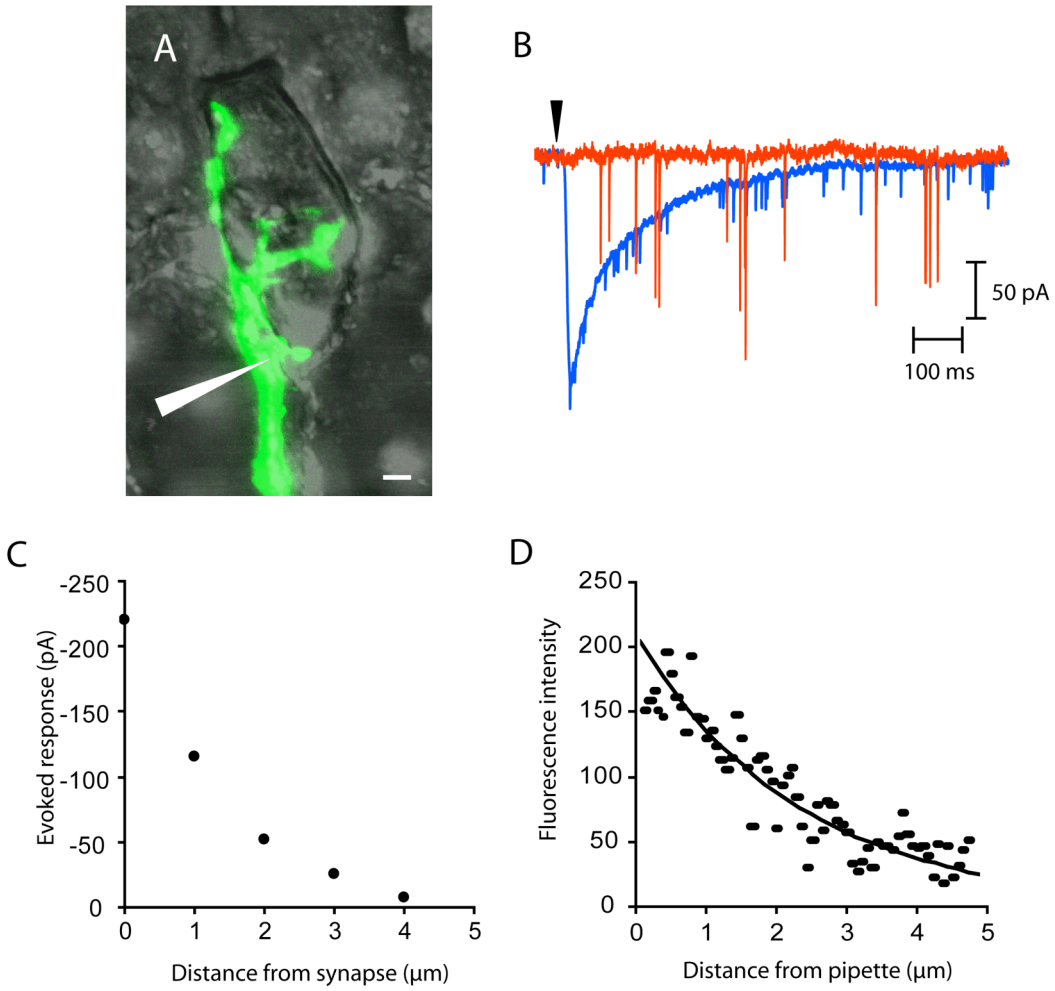
A
B
50 pA
100 ms
C
Evoked response (pA)
-250
-200
-150
-100
-50
0
0
1
2
3
4
5
Distance from synapse (µm)
D
Fluorescence intensity
250
200
150
100
50
0
0
1
2
3
4
5
Distance from pipette (µm)

Figure 4.5

Spatially localized iontophoresis of glutamate

(**A**) A confocal z-stack with the corresponding transmitted light image displays an afferent fiber labeled with 50 μM Alexa 488 during whole-cell recording. Multiple terminals extend onto the innervated hair cell. The arrowhead depicts the location of the glutamate-filled iontophoretic pipette. Postsynaptic currents evoked by iontophoretic stimuli were recorded at a fiber holding potential of -90 mV. Scale bar, 2 μm. (**B**) A 10-ms, 15-nA negative current (blue) evokes a robust postsynaptic current, but a positive current (red) elicits no response. The arrowhead denotes the onset of the iontophoretic stimulus. The latency to the postsynaptic response likely reflects the relative depletion of glutamate at the tip induced by a 10-nA holding current. (**C**) The evoked postsynaptic response recorded from the afferent fiber in **A** decays as the iontophoretic pipette tip is displaced laterally from the synapse. (**D**) The fluorescence of Oregon Green, a compound with transfer properties similar to those of L-glutamate, decays with distance from the tip of the pipette. The iontophoretic pipette was filled with 5 mM Oregon Green and imaged by confocal microscopy using a line-scan protocol. Note the comparable spatial scales in panels **C** and **D**.

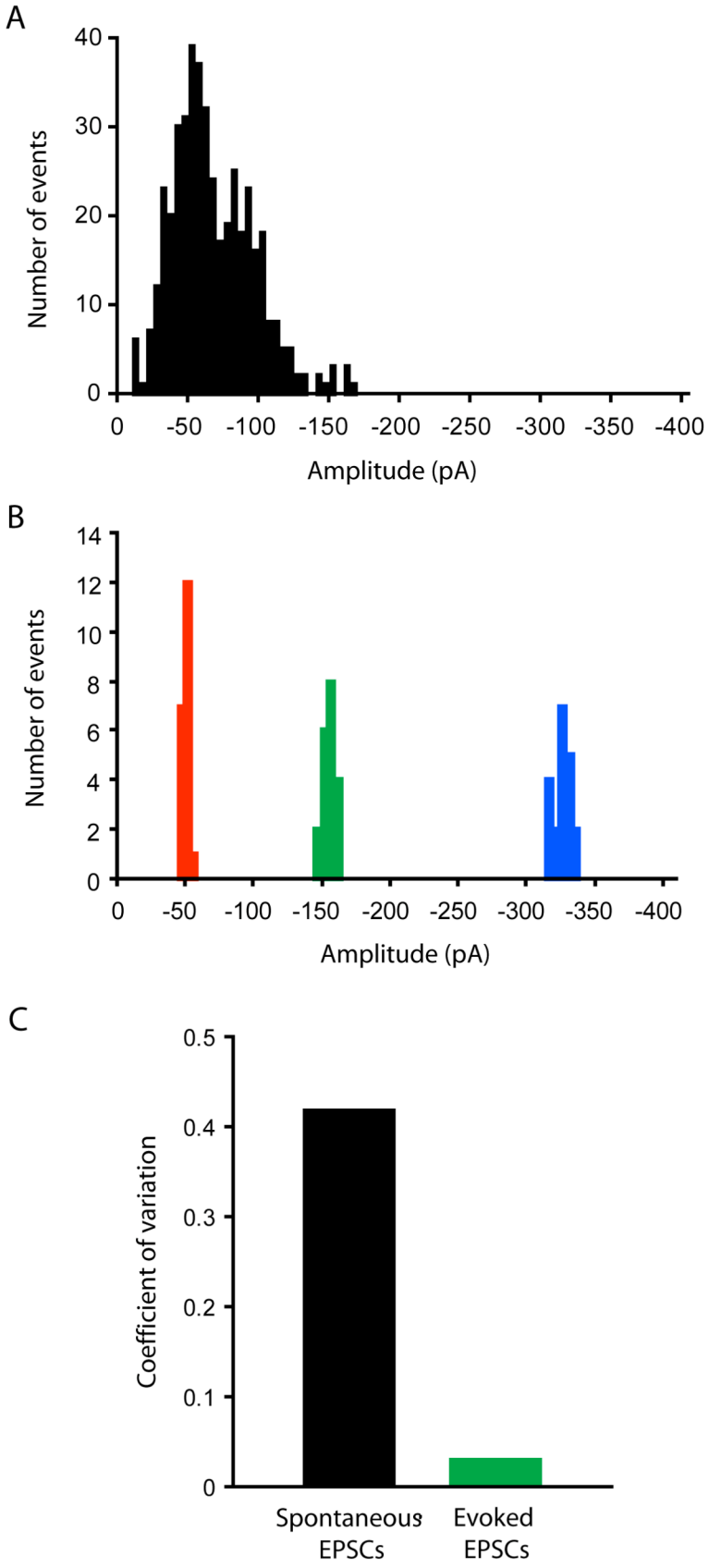
A
40
30
20
10
0
Number of events
0
-50
-100
-150
-200
-250
-300
-350
-400
Amplitude (pA)
B
14
12
10
8
6
4
2
0
Number of events
0
-50
-100
-150
-200
-250
-300
-350
-400
Amplitude (pA)
C
0.5
0.4
0.3
0.2
0.1
0
Coefficient of variation
Spontaneous EPSCs
Evoked EPSCs

Figure 4.6

Postsynaptic response to constant glutamate concentration

(**A**) Spontaneous EPSCs in an afferent fiber display a range of amplitudes. (**B**) Postsynaptic currents evoked by repeated application of a constant glutamate concentration in the same fiber show a tight distribution of amplitudes at low (red), medium (green), and high (blue) levels of stimulation. Glutamate was applied from an iontophoretic pipette using 10-ms pulses for 20 repetitions at 500-ms intervals. (**C**) The coefficient of variation of spontaneous EPSC amplitudes (42%) is an order of magnitude larger than that of postsynaptic currents elicited by a constant glutamate concentration (3%) in the same fiber.

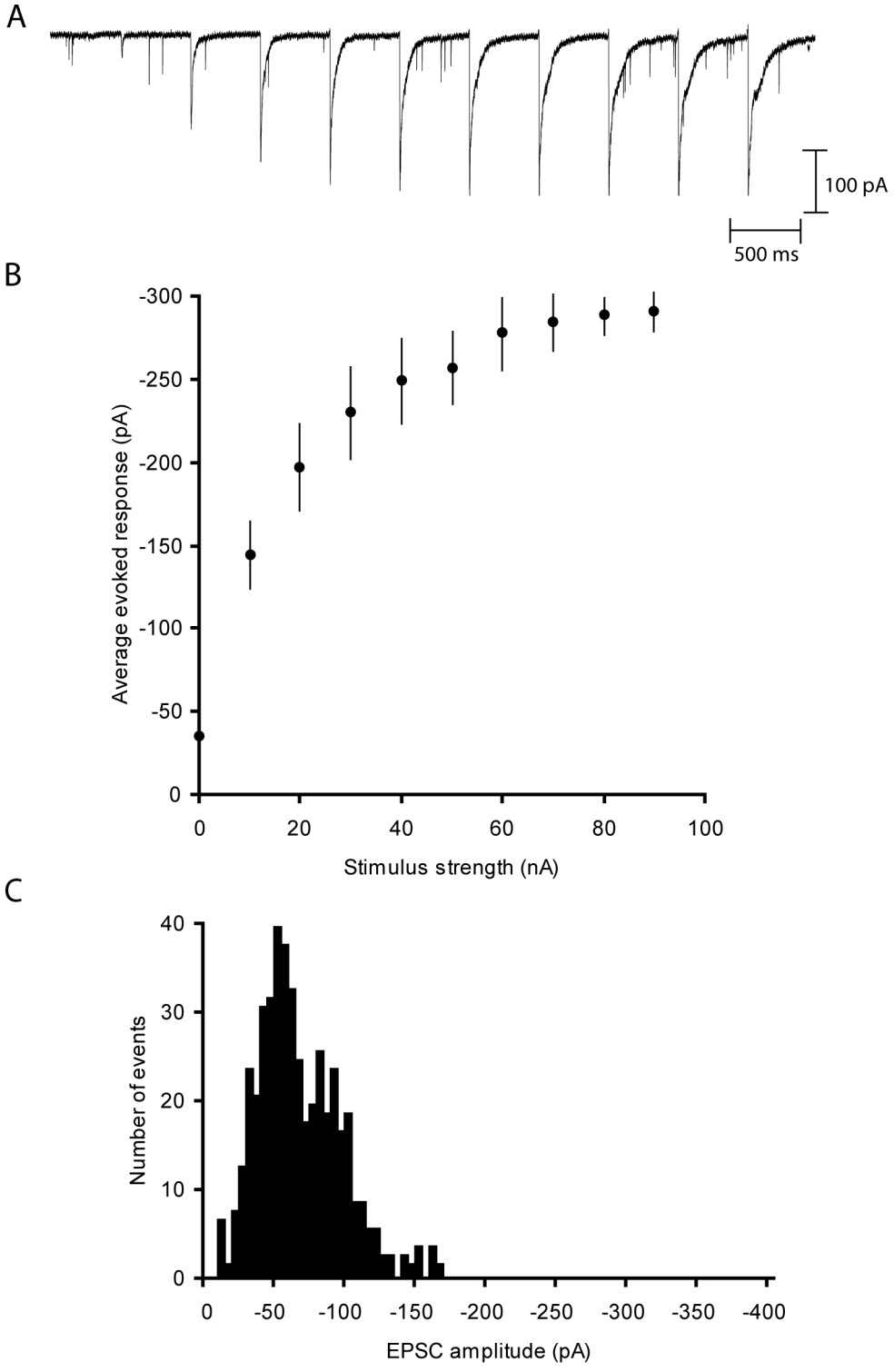
A
100 pA
500 ms
B
Average evoked response (pA)
-300
-250
-200
-150
-100
-50
0
0
20
40
60
80
100
Stimulus strength (nA)
C
Number of events
40
30
20
10
0
0
-50
-100
-150
-200
-250
-300
-350
-400
EPSC amplitude (pA)

Figure 4.7

Postsynaptic dose-response relation to glutamate

(**A**) Evoked postsynaptic currents saturate in response to iontophoretic pulses of increasing concentrations of glutamate. Data shown are from a single trial during which glutamate was applied iontophoretically with a 20-ms current ranging from 0 to -90 nA in 10 nA steps. The afferent fiber was held at a potential of -90 mV. (**B**) The dose-response relationship between glutamate concentration and postsynaptic response saturates near 300 pA in the same fiber. Data were obtained from 3 trials of the stimulation protocol described in (**A**). The maximal amplitude was -291±12 pA. (**C**) The amplitude distribution of spontaneous EPSCs recorded in the same fiber reveals that most events are far from saturating postsynaptic receptors. The mean amplitude of 429 spontaneous EPSCs in this afferent fiber was -68±30 pA.

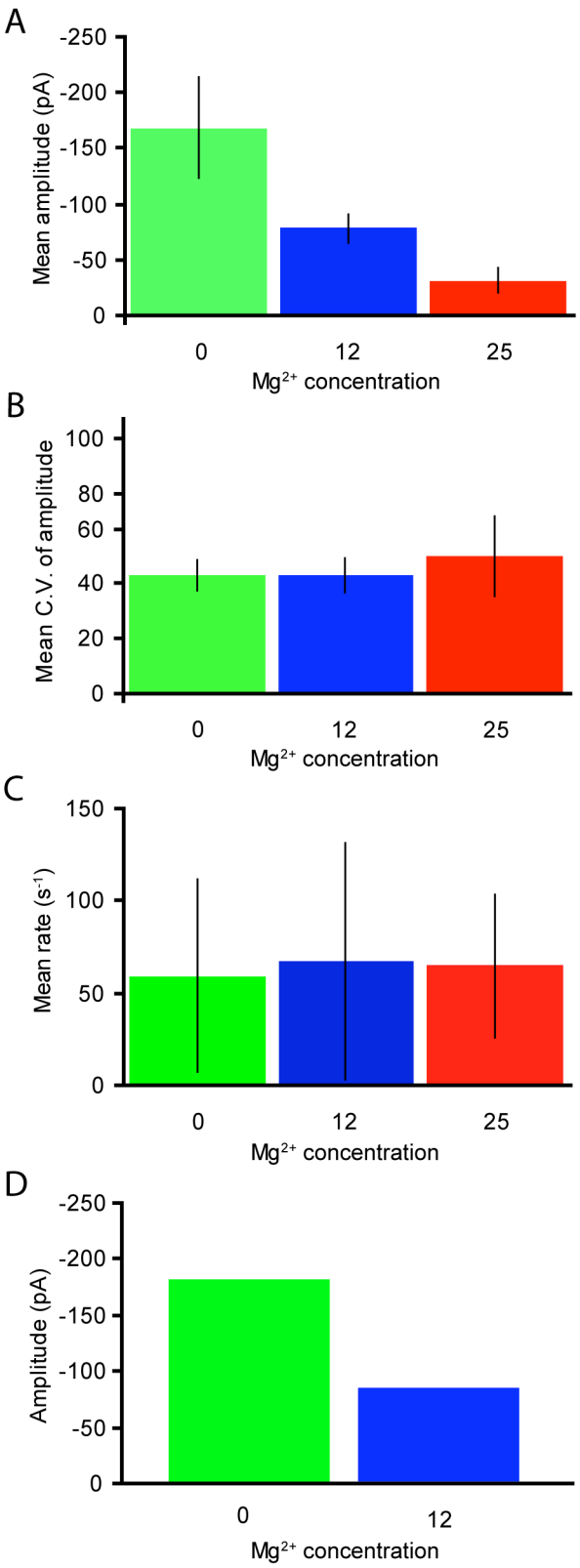
A
-250
-200
-150
-100
-50
0
Mean amplitude (pA)
0
12
25
Mg2+ concentration
B
100
80
60
40
20
0
Mean C.V. of amplitude
0
12
25
Mg2+ concentration
C
150
100
50
0
Mean rate (s-1)
0
12
25
Mg2+ concentration
D
-250
-200
-150
-100
-50
0
Amplitude (pA)
0
12
Mg2+ concentration

Figure 4.8

Effect of extracellular Mg^{2+} on spontaneous and evoked EPSCs

(**A**) Extracellular Mg^{2+} produces a marked decrease in the average amplitude of spontaneous EPSCs. (**B**) Extracellular Mg^{2+} has no significant effect on the coefficient of variation of EPSC amplitudes. (**C**) Extracellular Mg^{2+} does not alter the frequency of spontaneous EPSCs. (**D**) Iontophoretic application of glutamate evokes a smaller postsynaptic response in the presence of extracellular Mg^{2+}. The reduction in the amplitude of the evoked postsynaptic response is comparable to the effect observed in (**A**), suggesting that the predominant effect of extracellular Mg^{2+} is postsynaptic receptor block. Data shown in panels **A**, **B**, and **C** are means with standard errors of the means for four experiments.

A

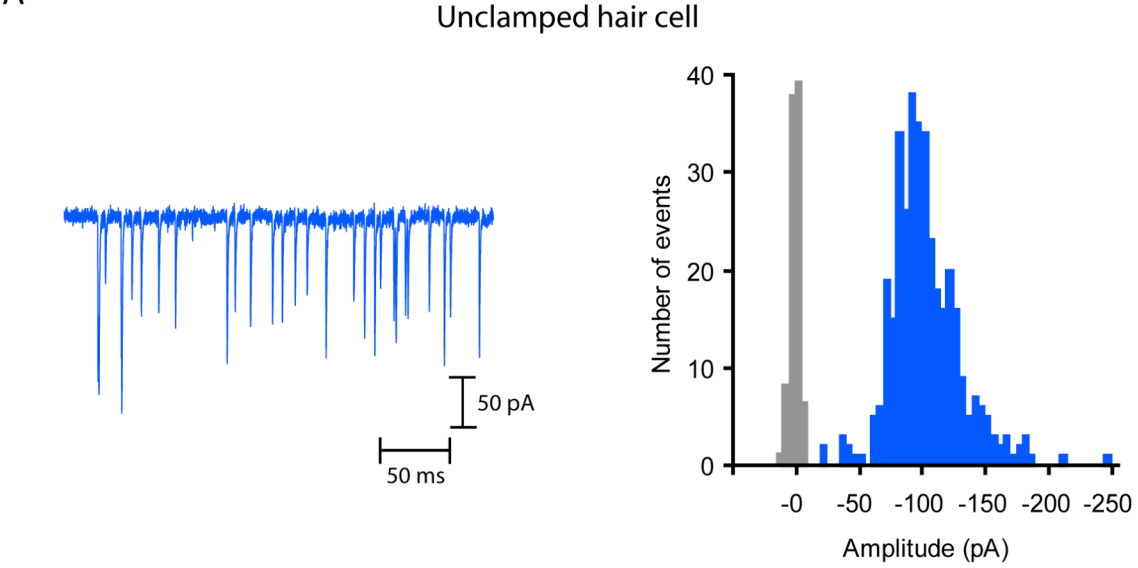
Unclamped hair cell
50 pA
50 ms
Number of events
40
30
20
10
0
-0
-50
-100
-150
-200
-250
Amplitude (pA)

B

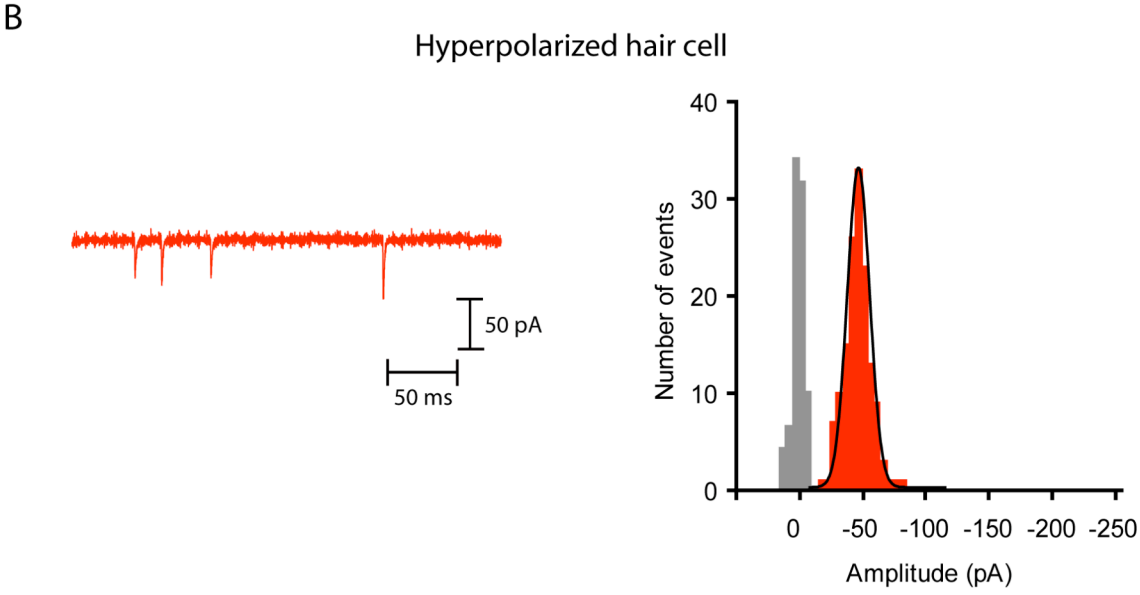
Hyperpolarized hair cell
50 pA
50 ms
Number of events
40
30
20
10
0
0
-50
-100
-150
-200
-250
Amplitude (pA)

Figure 4.9

Effect of hair-cell hyperpolarization

(**A**) Spontaneous EPSCs from an unclamped hair cell have a large range of amplitudes (*Left*). The amplitude distribution of spontaneous EPSCs (*Right*) has a mean value of -99±30 pA at a fiber holding potential of -70 mV. (**B**) Voltage-clamping the presynaptic hair cell to -80 mV eliminates all large events recorded from the same fiber and reduces the frequency of the events (*Left*). Hyperpolarizing the connected hair cell to -80 mV shifted the amplitude distribution (*Right*) to an average of -46±13 pA (n=145). For both histograms, EPSCs were binned at 10-pA intervals. The noise amplitude distributions (gray) are scaled to the maximum of the EPSC distributions.

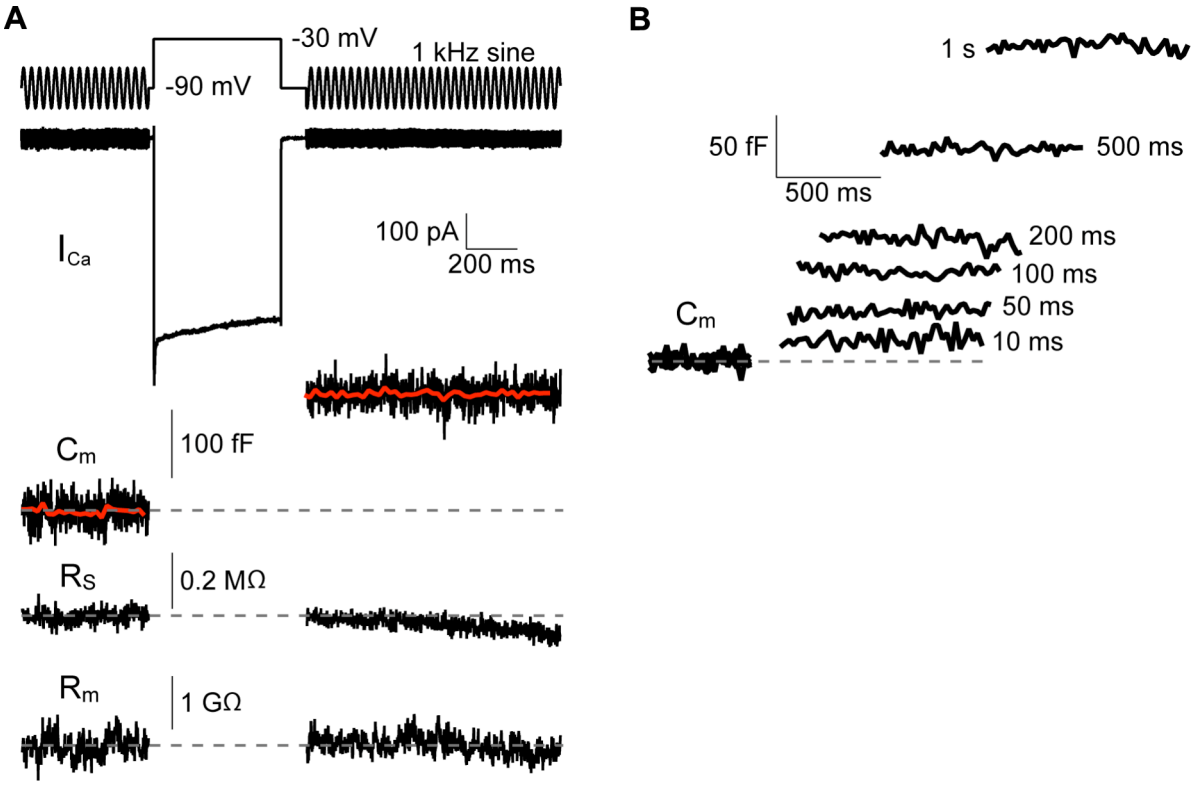
A
-30 mV
1 kHz sine
-90 mV
I_{Ca}
100 pA
200 ms
C_m
100 fF
R_S
0.2 MΩ
R_m
1 GΩ
B
1 s
50 fF
500 ms
500 ms
200 ms
100 ms
50 ms
10 ms
C_m

Figure 4.10

Presynaptic capacitance measurements

(**A**) A voltage-clamped hair cell was depolarized from a holding potential of -90 mV to -30 mV to evoke exocytosis. During the depolarizing stimulus, a presynaptic Ca^{2+} current (I_{Ca}) was recorded. To measure the presynaptic membrane capacitance, a sinusoid (1 kHz, 50 mV peak-to-peak) was superposed on the holding potential before and after the depolarization. From the measured current response to the sinusoid, membrane capacitance (C_m), series resistance (R_s), and membrane resistance (R_m) were calculated. The increase in C_m reflects a rise in membrane surface area due to synaptic vesicle fusion events. The red trace is the averaged value of the C_m data points. Note that R_s and R_m remain constant. (**B**) C_m increases with the duration of the depolarizing stimulus. The traces shown are responses to single depolarizing pulses presented to the cell of panel **A**.

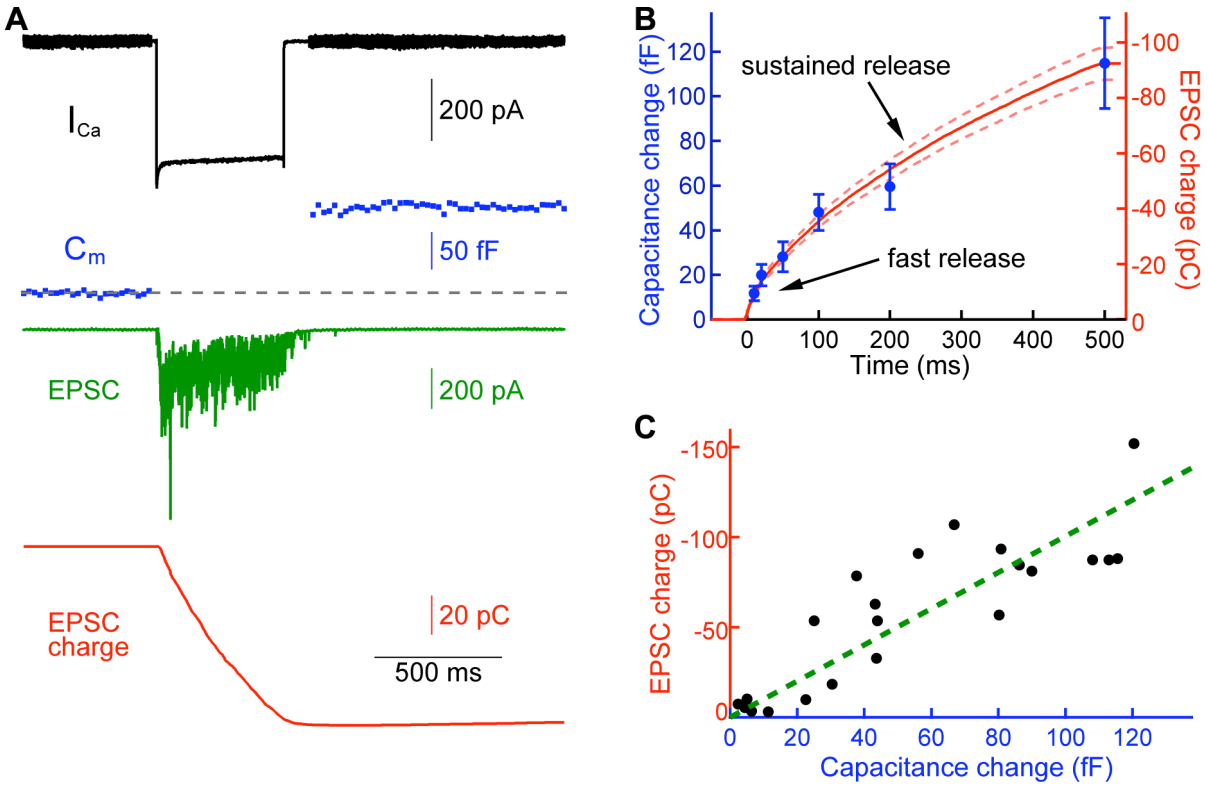
A
I_{Ca}
200 pA
C_m
50 fF
EPSC
200 pA
EPSC charge
20 pC
500 ms
B
sustained release
fast release
Capacitance change (fF)
EPSC charge (pC)
Time (ms)
C
EPSC charge (pC)
Capacitance change (fF)

Figure 4.11

Paired recordings with capacitance measurements

(**A**) In a representative hair cell-afferent fiber paired recording, depolarization of the hair cell from -90 mV to -30 mV elicits a presynaptic Ca^{2+} current (black) and capacitance increase (blue) and a postsynaptic EPSC (green). The total charge transferred (red) is the integral of the evoked EPSC. (**B**) The postsynaptic charge transferred (red, n=11; dashed lines indicate standard error range) is well correlated with the presynaptic membrane capacitance increase (blue; n=6) induced by depolarizing pulses of different durations. (**C**) For each paired recording, the total postsynaptic charge transferred was plotted against the presynaptic membrane capacitance increase. The data were fit with a straight line through the origin with a slope of 1.01 $kC \cdot F^{-1}$ (correlation coefficient: 0.86).

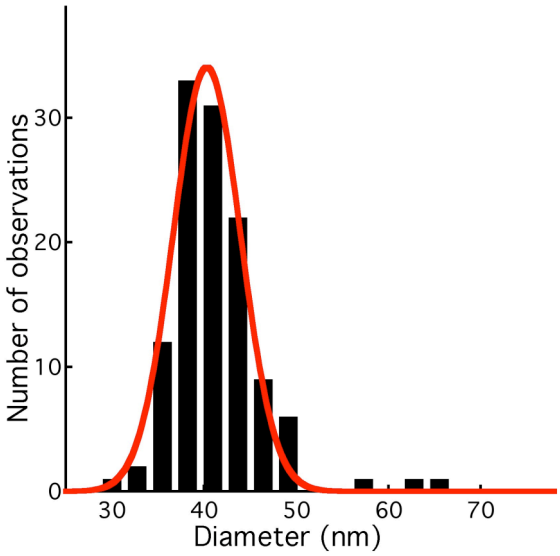
Number of observations
0
10
20
30
30
40
50
60
70
Diameter (nm)

Figure 4.12

Electron-microscopic analysis of synaptic vesicle diameters

The amplitude distribution of synaptic vesicle diameters is fit well by a Gaussian function (red) with a mean value of 40.3 nm. After calibration of the electron microscope, the mean vesicle diameter was determined to be 37.6 nm.

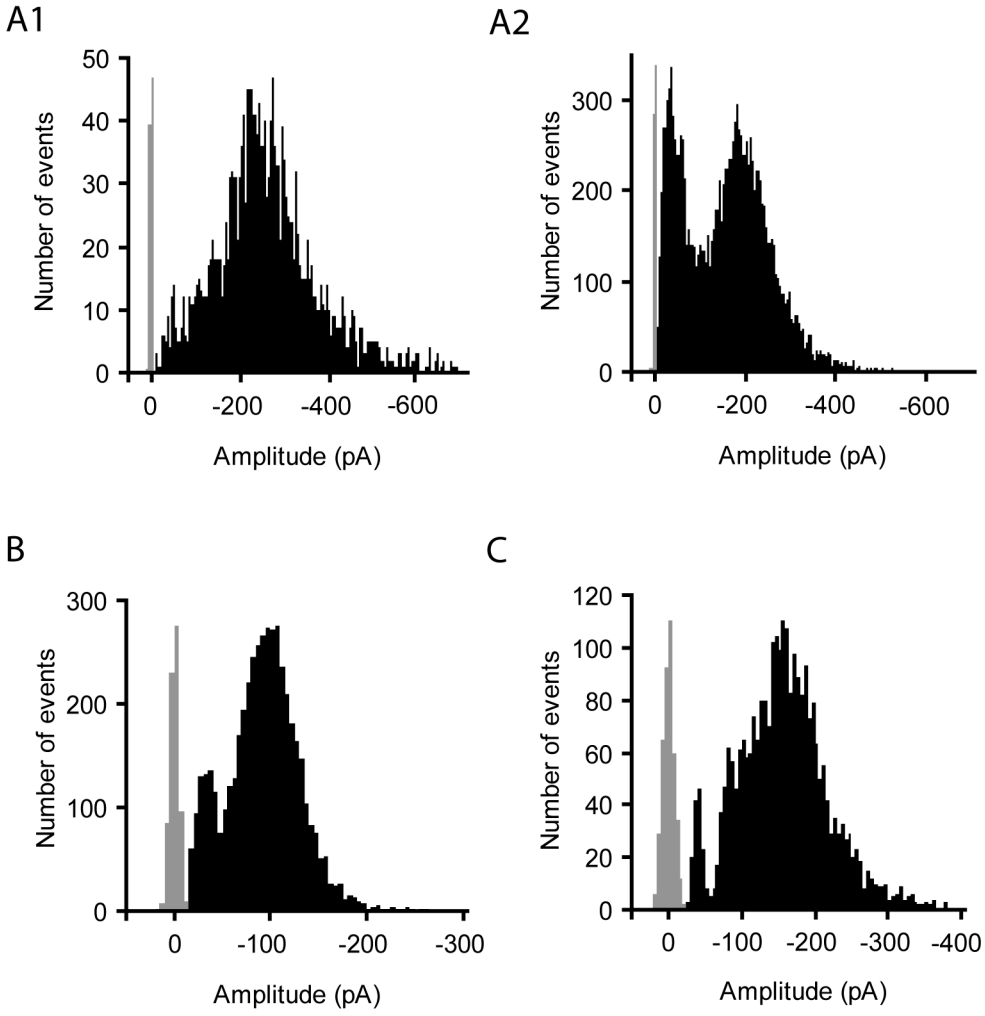
A1
Number of events
50
40
30
20
10
0
0
-200
-400
-600
Amplitude (pA)
A2
Number of events
300
200
100
0
0
-200
-400
-600
Amplitude (pA)
B
Number of events
300
200
100
0
0
-100
-200
-300
Amplitude (pA)
C
Number of events
120
100
80
60
40
20
0
0
-100
-200
-300
-400
Amplitude (pA)

Figure 4.13

A quantal peak in EPSC amplitude histograms

(**A1**) The amplitude distribution of spontaneous EPSCs recorded in control solution displays a single modal peak. The mean amplitude of 1,810 EPSCs was -275±115 pA in this afferent fiber. The occurrence rate was 60 s^{-1}. (**A2**) The addition of 50 μM BayK-8644 and simultaneous reduction in the extracellular Ca^{2+} concentration in the same recording leads to the emergence of a secondary peak with a modal amplitude of -55 pA, the estimated magnitude of the quantal response. This quantal peak emerges despite the persistence of the larger mode of release. Importantly, the kinetics of events in the smaller peak did not differ significantly from those in the larger peak. For 147 EPSCs with amplitudes of -50±1 pA, the mean rise and decay times were 0.22±0.10 ms and 0.51±0.28 ms, respectively. For 105 events with amplitudes of -200±1 pA, the corresponding kinetic parameters were 0.22±0.08 ms and 0.47±0.14 ms. (**B**) After 15 minutes of recording, a quantal peak emerges in another recording (n=2,752). (**C**) Focal Ca^{2+} iontophoresis in a nominally Ca^{2+}-free solution elicits a discrete quantal peak in an afferent fiber recording (n=2,999). Amplitudes were binned at 5-pA intervals for all histograms.

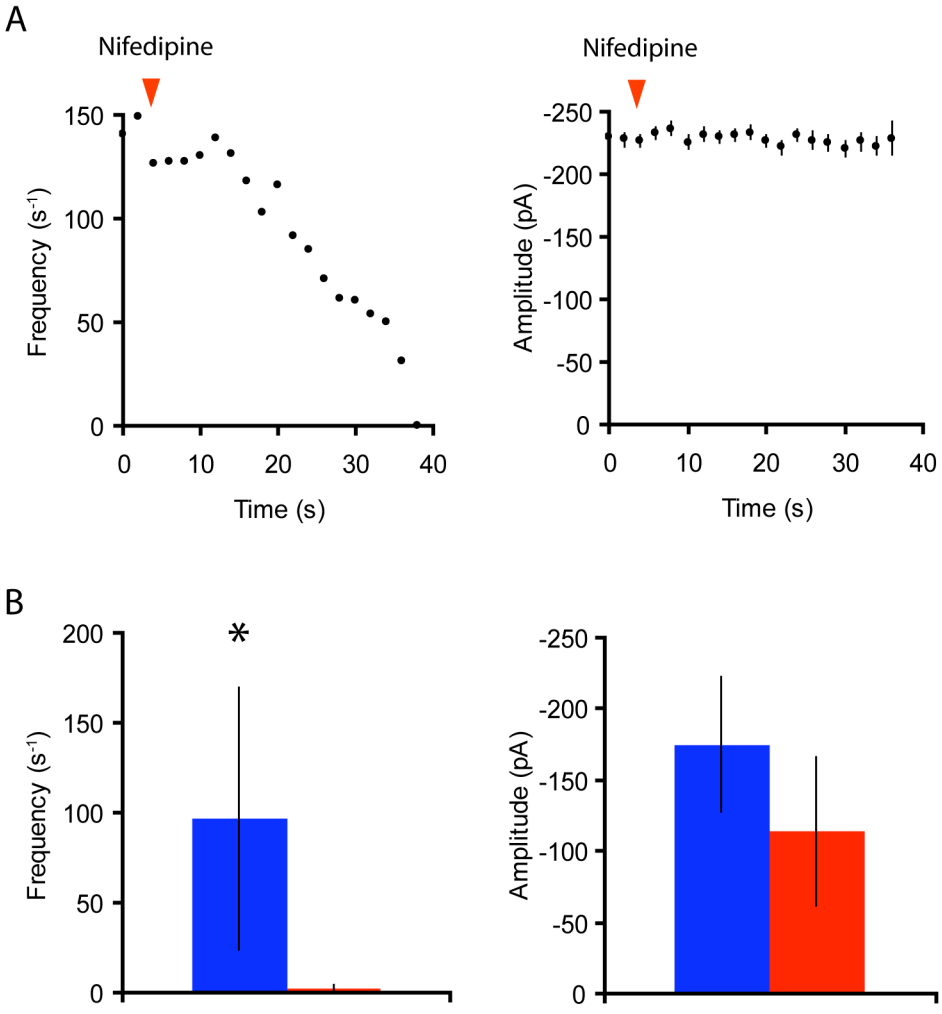
A
Nifedipine
Frequency (s-1)
150
100
50
0
0
10
20
30
40
Time (s)
Nifedipine
Amplitude (pA)
-250
-200
-150
-100
-50
0
0
10
20
30
40
Time (s)
B
*
Frequency (s-1)
200
150
100
50
0
Amplitude (pA)
-250
-200
-150
-100
-50
0

Figure 4.14

Differential effects of Ca^{2+} channel inhibition

(**A**) Application of 100 μM nifedipine during an afferent fiber recording produces a precipitous decline in the frequency of spontaneous EPSCs (*Left*), but does not alter their average amplitude over the same time period (*Right*). (**B**) The addition of either 50-100 μM nifedipine or 500-1000 μM extracellular Cd^{2+} led to a statistically significant reduction in the frequency of spontaneous EPSCs (left panel), but only a small decrease in their amplitudes (right panel). EPSCs recorded for 30 seconds in control solution were compared to those recorded for 30 seconds at one minute after addition of either reagent. Average EPSC frequency fell from 97 s^{-1} to 2 s^{-1}; average EPSC amplitude decreased from -175±48 pA to -114±52 pA. Data shown are mean values with standard errors of the mean from 14 experiments (8 nifedipine; 6 Cd^{2+}). Note that the average EPSC amplitude during Ca^{2+} channel inhibition is approximately double that of the putative quantal size. After several minutes with either Ca^{2+}-channel blocker, the frequency of events decreased further and predominantly quantal events with a mean of approximately -50 pA were observed.

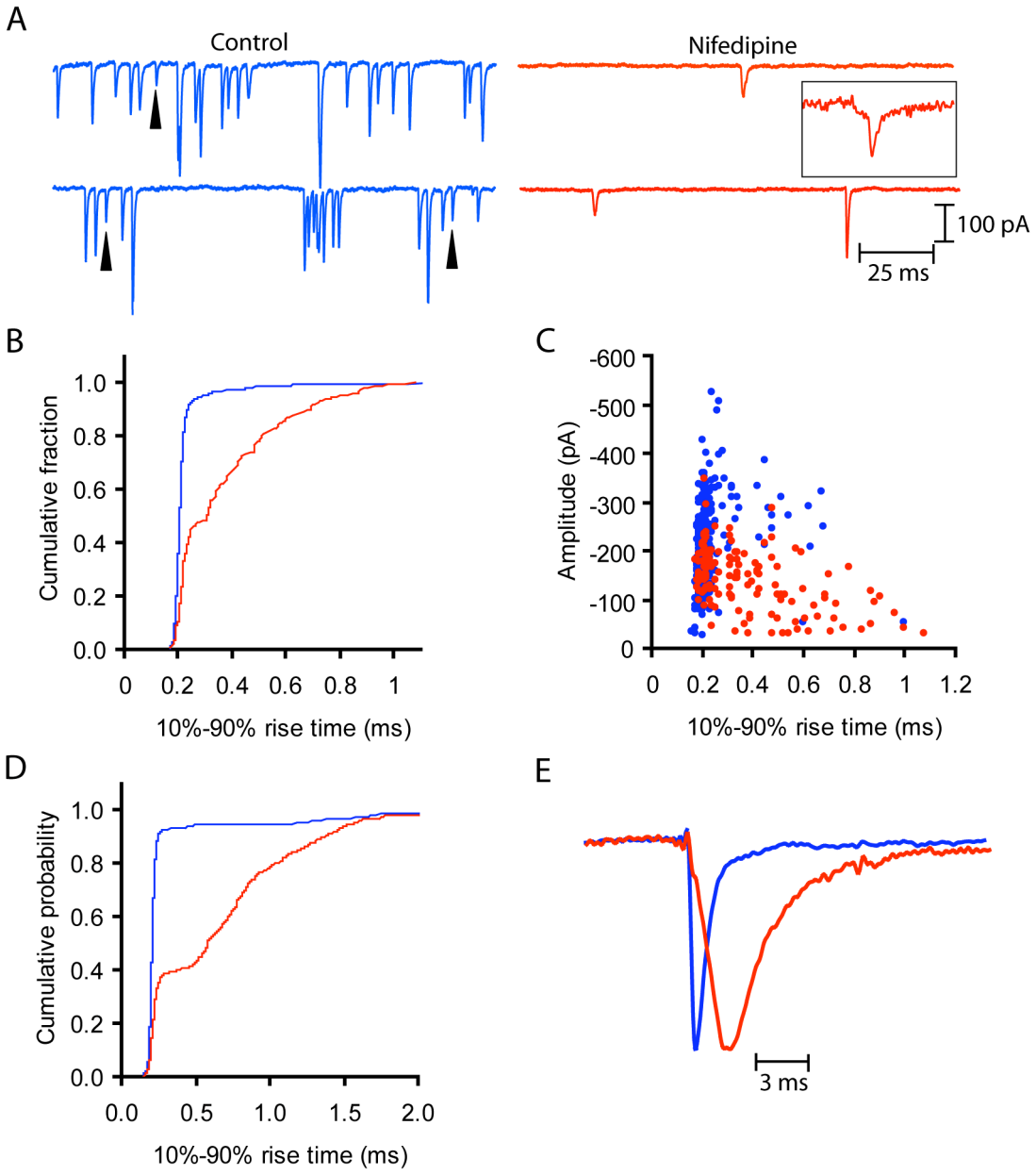
A
Control
Nifedipine
100 pA
25 ms
B
Cumulative fraction
1.0
0.8
0.6
0.4
0.2
0.0
0
0.2
0.4
0.6
0.8
1
10%-90% rise time (ms)
C
Amplitude (pA)
-600
-500
-400
-300
-200
-100
0
0
0.2
0.4
0.6
0.8
1
1.2
10%-90% rise time (ms)
D
Cumulative probability
1.0
0.8
0.6
0.4
0.2
0.0
0.0
0.5
1.0
1.5
2.0
10%-90% rise time (ms)
E
3 ms

Figure 4.15

Anomalous kinetic behavior of EPSCs

(A) Spontaneous EPSCs in control solution (*Left*) are widely distributed in amplitude, but have similar kinetics. Arrowheads denote small EPSCs. In the presence of nifedipine (*Right*), infrequent, small EPSCs display slower waveforms than their counterparts in control solution. Small events in nifedipine or a low extracellular Ca^{2+} concentration occasionally display humps on their rising phase reminiscent of an amperometric "foot" (inset). (**B**) The rise-time kinetics of EPSCs in control solution (blue) is highly uniform compared to that in nifedipine (red). In the presence of nifedipine, there appear to be two kinetically distinct populations of EPSCs. (**C**) EPSCs in control solution (blue) are faster and of larger average amplitude than those in the presence of nifedipine (red). (**D**) In another afferent fiber recording, EPSCs in control solution display predominantly fast kinetics (blue). After several minutes in a nominally Ca^{2+}-free solution (red), a distinct population of EPSCs with long rise times becomes prominent (red). 7% of spontaneous EPSCs in control solution had rise times greater than 0.35 ms *versus* 60% in the Ca^{2+}-free solution. (**E**) The averages of 203 fast EPSCs and 295 slow EPSCs in Ca^{2+}-free solution, normalized in amplitude and aligned by rise time, reveal significant kinetic differences. The average 10%-90% rise time quintupled from 0.22 ms to 1.08 ms, and the average 90%-37% decay time doubled from 0.55 ms to 0.95 ms. Although the average peak amplitude of slow EPSCs was half that of fast EPSCs, their average areas were similar. Both waveforms were fit well by single exponential functions.

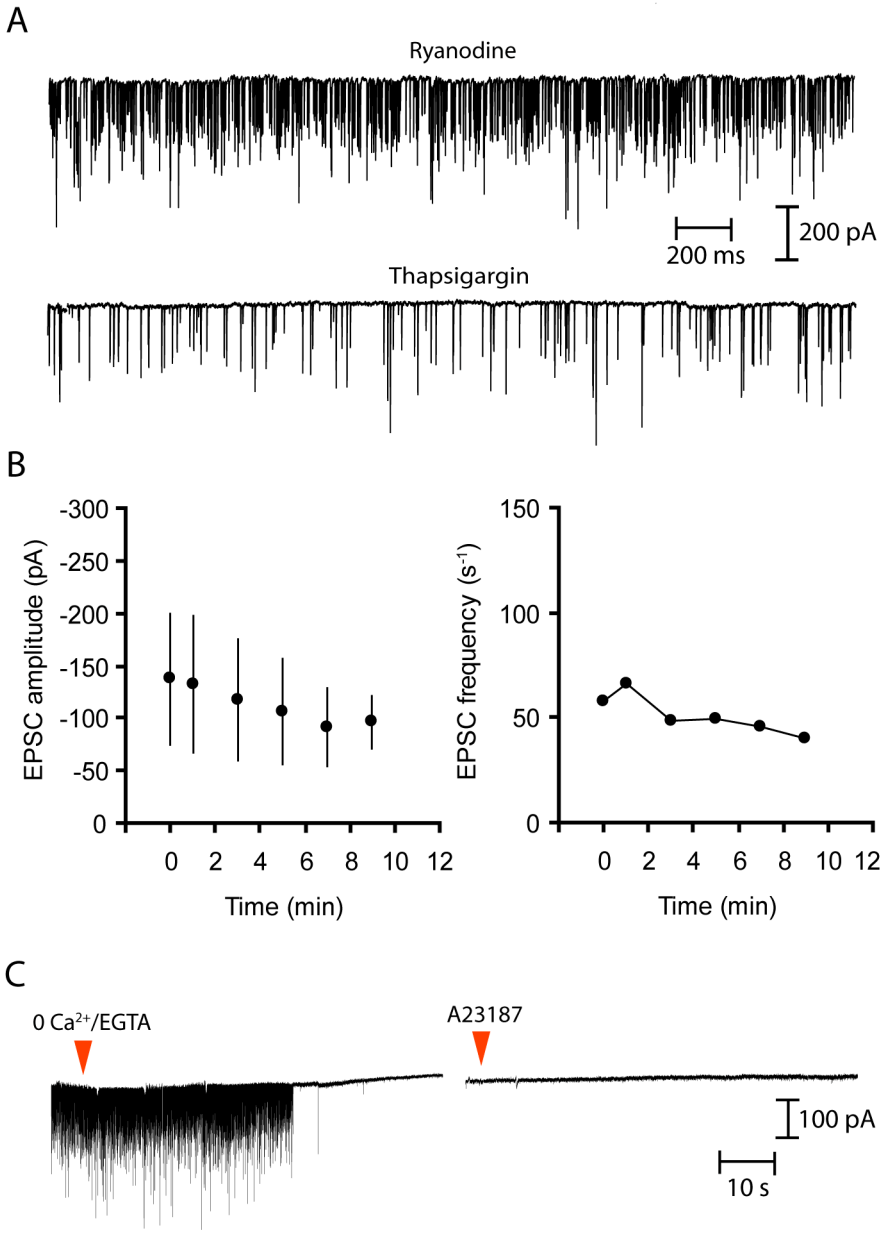
A
Ryanodine
200 ms
200 pA
Thapsigargin
B
EPSC amplitude (pA)
-300
-250
-200
-150
-100
-50
0
0 2 4 6 8 10 12
Time (min)
EPSC frequency (s-1)
150
100
50
0
0 2 4 6 8 10 12
Time (min)
C
0 Ca2+/EGTA
A23187
100 pA
10 s

Figure 4.16

Effect of Ca^{2+} release from internal stores

(**A**) A 30-minute preincubation with either 100 μM ryanodine (upper trace) or 50 μM cyclopiazonic acid/1 μM thapsigargin (lower trace) does not prevent high-frequency multiquantal EPSCs at the hair-cell synapse. For the upper record, the average EPSC amplitude was -195±75 pA and the average rate was 170 s^{-1}. For the lower record, the average EPSC amplitude was -181±67 pA and the average rate was 57 s^{-1}. (**B**) Addition of 100 μM ryanodine (at t=0) in 4 recordings did not produce a significant decrease in the average amplitude or frequency of spontaneous EPSCs. The initial average EPSC amplitude was -137±63 pA; the average EPSC amplitude after 10 minutes in ryanodine was -97±26 pA. A similar decrease in amplitudes was often observed in control recordings over the same time period. (**C**) The Ca^{2+} ionophore A23187 (10 μM) fails to elicit exocytosis in the absence of extracellular Ca^{2+}. About 1.5 minutes elapsed between the first and second traces. The concentration of unbuffered, free Ca^{2+} in this experiment was estimated to be approximately 20 nM. Similar results were obtained with ionomycin (10 μM) and thapsigargin (5 μM) in 5 additional experiments in which the unbuffered, free Ca^{2+} concentration was estimated to be lower than 100 nM. Note that with an estimated 250 nM free Ca^{2+} in another experiment, a burst of EPSCs was elicited roughly 20 seconds after addition of A23187.

CHAPTER FIVE

Conclusions and future directions

This work describes the development of a novel *in vitro* preparation that provides access to the hair cell's afferent synapse. The functional properties of this ribbon-type synapse have been explored with a variety of electrophysiological techniques meant to tease apart the contributions of the pre- and postsynaptic elements to information transfer.

Multiquantal release and linearity at the hair-cell synapse

Having determined the magnitude of the quantal response at this hair-cell synapse, it is evident that the majority of the spontaneous and evoked events are multiquantal despite possessing strikingly uniform kinetics. These multiquantal events arise from fusion events at individual active zones, rather than the concerted release of transmitter at different active zones. Furthermore, because postsynaptic receptors are not saturated by quantal events and report transmitter concentration with high fidelity, multiquantal events may be functionally significant. At most central and peripheral synapses, the relation between Ca^{2+} entry through voltage-gated channels and exocytosis is higher-order, presumably reflecting the highly cooperative nature of the Ca^{2+}-dependent fusion reaction (Dodge and Rahamimoff, 1967; Mintz *et al.*, 1995; Borst and Sakmann, 1999). The hair-cell synapse, however, displays a linear relation between the presynaptic Ca^{2+} current, presynaptic vesicle fusion, and postsynaptic response, permitting auditory receptor cells

to transmit graded information with minimal distortion over a physiological range of membrane potentials.

The results presented here demonstrate that the linearity of the synaptic transfer function is imparted primarily by an increase in the *frequency* of exocytotic events. In contrast, the average amplitude of postsynaptic events saturates rapidly with low levels of stimulation. The rate of change in amplitude is steep only within a range of hair-cell potentials and presynaptic Ca^{2+} currents near the threshold for exocytosis, where the relation between the presynaptic Ca^{2+} current and the postsynaptic response may also deviate from linearity. Spontaneous multiquantal events in the *in vitro* preparation typically reflect a point on the curve well beyond the saturation level. This explains why hair-cell depolarization here and in other systems causes a marked increase in the frequency of spontaneous events, but fails to produce a change in their amplitudes (Cochran, 1995; Glowatzki and Fuchs, 2002; Goutman and Glowatzki, 2007). The Ca^{2+} dependence of event frequency is consistent with vesicle fusions occurring under the control of a Ca^{2+} nanodomain (Brandt *et al.*, 2005). Primed vesicles may associate closely with Ca^{2+} channels, such that the Ca^{2+} influx through a single channel is sufficient to produce an all-or-none fusion reaction that overcomes the inherently higher-order dependence on Ca^{2+}. This strategy may also provide a significant temporal advantage: a fusion-competent vesicle in close proximity to a Ca^{2+} channel will experience a high Ca^{2+} concentration nearly instantaneously upon the opening of that channel, thus eliciting vesicle fusion with minimal delay.

How might the auditory system apply the linear relation between Ca^{2+} current and postsynaptic event frequency to encoding acoustic stimuli? An increase in the intensity

of a sound is expected to depolarize a hair cell, increase the number of open Ca^{2+} channels, and correspondingly increase the number of presynaptic release events. If each of these events—regardless of its amplitude—were sufficient to generate a postsynaptic action potential, the firing rate of the afferent fiber might indicate the amplitude of the stimulus. The linear synaptic relation could therefore be used to produce a linear rate code for stimulus intensity in the peripheral auditory system. Further experiments that examine the translation of postsynaptic currents to action potentials in afferent fibers will help to determine the functional consequences of neurotransmitter release in this system.

The mechanism of multiquantal release

Three potential mechanisms—coincident, sequential, and compound fusion—have been put forward to explain highly synchronous multiquantal release in this system (**Figure 1.2**).

Coincident fusion of docked vesicles might arise by any of several means. First, coupled gating of voltage-gated Ca^{2+} channels might provide simultaneous Ca^{2+} signals to several vesicles; however, there is no evidence for cooperativity between L-type Ca^{2+} channels. Second, a unique class of Ca^{2+} channels could promote the fusion of larger vesicles. Although an additional class of Ca^{2+} channels with N-type characteristics is expressed in hair cells (Su *et al.*, 1995; Rodriguez-Contreras and Yamoah, 2001), pharmacological evidence indicates that only L-type channels contribute to exocytosis (Robertson and Paki, 2002; Brandt *et al.*, 2003). Third, Ca^{2+}-induced Ca^{2+} release (CICR) could serve as a signal that coordinates the fusion of multiple vesicles; however, results reported in this work (**Figure 4.16**) and others (Neet *et al.*, 2007) suggest that CICR is

not involved. Fourth, docked vesicles might be synchronized by Ca^{2+} influx through a single L-type Ca^{2+} channel, in agreement with the nanodomain hypothesis ((Brandt *et al.*, 2005); however, quantal events predominate during presynaptic hyperpolarization (**Figure 4.9**). The opening of even a single Ca^{2+} channel during hair-cell hyperpolarization should permit a large influx of Ca^{2+} due to the increase in driving force. Therefore, if vesicle fusions are synchronized by Ca^{2+} from a single channel, infrequent, *large* EPSCs should predominate during hyperpolarization—the opposite of what has been observed. Thus, coincident vesicle fusion by the above mechanisms seems unlikely to underlie large postsynaptic events.

Compound fusion may better explain multiquantal events in this system, given the results of experiments reprised below. First, multiquantal events persist for some time in the presence of Ca^{2+}-channel inhibition, despite occurring at a severely reduced rate (**Figure 4.14**). Only after several minutes in a low-Ca^{2+} background fostered by Ca^{2+}-channel inhibitors or a reduced extracellular Ca^{2+} concentration do event amplitudes decrease significantly. Second, minimal iontophoretic stimulation evokes large EPSCs that correspond to the fusion of approximately three vesicles (**Figure 4.4**), indicating that multiquantal release can occur under conditions of low release probability. Importantly, these two observations are not consistent with simultaneous but independent fusion events; in that case, lowering the release probability should correspondingly lower the probability of multiquantal release. Rather, they suggest that fusion-competent, multiquantal compartments were *preformed* prior to the decline in release probability.

Third, the lack of definable quantal peaks in typical EPSC amplitude histograms (**Figure 2.7**) has been perplexing given the tight distribution of the quantal peak obtained

during hair-cell hyperpolarization, the evidence that spontaneous activity does not tend to saturate postsynaptic receptors, and the low variability in postsynaptic responses to iontophoresed glutamate. However, if larger vesicular structures containing variable amounts of transmitter were exocytosed, a broad distribution of postsynaptic response amplitudes would be anticipated.

Fourth, in the rare instances in which two peaks became apparent in EPSC amplitude histograms, a quantal peak emerged while the original multiquantal peak retained its broad Gaussian distribution (**Figure 4.13**). This result suggests that two independent processes—one producing quantal, the other multiquantal events—were occurring simultaneously. In other words, single vesicles may have been fusing in parallel with larger vesicular compartments.

Fifth, electron-microscopic images of hair-cell active zones in control conditions typically show large, membrane-bounded compartments in the vicinity of the active zone (**Figure 2.4D**). These irregular structures could represent the anatomical correlate of compound exocytotic events. Although none of the above data *demonstrate* the occurrence of compound exocytosis, results obtained with anatomical, pharmacological, and physiological techniques are all *consistent* with this mechanism as the basis for the generation of multiquantal events.

Are there precedents for compound exocytosis in other cells? Homotypic vesicle fusion has been described in secretory cells such as chromaffin, mast, and pancreatic acinar cells that release chemical mediators in a regulated vesicular process analogous to that of neuronal exocytosis. Sequential and compound fusions occur in these systems, and both processes may coexist in a given cell (Cochilla *et al.*, 2000; Hafez *et al.*, 2003;

Nemoto *et al.*, 2001; Scepek and Lindau, 1993). Importantly, compound fusion requires the elevation of free Ca^{2+} in these systems (Hartmann *et al.*, 2003; Vogel and Zimmerberg, 1992). The homotypic fusion of synaptic vesicles might well employ the same molecular players involved in exocytosis. Synaptic vesicles possess not only vesicle-SNAREs, but also the target-SNAREs syntaxin and SNAP-25 (Walch-Solimena *et al.*, 1995). Such coexpression could facilitate Ca^{2+}-dependent fusion reactions between neighboring vesicles on the synaptic ribbon.

An intriguing variant on the conventional notion of compound fusion is the exocytosis of membranous compartments previously retrieved by bulk endocytosis. This process has been suggested to occur at the ribbon-type active zones of retinal bipolar neurons on the basis of vesicle-imaging experiments (Coggins *et al.*, 2007). Electron-microscopic analysis in these cells has revealed large, cistern-like vesicles tethered to the synaptic ribbon (Matthews and Sterling, 2008), structures quite similar to those observed at active zones in this hair-cell preparation. The authors suggested that these structures were the result of compound vesicle fusions and they may, in fact, represent the exocytosing endosomes of Coggins *et al*.

If either Ca^{2+}-dependent compound fusion or exocytosis of endosomes were to occur, the degree of "multiquantalness" of a release event—and thus the size of the corresponding postsynaptic response—would depend upon the extent of presynaptic stimulation. With Ca^{2+}-dependent compound fusion, hair-cell depolarization would lead to a rise in the concentration of free Ca^{2+} at the active zone that enables fusion reactions between adjacent synaptic vesicles. With endosomal exocytosis, hair-cell depolarization would produce a high rate of exocytosis that leads to bulk endocytosis and subsequent

recycling of those compartments to presynaptic docking sites. Both scenarios are consistent with the experimental results described above.

Physiological role of multiquantal release

The predominance of multiquantal release at hair-cell synapses raises the question of the rationale for such an energetically expensive process. I propose two potential, not necessarily mutually exclusive, explanations for the prevalence of multiquantal exocytosis in this system.

In the auditory epithelium, a tonotopic array of hair cells provides finely graded frequency information to central processing centers. To prevent undue mixing of information between frequency channels, an afferent fiber ordinarily receives input from only one or a few hair cells. With few active zones and docked vesicles available for signaling, the auditory system may compensate by raising the release probability at each active zone. Under these circumstances, multiquantal events may simply be a consequence of the high release probability necessary for encoding sensory signals.

An alternative possibility is that the size of presynaptic fusion events is dynamically regulated. Because postsynaptic receptors are not saturated by quantal events, multiquantal release could in principle enhance the information capacity of the synapse by encoding signal intensity, providing precisely phase-locked temporal information, or reducing the background noise that arises from the high sensitivity of auditory receptor cells.

What functional advantages might compound exocytosis impart to the synapse? Hair cells support high rates of continuous transmitter release by fusing vesicles rapidly

and providing a large pool of vesicles at the active zone (Parsons *et al.*, 1994; reviewed in Prescott and Zenisek, 2005). Compound fusion could permit the equivalent of several vesicles to release their contents without trafficking to the plasma membrane, thus increasing the extent of transmitter release but not the number of occupied docking sites. Furthermore, large amounts of transmitter could be released without requiring multiple vesicles to find their docking partners at the plasma membrane, thus potentially increasing response speed. Release from endosomal compartments, in particular, could lessen the burden on both the endocytotic and exocytotic machinery. Compound exocytosis may therefore provide a way to maximize the information capacity of the synapse while minimizing spatial and temporal costs at the active zone.

APPENDIX ONE

Transfer characteristics of the hair cell's afferent synapse

Keen, EC and Hudspeth, AJ

PNAS **103:5537-5542 (2006)**

Transfer characteristics of the hair cell's afferent synapse

Erica C. Keen and A. J. Hudspeth*

Howard Hughes Medical Institute and Laboratory of Sensory Neuroscience, The Rockefeller University, 1230 York Avenue, New York, NY 10021-6399

Contributed by A. J. Hudspeth, February 14, 2006

The sense of hearing depends on fast, finely graded neurotransmission at the ribbon synapses connecting hair cells to afferent nerve fibers. The processing that occurs at this first chemical synapse in the auditory pathway determines the quality and extent of the information conveyed to the central nervous system. Knowledge of the synapse's input–output function is therefore essential for understanding how auditory stimuli are encoded. To investigate the transfer function at the hair cell's synapse, we developed a preparation of the bullfrog's amphibian papilla. In the portion of this receptor organ representing stimuli of 400–800 Hz, each afferent nerve fiber forms several synaptic terminals onto one to three hair cells. By performing simultaneous voltage-clamp recordings from presynaptic hair cells and postsynaptic afferent fibers, we established that the rate of evoked vesicle release, as determined from the average postsynaptic current, depends linearly on the amplitude of the presynaptic Ca^{2+} current. This result implies that, for receptor potentials in the physiological range, the hair cell's synapse transmits information with high fidelity.

auditory system | exocytosis | glutamate | ribbon synapse | synaptic vesicle

The remarkable acuity and temporal precision of the auditory system are contingent on exocytosis at the hair cell's ribbon synapses, whose transfer characteristics are largely determined by the dependence of vesicle fusion on Ca^{2+} influx through voltage-gated channels. The relation of presynaptic voltage and Ca^{2+} influx to transmitter release at ribbon synapses is of particular interest in light of several unusual features of the hair cell's synaptic signaling. Afferent synapses encode inputs with graded membrane potentials (reviewed in ref. 1), transmit information with microsecond temporal fidelity (2), demonstrate multivesicular release (3–5), sustain high rates of exocytosis for prolonged periods (6–8), and display frequency tuning (9). Transmitter release is triggered by an atypical class of voltage-gated Ca^{2+} channels [noninactivating, L-type channels with α_{1D} principal subunits (10)] clustered at the presynaptic active zones (11–14). Finally, synaptotagmins I and II, the putative Ca^{2+} sensors for vesicle fusion in the brain, have not yet been detected at hair-cell synapses (15); instead, an alternative Ca^{2+} sensor, such as otoferlin (16), may effect exocytosis at these sites.

The operation of the hair cell's synapse has been investigated only indirectly by recording signals independently from either its presynaptic or postsynaptic element. Presynaptic measurements of membrane capacitance, an index of synaptic vesicle fusion, have provided information about the relation between presynaptic Ca^{2+} signals and vesicle release. Flash photolysis of caged Ca^{2+} indicates that the rate of exocytosis displays a fifth-order dependence on the cytoplasmic Ca^{2+} concentration (17), whereas hair-cell depolarization elicits vesicle release that is directly proportional to the presynaptic Ca^{2+} current (18, 19). Independent manipulation of either the number or the single-channel current of activated Ca^{2+} channels suggests that very few channels regulate the release of each synaptic vesicle (20). Exocytosis thus appears to be influenced by the Ca^{2+} concentration in the immediate vicinity of open channels rather than by the spatially averaged concentration originating from a cluster of channels. On the postsynaptic side, recordings of spontaneous excitatory postsynaptic currents (EPSCs) from the afferent nerve terminals of immature mammals have revealed a broad amplitude distribution suggestive of highly synchronized multivesicular release (3). Recordings of sound-evoked excitatory postsynaptic potentials and action potentials have elucidated other properties of information transfer across the synapse, including adaptation (21, 22) and frequency selectivity manifested by the sharp tuning curves and ready phase-locking of afferent fibers to low-amplitude stimuli (23).

Although these experiments have provided insight into the operation of the hair cell's synapse, it has not been possible to investigate directly the transfer characteristics of this synapse through simultaneous recordings from its pre- and postsynaptic elements. Such recordings offer the advantages of high temporal resolution, control over the presynaptic cell's voltage and intracellular milieu, and detection of only physiologically relevant vesicle release to the exclusion of that from outlying vesicles. We introduce here a preparation that permits such paired recordings, and we present data on the input–output function at the hair cell's afferent synapse.

Results

Experimental Preparation. We investigated the synaptic interaction between hair cells and afferent nerve fibers in the bullfrog's amphibian papilla. As the principal auditory receptor organ of anurans, the amphibian papilla detects airborne vibrations in the frequency range of 100–1,250 Hz. By controlled splitting of the sensory epithelium down its long axis, we exposed the unmyelinated afferent terminals innervating hair cells in the papilla's medial and caudal regions (Fig. 1*A*). Fracture ordinarily occurred along a row of hair cells lying near the midpoint of the organ's mediolateral axis. The frequency selectivity of both hair cells and afferent fibers defines a tonotopic gradient along the amphibian papilla (24–27). On the basis of this frequency map, the exposed cells would be expected to display characteristic frequencies of 400–800 Hz.

We used morphological techniques to characterize the innervation pattern in the region of interest. We immunolabeled hair cells with an antiserum directed against parvalbumin 3, an abundant cytoplasmic Ca^{2+} buffer, and afferent fibers with 3A10 monoclonal antibodies directed against neurofilament-associated proteins. The afferent terminals were typically 1–3 μm in diameter immediately postsynaptic to a hair cell and branched to contact one to three hair cells (Fig. 1*B*). Labeling of fibers and hair cells in the split epithelium confirmed that some of these synaptic contacts are preserved in the preparation used for electrical recording (Fig. 1*C*). To examine the trajectories of

Conflict of interest statement: No conflicts declared.

Freely available online through the PNAS open access option.

Abbreviations: AMPA, α-amino-3-hydroxy-5-methyl-4-isoxazolepropionic acid; EPSC, excitatory postsynaptic current.

*To whom correspondence should be addressed at: The Rockefeller University, Box 314, 1230 York Avenue, New York, NY 10021-6399. E-mail: hudspaj@rockefeller.edu.

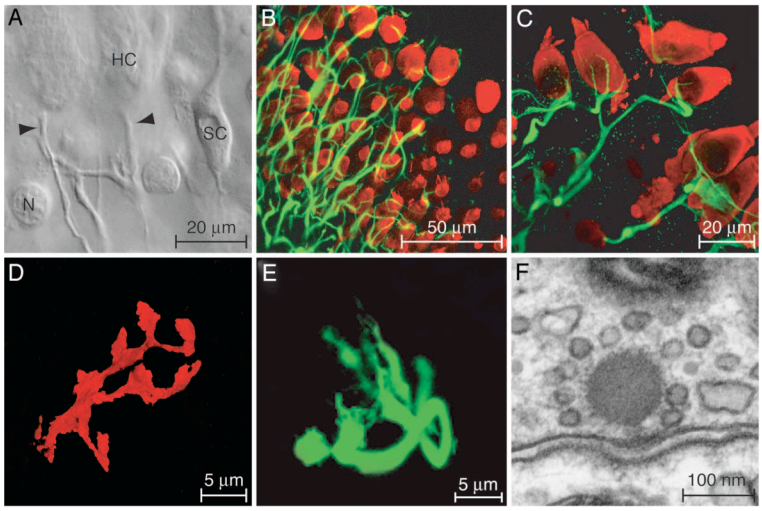

Fig. 1. *In vitro* preparation of the amphibian papilla. (*A*) A differential-interference-contrast micrograph depicts a portion of the split sensory epithelium in which the unmyelinated eighth-nerve fibers contact the basolateral surfaces of two hair cells (HC). Arrowheads, nerve terminals; SC, supporting cell; N, nucleus of dead supporting cell. (*B*) A stack of confocal images of the intact epithelium depicts hair cells immunolabeled for parvalbumin 3 (red) and afferent nerve terminals labeled for neurofilament-associated proteins (green). (*C*) A higher-magnification view of a split preparation shows the fine branches of afferent terminals juxtaposed to the basolateral surfaces of hair cells. (*D*) The terminal branches of a fiber labeled with a fluorescent lipophilic tracer surround a single hair cell. (*E*) An afferent terminal is labeled with a fluorescent tracer after whole-cell recording. (*F*) As visualized by transmission electron microscopy, an afferent synapse from the amphibian papilla displays prominent pre- and postsynaptic densities and an osmiophilic presynaptic dense body, or synaptic ribbon, to which a halo of synaptic vesicles is tethered.

individual afferent fibers, we labeled fibers terminating in the mid- to high-frequency portion of the sensory epithelium by diffusion of 1,1′-dioctadecyl-3,3,3′,3′-tetramethylindocarbocyanine perchlorate [diIC_{18}(3)] along the nerve bundle. In agreement with prior studies (24, 26), this approach demonstrated that each fiber in the region of interest branches only sparsely. In contradistinction to the one-to-one synaptic connectivity observed in the mammalian auditory periphery (28), however, each fiber terminates in multiple branches on a given hair cell (Fig. 1*D*). To examine the synaptic contacts more closely, we included in the recording pipettes a fluorophore that permitted cytoplasmic labeling of single afferent fibers. Confocal imaging confirmed that our electrical recordings originated from a fiber postsynaptic to a single hair cell and revealed the synaptic contacts terminating on that hair cell (Fig. 1*E*).

To investigate the fine structure of presynaptic active zones in the hair cells of interest, we performed electron microscopy on the mid- to high-frequency region of the amphibian papilla. In accordance with the general pattern of ribbon-type synapses in hair cells, including those in the papilla's rostral and caudal regions (29), each active zone displayed well defined presynaptic and postsynaptic densities and was marked by a prominent, ≈150-nm-diameter presynaptic dense body enveloped by synaptic vesicles (Fig. 1*F*).

Properties of EPSCs. Voltage-clamp recordings were obtained from afferent fibers near their terminations on the basolateral surfaces of hair cells in the mid- to high-frequency region of the amphibian papilla. Establishment of the whole-cell recording configuration was evident from the appearance of spontaneous EPSCs, which occurred at rates of 5–130 s^{-1} in control perilymph (Fig. 2*A*). The waveforms of these EPSCs were predominantly monophasic; however, a fraction of EPSCs, ≈5% in most recordings, displayed complex rise or decay waveforms (Fig. 2*B*). These multiphasic EPSCs were typically larger in amplitude than monophasic EPSCs. Spontaneous EPSCs recorded from an individual fiber showed a wide distribution of amplitudes, which varied over an order of magnitude (Fig. 2*C*). Although the smallest rise and decay times were observed for the smallest events, these kinetic parameters were not appreciably greater for larger events, suggesting that the release of multiple vesicles was highly synchronized (Fig. 2*D*). In a typical fiber recording, the mean 10–90% rise time for 700 spontaneous EPSCs smaller than 75 pA was 0.23 ± 0.09 ms, whereas the value for 363 events larger than 100 pA was 0.22 ± 0.10 ms. The mean decay time constant for the small EPSCs was 0.40 ± 0.08 ms and that for large EPSCs was 0.41 ± 0.06 ms. Although these recordings were postsynaptic to a single hair cell, they may have included EPSCs originating from several presynaptic active zones innervated by a branched afferent terminal. We therefore cannot determine in the current experimental configuration whether the multivesicular events represent release from a single presynaptic active zone.

Dependence of EPSCs on Glutamate Receptors. The small rise times and exponential decays of EPSCs accorded with the expected kinetics of currents mediated by glutamate receptors of the α-amino-3-hydroxy-5-methyl-4-isoxazolepropionic acid (AMPA) type in the auditory system (ref. 3 and reviewed in ref. 30). The rise and decay times of monophasic EPSCs were variable in individual fibers (Fig. 3*A*). For 3,944 EPSCs in three fibers held at −70 mV, the mean 10–90% rise time was 0.37 ± 0.28 ms, and the mean decay time constant was 0.59 ± 0.19 ms.

To investigate the voltage sensitivity of the postsynaptic responses, we recorded spontaneous EPSCs while a fiber was

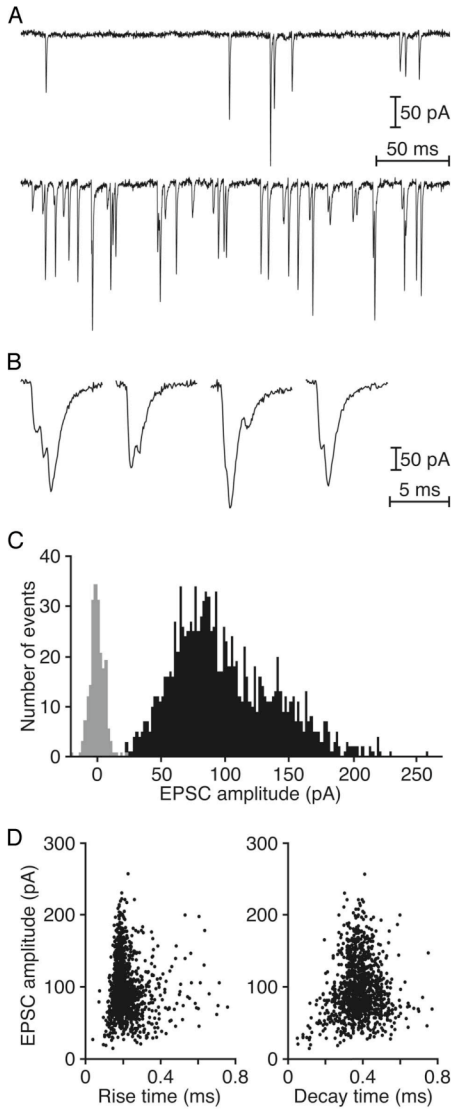

Fig. 2. Spontaneous EPSCs in afferent fibers. (*A*) The spontaneous EPSCs recorded from two terminals vary in amplitude and timing but display predominantly monophasic waveforms. (*B*) A subset of EPSCs display complex waveforms suggestive of multivesicular release slightly dispersed in time. (*C*) The amplitude distribution of spontaneous EPSCs (black) recorded in a particular afferent fiber extends over more than one order of magnitude. Analysis of these 1,216 events showed a mean amplitude of 100 ± 39 pA and an occurrence rate of 24 s^{-1}. The scaled distribution of noise amplitudes is shown in gray. (*D*) The 10–90% rise times (*Left*) and time constants of decay (*Right*) for EPSCs from the same fiber display tight distributions, suggesting that multiple release events are highly synchronized.

maintained at holding potentials from −100 mV to +50 mV. The kinetics and amplitudes of spontaneous EPSCs were voltage-dependent; the responses slowed at more positive potentials and reversed sign near 0 mV (Fig. 3*B*). Cyclothiazide, an agent that reduces the desensitization of AMPA receptors, doubled the decay time constant of EPSCs (Fig. 3*C*). Application of 6-cyano-7-nitroquinoxaline-2,3-dione (CNQX), an antagonist of AMPA and kainate receptors, completely and reversibly blocked EPSCs (Fig. 3*D*). These results indicate that EPSCs at the amphibian papilla's afferent synapse are mediated by AMPA receptors.

Dependence of EPSCs on Ca^{2+} Influx Through L-Type Channels. When added to the external solution, nifedipine, a specific antagonist of L-type voltage-gated Ca^{2+} channels, reversibly abolished spontaneous EPSCs (Fig. 3*E*). The release of synaptic transmitter therefore depends on Ca^{2+} influx through L-type Ca^{2+} channels, which is consistent with recordings from primary auditory afferent neurons showing that both spontaneous and sound-evoked transmitter release are sensitive to dihydropyridines (14).

Paired Recordings. To determine directly the dependence of the postsynaptic response on the presynaptic membrane potential, and especially on the presynaptic Ca^{2+} current, we performed paired voltage-clamp recordings on hair cells and afferent fibers. A recording was first obtained from an afferent fiber near its termination on the basolateral surface of a hair cell. In a total of six instances, we were then able to make a simultaneous whole-cell recording from the innervated hair cell. In five of these cases, the afferent fiber contacted solely the voltage-clamped hair cell, as verified by fluorescent dye labeling of the fiber and by the near elimination of postsynaptic currents when the hair cell was hyperpolarized to −80 mV.

After the two simultaneous recordings had been established, we explored the relationship between presynaptic voltage and vesicle release by stepping the hair cell's membrane potential from a holding level of −80 mV to test values between −70 mV and +10 mV. Evoked EPSCs were observed during the presentation of depolarizing pulses and persisted for the duration of each stimulus (Fig. 4). The rate of release did not necessarily remain constant; EPSCs in some experiments displayed adaptive changes during large presynaptic depolarizations, and in others showed an increase in rate suggestive of a progressive accumulation of cytoplasmic Ca^{2+}. The evoked EPSCs of some cell pairs were superimposed, precluding comparative analysis of the amplitude distributions of spontaneous and evoked currents from such fibers. In two of the paired recordings, however, individual EPSCs were discernible during maximal presynaptic stimulation. The amplitudes of the largest evoked EPSCs under these circumstances did not exceed those of the largest spontaneous EPSCs (data not shown).

We were also able to investigate the relationship between presynaptic Ca^{2+} influx and vesicle release by using the voltage-step protocol. Depolarizing voltage pulses activated an inward current in the hair cell and evoked EPSCs in the afferent fiber (Fig. 5*A*). The presynaptic inward current revealed with a Cs^{+}-based internal solution was noninactivating and nifedipine-sensitive, which, together with its voltage–current relation, signified Ca^{2+} influx through L-type Ca^{2+} channels (data not shown).

As a measure of the postsynaptic response, we integrated the evoked EPSC and divided the result by the duration of the depolarizing stimulus. This average postsynaptic current was presumably proportional to the number of glutamate receptors that bound the released transmitter, and in turn to the number of synaptic vesicles that liberated their contents. The postsynaptic current depended on the hair cell's membrane potential and mirrored the steep voltage dependence of the presynaptic

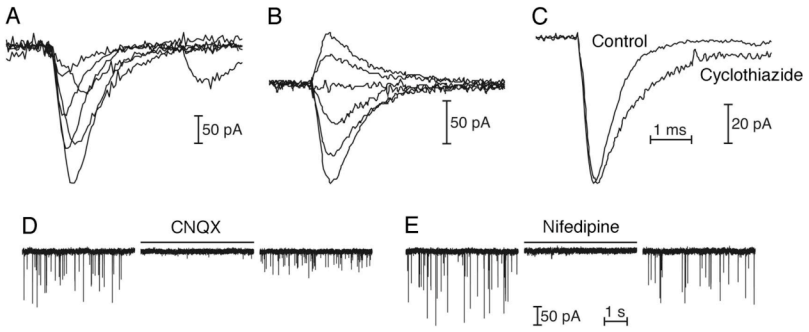

Fig. 3. Spontaneous EPSCs mediated by AMPA receptors. (*A*) Superimposed records from one fiber reveal the rapid onset and slower, exponential decay of monophasic EPSCs, as well as the variation in rise time. (*B*) As the postsynaptic membrane potential was varied, averaged EPSCs reversed sign near 0 mV and slowed at more positive potentials. From top to bottom, the holding potentials were +50 mV, +30 mV, 0 mV, −20 mV, −70 mV, and −100 mV. (*C*) Addition of 100 μM cyclothiazide halved the average decay rate of spontaneous EPSCs, increasing the time constant from 0.65 ± 0.13 ms ($n = 91$) to 1.25 ± 0.27 ms ($n = 38$). (*D*) An antagonist of AMPA and kainate receptors, 6-cyano-7-nitroquinoxaline-2,3-dione (CNQX), reversibly blocked EPSCs at a concentration of 10 μM. (*E*) Nifedipine, a specific antagonist of L-type Ca^{2+} channels, reversibly blocked EPSCs at a concentration of 50 μM.

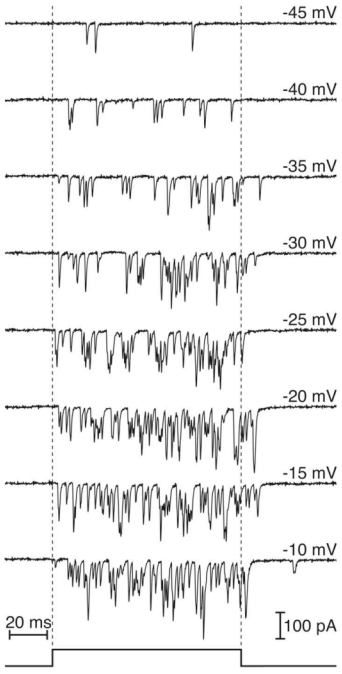

Fig. 4. Relationship between presynaptic voltage and evoked EPSCs. In a simultaneous voltage-clamp experiment, the hair cell was confronted with a series of 100-ms depolarizations whose timing is displayed at the bottom of the figure. For depolarizations that evoked near-maximal Ca^{2+} currents, the latency between stimulus onset and the first response decreased, and evoked EPSCs persisted after the termination of the pulse.

Ca^{2+} current (Fig. 5*B*). The Ca^{2+} current activated near −55 mV and was maximal at −20 mV; similarly, the postsynaptic current displayed an activation threshold between −55 mV and −50 mV and peaked at −20 mV to −10 mV.

At the presynaptic active zones of hair cells, the local Ca^{2+} concentration is expected to be directly proportional to the Ca^{2+} current (31). To determine the dependence of synaptic release on Ca^{2+}, we therefore plotted the average amplitude of the postsynaptic current against the presynaptic Ca^{2+} current at each test potential. Both signals displayed considerable variation between cell pairs, perhaps as a consequence of the heterogeneous electrical properties of amphibian papilla hair cells (27) and differences in the number of postsynaptic AMPA receptors. Nevertheless, the data from five sets of recordings were well approximated by linear fits over a range of presynaptic potentials that corresponds to physiological stimulation (Fig. 5*C*). In some instances, the average postsynaptic current saturated as the presynaptic Ca^{2+} current increased still further.

Discussion

Paired Recordings at Hair-Cell Afferent Synapses. Investigation of the input–output function at ribbon synapses in the auditory system is critical for understanding the mechanisms by which the electrical responses of hair cells are translated into a neural spike code. The split sensory epithelium of the bullfrog's amphibian papilla permits the study of synaptic signaling across this first synapse in the auditory pathway. The preparation preserves functional synapses in the epithelium yet exposes postsynaptic terminals for electrophysiological analysis. By using this preparation, it is possible to study not only spontaneous vesicle release from hair cells but also the transfer characteristics of the synapse with paired whole-cell recordings. Because this experimental preparation originates from an adult animal, its properties presumably reflect mature synaptic transmission. That no enzyme is used during the dissection or recording procedures further ensures the normal operation of the synapse.

Properties of EPSCs. The spontaneous EPSCs that we observed in afferent fibers of the amphibian papilla are consistent with anatomical observations of membrane recycling at unstimulated active zones and with physiological observations of spontaneous firing in eighth-nerve fibers (32, 33). The waveforms and phar-

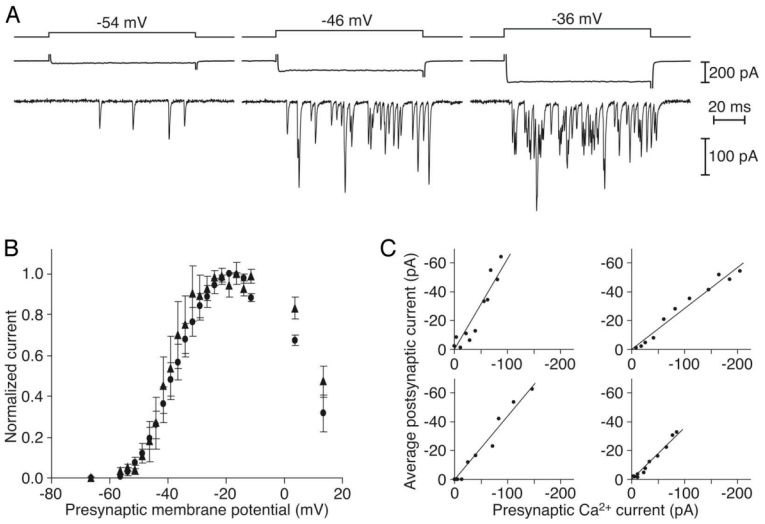

Fig. 5. Voltage and Ca^{2+} sensitivity of transmitter release. (*A*) Recordings during a simultaneous voltage-clamp experiment depict presynaptic Ca^{2+} currents (middle traces) and EPSCs (bottom traces) evoked by 100-ms hair-cell depolarizations (top traces). (*B*) Both the presynaptic Ca^{2+} current (circles) and the postsynaptic current (triangles) display a sigmoidal dependence on the test potential. Data are presented as normalized means ± standard errors of the means for four experiments. (*C*) In each of four paired recordings, the dependence of the postsynaptic current on the presynaptic Ca^{2+} current is approximately linear over a physiologically relevant range of hair-cell membrane potentials, here −56 mV to −31 mV. Clockwise from the upper left, the linear regression coefficients (r^2) are 0.88, 0.97, 0.97, and 0.95.

macological sensitivities of these currents accord with evidence that synaptic transmission at mammalian auditory ribbon synapses is mediated by AMPA-type glutamate receptors with rapid kinetics (3). The broad amplitude distributions of EPSCs from individual fibers suggest that multiple vesicles are released, whether from single or from multiple active zones, with a high degree of temporal precision.

Input–Output Function at Hair-Cell Synapses. Despite nonlinear stimulus processing in both the presynaptic hair cell and the postsynaptic afferent fiber, the intervening synapse evidently operates in a linear regime under our experimental conditions. Such a relationship has also been observed for the ribbon synapses of rod photoreceptors, at which the linearity between presynaptic Ca^{2+} signals and vesicle fusion facilitates the encoding of small changes in illumination (34). In several auditory receptor organs, presynaptic vesicle fusion has been shown to depend linearly on the presynaptic Ca^{2+} current (18, 19). The present demonstration that this linear relation extends across the synapse to the postsynaptic current implies that the postsynaptic receptors faithfully transmit the information conveyed by hair-cell exocytosis.

In most instances, the postsynaptic response vanished at potentials more negative than −55 mV despite the persistence of a small Ca^{2+} current (Fig. 5*C*). This result is consistent with evidence that exocytosis displays a higher-order Ca^{2+} dependence at the threshold of synaptic responsiveness (17). Near the normal resting potential of −55 mV to −50 mV for hair cells of the amphibian papilla (35, 36), however, the linear relation was obtained consistently. In many receptor organs, including the amphibian papilla (27, 36), the responsiveness of hair cells is accentuated by resonant electrical tuning mediated by colocalized Ca^{2+} channels and Ca^{2+}-activated K^+ channels. Analysis of the ionic currents underlying this process indicates that the presynaptic Ca^{2+} current closely follows the membrane potential (37). Linearity at the afferent synapse therefore ensures that responses sharpened by electrical resonance are faithfully propagated to the afferent nerve fiber. More generally, we propose that the direct proportionality of vesicle release, and also the postsynaptic current as observed in our experiments, to Ca^{2+} influx facilitates the encoding of auditory stimuli by allowing the synapse to be sensitive to low-amplitude stimuli, to possess a wide dynamic range for finely graded intensity discrimination, and to transfer complex waveforms with minimal distortion.

Materials and Methods

Experimental Preparation. Amphibian papillae were dissected from adult bullfrogs (*Rana catesbeiana*) that had been sedated by cold, doubly pithed, and decapitated. Papillae were maintained in oxygenated artificial perilymph containing 120 mM NaCl, 2 mM KCl, 1–2 mM $CaCl_2$, 3 mM D-glucose, 1 mM creatine, 1 mM sodium pyruvate, and 5 mM Hepes at pH 7.25 (230 mosmol·kg^{-1}). Amiloride (100 μM) was included during the dissection to block mechanoelectrical transduction channels and thereby lessen Ca^{2+}-mediated excitotoxicity.

After the sensory epithelium had been exposed by cutting and folding back the papilla's cartilaginous roof, the overlying tectorial membrane was removed with fine forceps. The papilla was positioned on a 125-μm-diameter tungsten wire such that its tonotopic axis paralleled the wire. When the preparation was stretched against the wire by securing it at four locations, the opposing forces applied to the cartilaginous roof and to the tissue beneath the main nerve bundle exerted stress on the sensory epithelium. The resulting strain usually split the epithelium along its tonotopic axis, exposing afferent fibers at their terminations on hair cells.

Electrophysiology. Hair cells and afferent fibers were visualized by differential-interference-contrast video microscopy with a ×63 water-immersion objective lens, ×5 optical magnification, and ×2 digital magnification. Whole-cell, voltage-clamp recordings were performed with two Axopatch 200A amplifiers (Axon Instruments, Union City, CA). Stimuli were presented and data acquired with programs written in LABVIEW (National Instruments, Austin, TX). Currents were low-pass filtered at 8 kHz and sampled at 50-μs intervals. During afferent fiber recordings, 1 μM tetrodotoxin was included in the perilymph to block voltage-gated Na^+ channels.

Recordings were obtained at room temperature with borosilicate glass pipettes pulled to resistances of 2–4 MΩ for hair-cell recordings and 8–10 MΩ for afferent fiber recordings. The internal solution for both recordings contained 110 mM CsCl, 0.5 mM $MgCl_2$, 2 mM EGTA, 5 mM Na_2ATP, and 10 mM Hepes at pH 7.3 (230 mosmol·kg^{-1}). A Cs^+-based internal solution was used to permit measurement of the presynaptic Ca^{2+} current, block some nonlinear K^+ conductances, and increase the postsynaptic input resistance. We chose not to introduce further blocking agents that might interfere with vesicle release; therefore, the presynaptic Ca^{2+} current was sometimes contaminated by the presence of residual, outward K^+ currents. Because these K^+ currents activated slowly, however, the initial peak inward current accurately reflected the magnitude of the Ca^{2+} current and was used for analysis. To assess the configuration of terminals from which we had recorded by confocal microscopy (LSM-510; Zeiss), we included the fluorophore Alexa 488 hydrazide at 50 μM in the postsynaptic internal solution.

Afferent terminals were held at a potential of −70 mV during postsynaptic recordings. For paired recordings, hair cells were maintained at −80 mV between stimulus presentations. Holding potentials were corrected post hoc for a 4-mV junction potential but not for the voltage drop across the uncompensated series resistance. Because the Ca^{2+} current in hair cells never exceeded 300 pA, this voltage error was at most 2 mV. The input resistances of afferent terminals measured 250–500 MΩ; the fibers' input capacitances were 1–4 pF. When measured in current-clamp mode, the resting potentials of afferent fibers were stable at −75 mV to −55 mV for up to 45 min of recording.

Data Analysis. The total charge transfer associated with each evoked postsynaptic current was calculated by integrating the change in the postsynaptic current during the presentation of a 100-ms test potential. The average postsynaptic current was defined as the total charge transfer divided by the duration of the stimulus. Data analysis was performed with MINIANALYSIS (SYNAPTOSOFT; Jaejin Software, Leonia, NJ), EXCEL (Microsoft), and MATHEMATICA (Wolfram Research, Champaign, IL). Unless otherwise noted, statistical results are reported as means ± standard deviations.

We thank Mr. B. Fabella for computer programming and Mr. A. Hinterwirth for the construction of apparatus. Dr. H. von Gersdorff, Dr. W. M. Roberts, and the members of our research group provided valuable comments on the manuscript. This work was supported by National Institutes of Health Grants DC00241 and GM07739. A.J.H. is an investigator of the Howard Hughes Medical Institute.

1. Prescott, E. D. & Zenisek, D. (2005) *Curr. Opin. Neurobiol.* **15,** 431–436.
2. Sullivan, W. E. & Konishi, M. (1984) *J. Neurosci.* **4,** 1787–1799.
3. Glowatzki, E. & Fuchs, P. A. (2002) *Nat. Neurosci.* **5,** 147–154.
4. Edmonds, B. W., Gregory, F. D. & Schweizer, F. E. (2004) *J. Physiol. (London)* **560,** 439–550.
5. Singer, J. H., Lassova, L., Vardi, N. & Diamond, J. S. (2004) *Nat. Neurosci.* **7,** 826–833.
6. Moser, T. & Beutner, D. (2000) *Proc. Natl. Acad. Sci. USA* **97,** 883–888.
7. Eisen, M. D., Spassova, M. & Parsons, T. D. (2004) *J. Neurophysiol.* **91,** 2422–2428.
8. Griesinger, C. B., Richards, C. D. & Ashmore, J. F. (2005) *Nature* **435,** 212–215.
9. Rutherford, M. A. & Roberts, W. M. (2006) *Proc. Natl. Acad. Sci. USA* **103,** 2898–2903.
10. Kollmar, R., Montgomery, L. G., Fak, J., Henry, L. J. & Hudspeth, A. J. (1997) *Proc. Natl. Acad. Sci. USA* **94,** 14883–14888.
11. Roberts, W. M., Jacobs, R. A. & Hudspeth, A. J. (1990) *J. Neurosci.* **10,** 3664–3684.
12. Issa, N. P. & Hudspeth, A. J. (1994) *Proc. Natl. Acad. Sci. USA* **91,** 7578–7582.
13. Platzer, J., Engel, J., Schrott-Fischer, A., Stephan, K., Bova, S., Chen, H., Zheng, H. & Streissnig, J. (2000) *Cell* **102,** 89–97.
14. Robertson, D. & Paki, B. (2002) *J. Neurophysiol.* **87,** 2734–2740.
15. Safieddine, S. & Wenthold, R. J. (1999) *Eur. J. Neurosci.* **11,** 803–812.
16. Mirghomizadeh, F., Pfister, M., Apayden, F., Petit, C., Kupka, S., Pusch, C. M., Zenner, H.-P. & Blin, N. (2002) *Neurobiol. Dis.* **10,** 157–164.
17. Beutner, D., Voets, T., Neher, E. & Moser, T. (2001) *Neuron* **29,** 681–690.
18. Johnson, S. L., Marcotti, W. & Kros, C. J. (2005) *J. Physiol. (London)* **563,** 177–191.
19. Schnee, M. E., Lawton, D. M., Furness, D. N., Benke, T. A. & Ricci, A. J. (2005) *Neuron* **47,** 243–254.
20. Brandt, A., Khimich, D. & Moser, T. (2005) *J. Neurosci.* **25,** 11577–11585.
21. Furukawa, T., Hayashida, Y. & Matsuura, S. (1978) *J. Physiol. (London)* **276,** 211–226.
22. Furukawa, T., Kuno, M. & Matsuura, S. (1982) *J. Physiol. (London)* **322,** 181–195.
23. Köppl, C. (1997) *J. Neurosci.* **17,** 3312–3321.
24. Lewis, E. R., Leverenz, E. L. & Koyama, H. (1982) *J. Comp. Physiol.* **145,** 437–445.
25. Yu, X., Lewis, E. R. & Feld, D. (1991) *J. Comp. Physiol. A* **169,** 241–248.
26. Simmons, D. D., Bertolotto, C. & Narins, P. M. (1992) *J. Comp. Neurol.* **322,** 191–200.
27. Smotherman, M. S. & Narins, P. M. (1999) *J. Neurosci.* **19,** 5275–5292.
28. Liberman, M. C. (1980) *Hear. Res.* **3,** 45–63.
29. Simmons, D. D., Bertolotto, C. & Leong, M. (1995) *Aud. Neurosci.* **1,** 183–193.
30. Trussell, L. O. (1999) *Annu. Rev. Physiol.* **61,** 477–496.
31. Roberts, W. M. (1994) *J. Neurosci.* **14,** 3246–3262.
32. Lenzi, D., Runyeon, J. W., Crum, J., Ellisman, M. H. & Roberts, W. M. (1999) *J. Neurosci.* **19,** 119–132.
33. Sewell, W. F. (1984) *J. Physiol. (London)* **347,** 685–696.
34. Thoreson, W. B., Rabl, K., Townes-Anderson, E. & Heidelberger, R. (2004) *Neuron* **42,** 595–605.
35. Pitchford, S. & Ashmore, J. F. (1987) *Hear. Res.* **27,** 75–83.
36. Ospeck, M., Eguiluz, V. M. & Magnasco, M. O. (2001) *Biophys. J.* **80,** 2597–2607.
37. Hudspeth, A. J. & Lewis, R. S. (1988) *J. Physiol. (London)* **400,** 275–297.

APPENDIX TWO

The unitary event underlying multiquantal excitatory postsynaptic currents at a hair-cell synapse

Li GL, Keen EC, Andor-Ardo D, Hudspeth AJ, and Von Gersdorff H.

(Under submittal)

The unitary event underlying multiquantal excitatory postsynaptic currents at a hair-cell synapse

Geng-Lin Li[1]*, Erica Keen[2]*, Daniel Andor-Ardó[2], A. J. Hudspeth[2], and Henrique von Gersdorff[1#]

[1]The Vollum Institute, Oregon Health & Science University, 3181 SW Sam Jackson Park Road, Portland, OR 97239, USA, and [2]Howard Hughes Medical Institute and Laboratory of Sensory Neuroscience, The Rockefeller University, 1230 York Avenue, New York, NY 10065, USA

* These authors contributed equally to this research.

[#] Corresponding author

ABSTRACT

Excitatory postsynaptic currents (EPSCs) at the synapses of sensory receptors and of some central-nervous-system neurons include large events thought to represent the synchronous release of the neurotransmitter from several synaptic vesicles in a process known as multiquantal release. However, determination of the unitary, quantal size underlying such putatively multiquantal events has proven difficult. Here we perform presynaptic membrane capacitance measurements together with paired recordings at an adult hair-cell ribbon synapse. These simultaneous pre- and postsynaptic measurements of exocytosis, together with electron-microscopic estimates of single-vesicle capacitance, allow us to estimate a single-vesicle EPSC charge of about -50 fC, a value in close agreement with the mean postsynaptic charge transfer of EPSCs recorded during periods of presynaptic hyperpolarization. By establishing the magnitude of the quantal response at this peripheral auditory synapse, we provide evidence that the majority of spontaneous and evoked EPSCs are multiquantal. We additionally demonstrate that the extent of multiquantal *versus* uniquantal release is Ca^{2+}-dependent.

INTRODUCTION

The release of chemical transmitter at a neuromuscular junction displays several properties that simplified its analysis at that specialized synapse. A single motor-nerve terminal has as many as a thousand presynaptic active zones, each of which contains a handful of docked synaptic vesicles. During normal neurotransmission, each vesicle's probability of release is low, about 0.1 to 0.2, and independent of that of other vesicles. Invasion of the presynaptic terminal by an action potential evokes an excitatory endplate current that represents the summation of many smaller events that are nearly—but not exactly—synchronous. Consistent with this hypothesis, lowering the probability of release by reducing the extracellular Ca^{2+} concentration reveals that each postsynaptic

event represents an integer multiple of a fixed quantum. Like a spontaneous miniature endplate current of similar magnitude, this quantum is thought to represent the postsynaptic response to the transmitter released from a single synaptic vesicle (Martin, 1976).

Although neurotransmission at synapses of the central nervous system shares the fundamental features of neuromuscular signaling, there are several important differences (Korn et al, 1993). Synaptic boutons are small and contain only one or a few active zones; as a consequence, the total number of vesicles released is small. The mechanism of transmitter release may vary between synapses or even at a particular synapse, with both complete exocytosis and kiss-and-run release of transmitter through a transitory fusion pore (Harata et al., 2001). The final feature, and the subject of the present communication, is so-called multiquantal release (Frerking et al., 1997): individual EPSCs vary severalfold in amplitude, suggesting that the larger events represent the synchronous release of transmitter equivalent to that contained in several vesicles. However, few studies have actually demonstrated this for spontaneous EPSCs (Tong and Jahr, 1994; Llano et al., 1998; Singer et al., 2002).

The ribbon synapses of vertebrate sensory receptors, including both neurons such as photoreceptors and epithelial cells such as hair cells, share numerous features with central-nervous synapses (Heidelberger et al., 2005; Sterling and Matthews, 2005). In particular, recordings from afferent fibers of the eighth cranial nerve reveal that individual postsynaptic events, whether spontaneous or evoked, vary widely in size (Glowatzki and Fuchs, 2002; Keen and Hudspeth, 2006). Although the large EPSC events have been presumed to be multiquantal, it has not proven

possible to demonstrate that each represents a multiple of a more basic response, that is, a quantum (Siegel, 1992; Rossi et al., 1994). Several factors complicate this endeavor. Fluctuation analysis of hair-cell capacitance measurements suggests a lower degree of multivesicular release by mature hair cells than is estimated from EPSC recordings of afferent fibers (Neef et al., 2007), and large EPSCs might originate from single vesicles with higher glutamate concentrations (Henze et al., 2002). In the present study, we have performed experiments meant to determine the quantal size underlying multiquantal EPSCs.

RESULTS

The amphibian papilla, the principal auditory receptor of the bullfrog, provides a useful experimental preparation for the investigation of neurotransmission at an adult ribbon synapse (Keen and Hudspeth, 2006). In the central portion of this organ, where afferent fibers are tuned to frequencies of 400-800 Hz (Smotherman and Narins, 2000), each hair cell contacts one or a few nerve fibers that may readily be visualized by differential-interference-contrast optics. At each of a hair cell's several active zones, synaptic vesicles are clustered around a roughly ellipsoidal presynaptic dense body, or synaptic ribbon. Upon release from vesicles, the excitatory neurotransmitter glutamate activates AMPA receptors in the postsynaptic membrane. It is straightforward to record by the whole-cell, tight-seal technique from both the presynaptic hair cells and the postsynaptic nerve fibers; simultaneous recordings from both elements of the synapse are also possible.

Spontaneous excitatory postsynaptic currents

Even in the absence of stimulation, afferent fibers displayed a brisk rate of spontaneous EPSCs (Figure 1A). Recordings from nine fibers revealed postsynaptic events at a rate of

$60 \pm 28\ s^{-1}$ and of widely varying magnitude. In determining the amplitude distribution of spontaneous EPSCs, we found that a low access resistance of the recording electrode, preferably less than 40 MΩ, was critical: the voltage error and filtering produced by a greater series resistance (R_s) systematically reduced the number of large events and skewed the amplitude distribution toward smaller events (Supplementary Figure 1). In satisfactory recordings with a stable low series resistance, the amplitude distribution of spontaneous EPSCs was typically well fit with a Gaussian function (Figure 1B). The amplitude of spontaneous EPSCs from seven fibers held at a membrane potential of -90 mV averaged -129 ± 24 pA and the coefficient of variation (CV) was 0.35.

Regardless of amplitude, most spontaneous EPSCs displayed smooth onset and decay phases (Figure 1C) without the interruptions characteristic of imperfectly superposed quantal events at the neuromuscular junction. Although lowering the ambient temperature from 22˚C to 15˚C desynchronizes release at the neuromuscular junction (Martin, 1976), this manipulation failed to reveal inflection points in the rise or decay phases of EPSCs (Supplementary Figure 2). For the average of ten events with amplitudes of -100 ± 1 pA from each of nine fibers, the 10% to 90% rise time was 0.25 ± 0.01 ms at 22˚C. In recordings from eight fibers, the decay phase of EPSCs was well fit by a single exponential function with an average time constant of 0.48 ± 0.01 ms (Figure 1D). These average EPSC rise and decay times half those reported for EPSCs of afferent fibers in the juvenile rat cochlea (Glowatski and Fuchs, 2001), but are very similar to those for miniature EPSCs at the compact neuromuscular junction of the larval zebrafish (Wen and Brehm, 2005).

If larger events arise from the superposition of multiple quantal events, they might be expected to display broadening owing to slight differences in the times at which their constituent vesicles undergo exocytosis (Wall and Usowicz, 1998). On the contrary, the temporal characteristics of EPSCs were independent of their amplitudes (Figure 1D). An analysis of seven fiber recordings showed no significant difference in the waveforms of

small and large EPSCs. Unlike the evoked postsynaptic events at the neuromuscular junction, then, the putatively multiquantal events at the hair cell's synapse reveal no substructure indicative of independent but nearly coincident vesicle fusions.

Possible superposition of events

Could large EPSCs be caused by the coincident fusion of single quanta? If the events are independent, the probability of coincidences depends only on the ability of the recording apparatus and our deconvolution algorithm to resolve individual EPSCs. A conservative estimate of the resolution of our maximum-entropy deconvolution algorithm at typical noise levels is that it can easily separate events as close as 0.5 ms. In a 10 s stretch of spontaneous activity in which we encountered 443 EPSCs, we would therefore expect fewer than ten to occur sufficiently close together to register as compound events. Yet more than 75% of the 443 events are large, leading to a mean size of two quanta. Is coincidence of independent events a good explanation for this? Intuitively, it seems not: the distribution of silences suggests a low rate of coincidence, about 2% for this record, yet the majority of the EPSCs are larger than the putatively quantal events.

Although we lack an understanding of the mechanism of vesicle release, we can consider two general modes of explanation. Our null hypothesis is that a single process generates independent events that occasionally coincide. Alternatively, there could be an additional process that orchestrates release such that compound events occur most of the time. Although coincidences would still occur under the alternate hypothesis, the additional cooperative process would explain most of the large events. When we compared the marginal likelihoods of these two hypotheses for the record described above, the weight of evidence in favor of the alternative explanation was a formidable $9 \cdot 10^{157}$. A similar calculation for a segment of same length but containing only one-tenth the number of events yielded a factor of $8 \cdot 10^{13}$. These results confirm the intuitive

impression that large EPSCs do not arise from the superposition of independently released quanta.

AMPA receptor antagonists

If large EPSCs represent multiquantal fusions at individual presynaptic active zones, they should generate a higher concentration of glutamate in the synaptic cleft than smaller, uniquantal events. A low-affinity, rapidly dissociating AMPA receptor antagonist, such as γ-D-glutamylglycine (γ-DGG), may be used to test whether larger EPSCs reflect the presence of more cleft glutamate. If this is the case, γ-DGG will block smaller EPSCs more effectively than larger ones (Wadiche and Jahr, 2001; Singer et al., 2004; Christie and Jahr, 2006).

When we applied γ-DGG, all EPSCs were reduced in amplitude compared to those recorded in control solution (Figure 2A). We determined the average amplitudes of two subsets of events (Figure 2A): those with amplitudes at the tenth percentile ($E_{10\%}$ values within ± 2 pA) and those with amplitudes at the ninetieth percentile ($E_{90\%}$ values within ± 2 pA). We normalized $E_{90\%}$ events in γ-DGG to their counterparts in control solution. Normalizing $E_{10\%}$ events by the same ratio revealed that $E_{10\%}$ events were blocked to a greater extent by γ-DGG (Figure 2B).

As a control, we applied NBQX, a high-affinity antagonist of AMPA receptors. In the presence of NBQX, $E_{90\%}$ and $E_{10\%}$ events were blocked to a similar extent (Figure 2C). The average normalized ratio of $E_{10\%}/E_{90\%}$ was statistically significant for γ-DGG *versus* control (n = 6), but not for NBQX *versus* control (n = 5; Figure 2D). These results suggest that the variability in EPSC amplitude is dominated by differences in presynaptic glutamate release rather than postsynaptic properties.

Ca^{2+} iontophoresis

Because afferent fibers in the amphibian papilla form multiple terminal branches onto hair cells, we ordinarily sample release events from several presynaptic active zones in our postsynaptic recordings. Thus, large EPSCs could in principle represent the simultaneous fusion of vesicles at distinct synaptic ribbons. To determine whether large events can originate from a single active zone, we bathed the preparation in a zero-Ca^{2+} solution to silence spontaneous activity and applied Ca^{2+} iontophoretically with a Ca^{2+}-filled pipette. Control experiments with fluorescent Ca^{2+} indicators confirmed that iontophoretic application was highly localized to the region near the application pipette (data not shown). Brief pulses of Ca^{2+} were sufficient to evoke EPSCs similar in amplitude to the largest spontaneous EPSCs recorded from the same fiber in control solution (Figure 3). Similar results were observed in three recordings. These experiments demonstrate that large EPSCs can arise from a single active zone and suggest that large spontaneous events originate from single synaptic ribbons.

Effect of hair-cell hyperpolarization

In an effort to demonstrate quantal components in the putatively multiquantal events, we next attempted to reduce the cytoplasmic concentration of Ca^{2+}, the presumed trigger for synaptic release, by presynaptic hyperpolarization during paired recordings. We compared spontaneous EPSCs before and after lowering the membrane potential of the hair cell from its control resting level of about -60 mV to -80 mV or -90 mV. Hyperpolarizing a hair cell reduced the frequency of EPSCs and selectively eliminated large events (Figure 4). The EPSC amplitude during hyperpolarization of ten hair cells to -90 mV fell to a mean value of -57 ± 13 pA. In the seven recordings with sufficient events for analysis, the coefficient of variation averaged 0.29, a value close to those obtained at the neuromuscular junction (Del Castillo and Katz, 1954) and at central synapses (Forti et al., 1997; Crowley et al., 2007; reviewed by Auger and Marty, 2000).

The effect of hyperpolarization on spontaneous EPSC amplitude was reversible; upon careful removal of the presynaptic patch pipette, large EPSC events reappeared, indicating that the small EPSCs did not reflect glutamate leakage from synaptic vesicles or an artifact of whole-cell dialysis. To determine the corresponding value for the postsynaptic charge transfer, we also calculated the integrals of the EPSCs recorded during hair-cell hyperpolarization. Because the waveforms of EPSCs do not vary with amplitude (Figure 1D), the charge-transfer distribution displayed a similar Gaussian profile with a mean value of -50.2 ± 2.8 fC when the hair cell was held at -90 mV.

Presynaptic capacitance measurements

During exocytosis, the incorporation of vesicular membrane into the plasma membrane transiently increases the capacitance of secretory cells (Neher and Marty, 1982; Angleson and Betz, 1997) and synaptic terminals (Heidelberger et al., 1994; von Gersdorff and Matthews, 1994; Sun and Wu, 2001; Hallerman et al., 2004). To obtain an estimate of the rate of vesicle fusion, we stimulated exocytosis by depolarizing a hair cell from a holding potential of -90 mV to -30 mV and measured the change in membrane capacitance. We simultaneously recorded the presynaptic Ca^{2+} current borne by L-type channels (Parsons et al., 1994; Rodriguez-Contreras and Yamoah, 2001; Schnee and Ricci, 2003).

At the holding potential of -90 mV, 15 hair cells from the bullfrog's amphibian papilla displayed an average capacitance of 11.6 ± 1.5 pF. A 500-ms depolarization increased their capacitance by 99 ± 39 fF. Because neither the series resistance nor the membrane resistance changed after the depolarization, the capacitance measurement was devoid of conductance artifacts (Figure 5A; see Horrigan and Bookman, 1994). The capacitance change increased monotonically for hair-cell depolarizations from 10 ms to 1000 ms (Figure 5B). Because the capacitance returned to its baseline value with an exponential time constant of approximately 11 s (data not shown), capacitance measurements made within 100-500 ms of the depolarizing pulse should not be

significantly affected by membrane retrieval. The extracellular application of 200-400 μM Cd^{2+} blocked both the presynaptic Ca^{2+} current and the capacitance increase in four experiments (Figure 5C), indicating that depolarization-evoked vesicle fusion requires Ca^{2+} influx.

Paired pre- and postsynaptic recordings

Simultaneous recordings from a hair cell and its innervating fiber permitted us to correlate the rate of vesicle fusion, as manifested by a change in the presynaptic capacitance, with the rate of transmitter release, as measured by an evoked postsynaptic current. Presynaptic depolarizations that produced robust capacitance changes also resulted in large postsynaptic responses with highly overlapping events (Figure 6A). As a measure of the postsynaptic response, we therefore measured the cumulative postsynaptic charge transfer, or integral of the postsynaptic current.

During a sustained depolarization, the postsynaptic charge transfer first rose briskly, then continued to increase at a lower, nearly constant rate (Figure 6B). Averaged over 11 recordings, the kinetics of the postsynaptic response accorded with that of the average presynaptic capacitance increase in six hair cells. These results are consistent with exocytosis from a readily releasable pool of vesicles followed by a reserve pool (Moser and Beutner, 2000; Spassova et al., 2004; Johnson et al., 2005; Schnee et al., 2005; Rutherford and Roberts, 2008). The close agreement between postsynaptic charge transfer and capacitance increases suggests that neither desensitization nor saturation of AMPA receptors occurs to a significant degree at this synapse. This conclusion agrees with that drawn from *in vivo* afferent-fiber recordings from the goldfish's sacculus, which showed no change in the size of miniature EPSP during periods of silence or intense sound stimulation (Furukawa et al., 1978). Ribbon synapses between bipolar and amacrine cells of the retina also display no desensitization during a prolonged presynaptic depolarization (Singer and Diamond, 2006).

The postsynaptic charge transfer increased concomitantly with the presynaptic capacitance (Figure 6C); the relation was approximately linear, as has also been observed at a retinal ribbon synapse (von Gersdorff et al., 1998) and a central auditory synapse when saturation of AMPA receptors is blocked (Sun and Wu, 2001; Sakaba, 2006). For a total of 22 depolarizations in 7 cell pairs, the slope of the relation was -1.01 ± 0.07 $kC \cdot F^{-1}$. As discussed below, this value can be used to obtain an independent estimate of the quantal response.

Electron microscopy and the capacitance of single vesicles

To estimate the capacitance change expected from fusion of a single synaptic vesicle, we conducted electron microscopy on hair cells in the region of the amphibian papilla from which our physiological results originated. At 23 ribbon-type active zones (Figure 7A), we measured the dimensions of 119 vesicles whose perimeters were bounded completely by trilaminar membrane, and which therefore lay largely or entirely within the 70-nm sections. The geometric mean of the greatest and least diameters, measured at the center of the trilaminar structure, was 37.6 ± 4.5 nm; the arithmetic mean was 37.8 ± 4.5 nm. The amplitude distribution was well fit by a Gaussian function with mean value of 40.3 nm (Figure 7B). The synaptic vesicles at this synapse are therefore of dimensions similar to those at the ribbon synapses of other hair cells (Lenzi *et al.*, 1999; Schnee et al., 2005; Neef et al., 2007). Assuming a standard specific membrane capacitance of 10 $mF \cdot m^{-2}$, we obtain a best estimate of the single-vesicle capacitance of 45 ± 11 aF.

DISCUSSION

The initial synapse of the auditory system offers the experimental advantage that both the presynaptic element—the sensory hair cell—and the postsynaptic element—the eighth-nerve afferent fiber—are accessible for recording. Moreover, the anatomical features of

the preparation are favorable. In the central nervous system, the complex anatomy of postsynaptic neurons complicates the analysis of electrical recordings, for some synaptic inputs lie at a greater electrotonic distance than others from the recording site (Bekkers and Stevens, 1995). At hair-cell synapses, however, both the pre- and the postsynaptic elements are electrically compact. Using the hair-cell synapses of the bullfrog's amphibian papilla, we have been able not only to conduct whole-cell fiber recordings to study excitatory postsynaptic currents, but also to make hair-cell capacitance measurements to examine the extent of exocytosis.

Paired recordings and the unitary charge transfer

The large variation in the amplitudes of single postsynaptic events at the synapses of the central nervous system and sensory organs suggests that neurotransmitter can be released in amounts corresponding to multiple quanta. However, because it is difficult to determine the response owing to transmitter release from a single vesicle, the unitary or quantal event, it is usually impossible to ascertain how many vesicles contribute to a multiquantal response. Under ordinary recording conditions, amplitude histograms of spontaneous EPSCs at hair-cell synapses show no apparent substructure indicative of independently fusing vesicles. The effect of hyperpolarization suggests, however, that these synapses can release transmitter in smaller quantities that yield postsynaptic events of about -50 fC. These EPSCs might represent the response to single-vesicle fusion events. Our dual recordings, which relate the postsynaptic response to the change in presynaptic capacitance, offer a means of buttressing this conclusion by providing an independent estimate of the unitary charge transfer.

We wish to determine the mean postsynaptic charge transfer q associated with the release of transmitter from a single vesicle, the fusion of which increases the presynaptic membrane's capacitance by an amount c. If a protracted depolarization of a hair cell

causes a measured increase C in the presynaptic membrane capacitance and evokes a postsynaptic response with a total charge transfer Q, then we expect that

$$\frac{q}{c} = \left(\frac{P}{R}\right)\frac{Q}{C} \text{ or } q = \left(\frac{\pi d^2 \mathcal{C} P}{R}\right)\frac{Q}{C}.$$

Here P is the probability that a vesicle's fusion occurs at a presynaptic active zone and can be sensed by the postsynaptic receptors and R is the innervation ratio of afferent fibers per stimulated hair cell. The fusion of a single vesicle increases the presynaptic capacitance by an amount $c = \pi d^2 \mathcal{C}$, in which d is the diameter of a vesicle and $\mathcal{C}$ is the specific capacitance of the vesicle membrane; our electron-microscopic results suggest that $c = 45$ aF. If $P = R = 1$, then the value of $Q/C = -1.01$ kC·F^{-1} adduced from our physiological measurements (Figure 6C) implies that $q = -50$ fC, a value in very good agreement with that obtained from histograms of the postsynaptic charge transfer during hair-cell hyperpolarization to -90 mV (Figure 4D).

The foregoing analysis rests upon three important assumptions. First, we suppose that most synaptic vesicles are released at presynaptic active zones, so that $P \approx 1$. For hair cells acutely isolated from the bullfrog's sacculus, though, there is some ectopic exocytosis (Lenzi et al., 2002; Zenisek *et al.*, 2003). If the same occurs for hair cells of the amphibian papilla, the value of P might be less than unity. It is also possible that some afferent terminals are separated from their hair cells during dissection, again with the consequence of a lower value for P. The second assumption is that each depolarized hair cell contacts only the single afferent fiber involved in a simultaneous recording, so that the innervation ratio $R \approx 1$. Several lines of evidence support the contention that each afferent fiber receives its input from but a single hair cell; in particular, holding the hair cell in a paired recording at a potential of -80 mV or -90 mV suppresses significantly the frequency of postsynaptic activity, whereas the death of the hair cell interrupts all postsynaptic activity (data not shown). It is less certain, however, that each hair cell synapses with only a single afferent fiber; if this is not the case, R might exceed unity.

Finally, we assume that the specific capacitance of the membrane of a synaptic vesicle is similar to that for other biological membranes, so that $C \approx 10\ mF \cdot m^{-2}$ (Fettiplace et al., 1971). Because each vesicle contains an extraordinary number of transmembrane proteins (Takamori *et al.*, 2006) the true value of C might differ from that of cell membranes. However, expression of a high density of transmembrane proteins in cultured cells has been shown to not alter the value of the specific membrane capacitance (Gentet et al., 2000).

Remarkably enough, the uncertainties associated with these three assumptions make contributions in the same direction to our estimate of q. If P were less than one or R exceeded unity, the consequence would be that some of the measured change in presynaptic capacitance would not be associated with a detectable postsynaptic response. As a result, the true value of q—and thus the amplitude of the unitary postsynaptic current—could only be *larger* than suggested by our calculation. The critical point is that the actual value of q is unlikely to be significantly *smaller* than we calculate. Our dual recordings therefore eliminate the greatest problem in most estimates of the magnitude of unitary events, namely that these events are so small that they are hidden in the noise of a recording.

The foregoing argument is subject to two reservations. First, we made no correction in our estimate of the vesicle diameter d for distortion produced by electron-microscopic preparation. In many instances, though, fixation, dehydration, and embedding inflict a shrinkage artifact of approximately 20% (Tatsuoka and Reese, 1989). If the actual vesicle diameter is greater than measured by this amount, we might overestimate q by about 40%. However, it is improbable that we would make an error of twofold or more, as would be required to miss unitary events of half the size detected. Moreover, synaptic vesicles preserved by high-pressure rapid freezing and examined by cryo-electron microscopy have diameters identical to those prepared conventionally (Takamori et al., 2006). The other qualification is that the release of some transmitter by

a kiss-and-run mechanism could artifactitiously lower our estimate of the capacitance increase associated with a given postsynaptic response. Optical measurements from isolated retinal bipolar cells and hair cells suggest, however, that most release involves the complete fusion of vesicles at synaptic ribbons (Llobet et al. 2003; Zenisek *et al.*, 2003), which are then replenished from a reserve pool (Lenzi et al., 2002; LoGiudice et al., 2008).

Number of AMPA receptors activated by one vesicle fusion

Our estimate of about -57 pA for the unitary response is reasonable in the light of other information about the ribbon synapses of hair cells. At the -90 mV holding potential of afferent fibers, this quantal size corresponds to a postsynaptic conductance of about 600 pS. If each AMPA receptor at the ribbon synapse in the bullfrog's amphibian papilla has the conductance of about 20 pS observed for AMPA receptors in the auditory system (Parks, 2000; Sahara and Takahashi, 2001), the unitary response we measure involves the gating of approximately 30 receptors. The largest putatively multiquantal responses that we have encountered, with magnitudes near -300 pA, would correspond to the activation of some 150 receptors. Freeze-fracture electron microscopy indicates that the postsynaptic membrane of afferent synapses in the mammalian cochlea is studded at a density of 3000 μm^{-2} with large particles thought to be AMPA receptors (Saito, 1990). The afferent terminals at the ribbon synapse of the sacculus, another receptor organ of the bullfrog's internal ear, display intramembrane particles of a similar density (Jacobs and Hudspeth, 1990). In the region of the amphibian papilla under investigation, the postsynaptic membrane specialization at each ribbon synapse is about 150 nm across and 250 nm in length (Simmons *et al.*, 1995; Keen and Hudspeth, 2006). If the membrane at this ribbon synapse holds AMPA receptors at the density observed by freeze-fracture electron microscopy, there are about 110 such receptors directly opposing each presynaptic active zone. The rough agreement between this value and that for the

maximal receptor activation provides further support for our estimate of the unitary response. A large density of AMPA receptors at the hair cell synapse allows avoidance of receptor saturation and thus increases the dynamic range of the synapse. By contrast, conventional bouton-type synapses have an AMPA receptor density of 1000 μm^{-2} and smaller quantal size (Raghavachari and Lisman, 2004).

Large EPSC events originate at individual synaptic ribbons

Because hair cells of the auditory papilla form several ribbon-type active zone sites onto one afferent terminal (Schnee et al., 2005; Keen and Hudspeth, 2006), large EPSCs could in principle represent the simultaneous fusion of single vesicles at different synaptic ribbons. However, brief, local iontophoresis of Ca^{2+} triggers large EPSCs (Figure 3B). Furthermore, the differential block of small and large EPSCs by γ-DGG argues that large EPSCs do not originate from the simultaneous exocytosis of single quanta at different locations along the afferent terminal. Finally, the statistics of EPSC occurrence renders the probability that large EPSCs represent the random superposition of small EPSCs vanishingly small. Large events therefore originate at individual active zones through the release of a bolus of glutamate onto a single postsynaptic cluster of AMPA receptors.

Coordinated, compound, and sequential exocytosis

Our results demonstrate the occurrence in afferent fibers of unitary events about -55 pA in amplitude. Whether recorded as spontaneous EPSCs or as components of evoked EPSCs, larger postsynaptic signals may therefore represent the summation of several such unitary events. The usual response of about -130 pA implies the release of transmitter equivalent to two or three quanta; the largest events, about -300 pA in magnitude, correspond to the synchronous exocytosis of five or six quanta. Because we detected no temporal substructure in the waveforms of large events, we do not have evidence that they arise from independent vesicle fusions and cannot distinguish among

three candidate mechanisms for the production of such signals: highly synchronous, perhaps cooperative fusion at distinct docking sites (Singer et al., 2004); compound fusion, in which several vesicles fuse together before undergoing exocytosis at a single site (Matthews and Sterling, 2008); and sequential fusion, in which exocytosis by one docked vesicle initiates the rapid, piggyback fusion of several additional ones stacked along the ribbon (Neef et al., 2007). Because we have not observed quantal peaks in amplitude histograms, we cannot rule out the further possibility that the amount of transmitter contained in a single vesicle is subject to endogenous regulation. If this were the situation at the hair-cell synapse, large EPSCs could arise from effectively multiquantal, but univesicular, fusion events (Henze et al., 2001).

Physiological role of multiquantal release

The predominance of multiquantal release at hair-cell synapses raises the question of the rationale for such an energetically expensive process. We propose two potential, and not necessarily mutually exclusive, explanations. In the auditory epithelium, a tonotopic array of hair cells provides finely graded frequency information to central processing centers. To prevent undue mixing of information between frequency channels, an afferent ordinarily receives input from only one or a few hair cells. With few active zones and docked vesicles available for signaling, the auditory system may compensate by raising the release probability at each active zone. Under these circumstances, multiquantal events may be merely a statistical consequence of the high release probability necessary for encoding sensory signals. An alternative possibility is that the size of presynaptic fusion events is dynamically regulated to encode signal intensity, provide precise phase-locked temporal information, or reduce the background noise that arises from the high sensitivity of auditory receptor cells. Further experiments will be needed to determine the contribution of multiquantal signaling to information transfer at this peripheral auditory synapse.

EXPERIMENTAL PROCEDURES

Preparation

Adult bullfrogs (*Rana catesbeiana*) were sedated in an ice bath for about 20 min, then double-pithed and decapitated. Amphibian papillae were dissected in oxygenated artificial perilymph containing (in mM): 120 NaCl, 2 KCl, 2 $CaCl_2$, 3 **D**-glucose, 1 creatine, and 5 HEPES at pH 7.30 (240 mOsmol·kg^{-1}). Hair cells and their innervating afferent fibers were exposed by procedures described previously (Keen and Hudspeth, 2006). During recordings, the preparation was placed in HEPES-buffered perilymph or perfused continuously at 2-3 ml/min with bicarbonate-buffered perilymph continuously bubbled with 95% O_2 and 5% CO_2 and containing (in mM): 95 NaCl, 2 KCl, 2 $CaCl_2$, 1 $MgCl_2$, 3 **D**-glucose, 1 creatine, 1 Na-pyruvate, and 25 $NaHCO_3$ at pH 7.30 (230 mOsmol·kg^{-1}). Tetrodotoxin was added to the recording solution at a concentration of 1 μM to block voltage-gated Na^+ channels.

Electrophysiology

Whole-cell recordings were obtained at room temperature with borosilicate glass pipettes pulled to resistances of 2-4 MΩ for hair cells and 8-10 MΩ for afferent fibers. Internal solutions were composed of either (in mM): 110 CsCl, 0.5 $MgCl_2$, 2 EGTA, 5 Na_2ATP, and 10 HEPES at pH 7.30 (240 mOsmol·kg^{-1}) or 80 Cs-gluconate, 20 CsCl, 10 TEA-Cl, 2 EGTA, 3 Mg-ATP, 0.5 Na-GTP, and 10 HEPES at pH 7.30 (240 mOsmol·kg^{-1}). Whole-cell voltage-clamp recordings of afferent fibers and hair cells were performed with an Axopatch 200A amplifier (Axon Instruments, Union City, CA) or a double EPC-9/2 amplifier (HEKA Elektronik, Lambrecht/Pfalz, Germany).

Hair cells and afferent fibers were held at -80 mV or -90 mV. Holding potentials were corrected for junction potentials (4 mV for the CsCl and 10 mV for the gluconate solution), but not for the voltage drop across the uncompensated series resistance. The

average series resistance (R_s) in the whole-cell mode was 17.8 ± 6.3 MΩ for the hair cell recordings (n=18) and 30.9 ± 8.7 MΩ for afferent fiber recordings (n = 15). The voltage-clamp time constant was about 100-200 μs for hair cell and afferent fiber recordings. An excessive series resistance could cause significant errors in EPSC amplitudes: amplitude distributions displayed a significant leftward shift if the series resistance exceeded 40 MΩ (Supplementary Figure 1), so we excluded from analysis all afferent-fiber recordings meeting that criterion.

For iontophoretic stimulation, borosilicate glass pipettes were pulled to resistances of 80-100 MΩ when filled with 0.5 M $CaCl_2$ at pH 7.0. The hair-cell synapse was bathed in a zero $CaCl_2$ plus 0.1 mM EGTA external solution. A steady-state holding current was applied to prevent diffusional leakage of Ca^{2+} from the pipette. Iontophoretic currents of 1-3 nA were delivered with an Axoclamp-2A amplifier (Axon Instruments, Union City, CA).

Stimuli were presented and data acquired with programs written in LabVIEW (National Instruments, Austin, TX) or with Pulse software (HEKA). Currents were low-pass filtered at 8 kHz and sampled at 50-μs intervals or filtered at 2 kHz and sampled at 10-μs intervals.

Statistical analysis of coincident EPSCs

We used a Poisson process to model the generation of events. The Poisson distribution gives the probability of single or compound events. The likelihood of a record with a set $\{a_i\}$ of m events of non-zero amplitude is

$$L = e^{-(M-m)\lambda} \prod_{i=1}^{m} \sum_{n=1}^{\infty} \frac{e^{-\lambda} \lambda^n q_n(a_i)}{n!}$$

in which $M = T / \Delta t$ is the length T of the record divided by the deconvolution resolution Δt, and $q_n(a)$ gives the likelihood of an event of size a being compounded of n events. The tension between the rate λ determined by the silence as opposed to the mean

amplitude of events is represented by competition between the initial exponential term and the product term. Significant jitter in the generation and detection of amplitudes $\{a_i\}$ means that q tends to be broad: most of the histograms we looked at did not display discernable peaks at integer multiples of the quantum. We require that both mean and variance of q_n should scale with n. In order to enforce positivity of event sizes—there are no EPSCs with current flowing in the wrong direction—we used $q_n(a) \sim \text{Gamma}(n\alpha^2\beta, \alpha\beta)$, in which α is the mean and β is the accuracy (inverse variance) when n=1. We also performed the calculation with $q_n(a) \sim \text{Normal}(n\alpha, n/\beta)$, but it did not make a significant difference. The model admits two kinds of solutions, corresponding to the null and alternate hypotheses. The latter intrinsically needs an extra parameter describing the rate at which orchestrated fusion occurs. However, by using a family of models that spans both null and alternate hypotheses, we simplify the problem (Gelman et al., 2004). When α is small and β is large, compound events are explained by the coincidence of multiple small events of size α. Conversely, when α is large and β is small, it is the action of orchestrated release that explains compound events. We marginalize over λ and β, leaving the marginal likelihood as a function of α only. Optimizing α gives the maximum-likelihood solution at $\hat{\alpha}$ from the family of models. The null hypothesis is simply the special case of $\alpha \equiv 1$ quantum. The ratio $L(\alpha = \hat{\alpha}) / L(\alpha = 1)$ can be interpreted as evidence in favor of the alternate hypothesis.

Capacitance measurements and data analysis

Whole-cell membrane capacitance measurements from hair cells were performed under voltage-clamp with the "Sine + DC" method (Lindau and Neher, 1988) using a double EPC9/2 amplifier and Pulse software (HEKA). Pipettes were coated with wax to minimize stray capacitance and to achieve better pipette capacitance compensation. A 1-kHz sinusoidal command voltage of 50 mV peak-to-peak magnitude was superposed on the hair-cell holding potential of -90 mV. The resulting current response was used to

calculate presynaptic capacitance, membrane resistance, and series resistance with the Pulse software emulator of a lock-in amplifier (Gillis, 2000).

Data analysis was performed with MINIANALYSIS (SYNAPTOSOFT; Jaejin Software, Leonia, NJ), EXCEL (Microsoft), MATHEMATICA (Wolfram Research, Champaign, IL), and IGOR Pro (Wavemetrics, Lake Oswego, OR). Spontaneous EPSC events were also detected and analyzed with software written by Dr. H. Taschenberger (Max Planck Institute, Göttingen, Germany) using an optimally scaled template method (Clements and Bekkers, 1997). Significance of average data point differences was tested using a paired Student's *t*-test. All statistical results are reported as means ± standard deviations for the indicated number of measurements.

ACKNOWLEDGMENTS

The authors thank W. Almers, M. Frerking, C. Jahr, and L. Trussell for discussions and the members of their research groups for helpful comments on the manuscript. This research was funded by National Institutes of Health grants DC04274 and DC00241. GLL was the recipient of a NOHR pilot grant; HvG received support from a Human Frontier Science Program grant; AJH is an Investigator of the Howard Hughes Medical Institute.

REFERENCES

Angleson, J.K., and Betz, W.J. (1997). Monitoring secretion in real time: capacitance, amperometry, and fluorescence compared. Trends Neurosci. *20*, 281-287.

Auger, C., and Marty, A. (2000). Quantal currents at single-site central synapses. J Physiol *526*, 3-11.

Awatramani, G.B., Price, G.D., and Trussell, L.O. (2005). Modulation of transmitter release by presynaptic resting potential and background calcium levels. Neuron *48*, 109-121.

Bekkers, J.M., and Stevens, C.F. (1996). Cable properties of cultured hippocampal neurons

determined from sucrose-evoked miniature EPSCs. J. Neurophysiol. 75, 1250-1255.

Christie, J.M., and Jahr, C.E. (2006). Multivesicular release at Schaffer collateral-CA1 hippocampal synapses. J Neurosci *26*, 210-216.

Clements, J.D., and Bekkers, J.M. (1997). Detection of spontaneous synaptic events with an optimally scaled template. Biophys J *73*, 220-229.

Crowley, J.J., Carter, A.G., and Regehr, W.G. (2007). Fast vesicle replenishment and rapid recovery from desensitization at a single synaptic release site. J Neurosci *27*, 5448-5460.

Del Castillo, J., and Katz, B. (1954). Quantal components of the endplate potential. J. Physiol. *124*, 560-573.

Edmonds, B.W., Gregory, F.D., and Schweizer, F.E. (2004). Evidence that fast exocytosis can be predominantly mediated by vesicles not docked at active zones in frog saccular hair cells. J Physiol *560*, 439-450.

Fettiplace, R., Andrews, D.M., and Haydon, D.A. (1971). The thickness, composition and structure of some lipid bilayers and natural membranes. J. Membr. Biol. 5, 277-296.

Forti, L., Bossi, M., Bergamaschi, A., Villa, A., and Malgaroli, A. (1997). Loose-patch recordings of single quanta at individual hippocampal synapses. Nature *388*, 874-878.

Frerking, M., Borges, S., and Wilson, M. (1997). Are some minis multiquantal? J Neurophysiol *78*, 1293-1304.

Furukawa, T., Hayashida, Y., and Matsuura, S. (1978). Quantal analysis of the size of excitatory post-synaptic potentials at synapses between hair cells and afferent nerve fibres in goldfish. J Physiol *276*, 211-226.

Gelman, A., Carlin, J.B., Stern, H.S. and Rubin, D.B. (2004) *Bayesian Data Analysis*, Second

Edition (Chapman and Hall/CRC, Boca Raton).

Gentet, L.J., Stuart, G.J., and Clements, J.D. (2000). Direct measurement of specific membrane capacitance in neurons. Biophys J *79*, 314-320.

Gillis, K.D. (2000). Admittance-based measurement of membrane capacitance using the EPC-9 patch-clamp amplifier. Pflugers Arch *439*, 655-664.

Glowatzki, E., and Fuchs, P.A. (2002). Transmitter release at the hair cell ribbon synapse. Nat Neurosci *5*, 147-154.

Goutman, J.D., and Glowatzki, E. (2007). Time course and calcium dependence of transmitter release at a single ribbon synapse. Proc Natl Acad Sci U S A *104*, 16341-16346.

Griesinger, C.B., Richards, C.D., and Ashmore, J.F. (2005). Fast vesicle replenishment allows indefatigable signaling at the first auditory synapse. Nature *435*, 212-215.

Hallermann, S., Pawlu, C., Jonas, P., and Heckmann, M. (2003). A large pool of releasable vesicles in a cortical glutamatergic synapse. Proc Natl Acad Sci U S A *100*, 8975-8980.

Harata, N., Pyle, J.L., Aravanis, A.M., Mozhayeva, M., Kavalali, E.T., and Tsien, R.W. (2001). Limited numbers of recycling vesicles in small CNS nerve terminals: implications for neural signaling and vesicular cycling. Trends Neurosci *24*, 637-643.

Heidelberger, R., Heinemann, C., Neher, E., and Matthews, G. (1994). Calcium dependence of the rate of exocytosis in a synaptic terminal. Nature *371*, 513-515.

Heidelberger, R., Thoreson, W.B., and Witkovsky, P. (2005). Synaptic transmission at retinal ribbon synapses. Prog Retin Eye Res *24*, 682-720.

Henze, D.A., McMahon, D.B., Harris, K.M., and Barrionuevo, G. (2002). Giant miniature EPSCs at the hippocampal mossy fiber to CA3 pyramidal cell synapse are monoquantal. J

Neurophysiol *87*, 15-29.

Horrigan, F.T., and Bookman, R.J. (1994). Releasable pools and the kinetics of exocytosis in adrenal chromaffin cells. Neuron *13*, 1119-1129.

Issa, N.P., and Hudspeth, A.J. (1994). Clustering of Ca^{2+} channels and Ca^{2+}-activated K^{+} channels at fluorescently labeled presynaptic active zones of hair cells. Proc Natl Acad Sci U S A *91*, 7578-7582.

Jacobs, R.A., and Hudspeth, A.J. (1990). Ultrastructural correlates of mechanoelectrical transduction in hair cells of the bullfrog's internal ear. Cold Spring Harb Symp Quant Biol *55*, 547-561.

Johnson, S.L., Marcotti, W., and Kros, C.J. (2005). Increase in efficiency and reduction in Ca^{2+} dependence of exocytosis during development of mouse inner hair cells. J Physiol *563*, 177-191.

Keen, E.C., and Hudspeth, A.J. (2006). Transfer characteristics of the hair cell's afferent synapse. Proc Natl Acad Sci U S A *103*, 5537-5542.

Korn, H., Bausela, F., Charpier, S., and Faber, D.S. (1993). Synaptic noise and multiquantal release at dendritic synapses. J. Neurophysiol. *70*, 1249-1254.

Lenzi, D., Crum, J., Ellisman, M.H., and Roberts, W.M. (2002). Depolarization redistributes synaptic membrane and creates a gradient of vesicles on the synaptic body at a ribbon synapse. Neuron *36*, 649-659.

Lenzi, D., Runyeon, J.W., Crum, J., Ellisman, M.H., and Roberts, W.M. (1999). Synaptic vesicle populations in saccular hair cells reconstructed by electron tomography. J Neurosci *19*, 119-132.

Lindau, M., and Neher, E. (1988). Patch-clamp techniques for time-resolved capacitance measurements in single cells. Pflugers Arch *411*, 137-146.

Llano, I., Gonzalez, J., Caputo, C., Lai, F.A., Blayney, L.M., Tan, Y.P., and Marty, A. (2000). Presynaptic calcium stores underlie large-amplitude miniature IPSCs and spontaneous calcium transients. Nat Neurosci *3*, 1256-1265.

Llobet, A., Beaumont, V., and Lagnado, L. (2003). Real-time measurement of exocytosis and endocytosis using interference of light. Neuron *40*, 1075-1086.

LoGiudice, L., Sterling, P., and Matthews, G. (2008). Mobility and turnover of vesicles at the synaptic ribbon. J Neurosci *28*, 3150-3158.

Matthews, G. and Sterling, P. (2008). Evidence that vesicles undergo compound fusion on the synaptic ribbon. J Neurosci *28*, 5403-5411.

Martin, A.R. (1976). Junctional transmission II. Presynaptic mechanisms. In Handbook of Physiology: Cellular Biology of Neurons, Vol. I, E. Kandel ed., pp. 329-355

Moser, T., and Beutner, D. (2000). Kinetics of exocytosis and endocytosis at the cochlear inner hair cell afferent synapse of the mouse. Proc Natl Acad Sci U S A *97*, 883-888.

Neef, A., Khimich, D., Pirih, P., Riedel, D., Wolf, F., and Moser, T. (2007). Probing the mechanism of exocytosis at the hair cell ribbon synapse. J Neurosci *27*, 12933-12944.

Neher, E., and Marty, A. (1982). Discrete changes of cell membrane capacitance observed under conditions of enhanced secretion in bovine adrenal chromaffin cells. Proc Natl Acad Sci U S A *79*, 6712-6716.

Parks, T.N. (2000). The AMPA receptors of auditory neurons. Hear. Res. *147*, 77-91.

Parsons, T.D., Lenzi, D., Almers, W., and Roberts, W.M. (1994). Calcium-triggered exocytosis and endocytosis in an isolated presynaptic cell: capacitance measurements in saccular hair cells. Neuron *13*, 875-883.

Raghavachari, S., and Lisman, J.E. (2004). Properties of quantal transmission at CA1 synapses. J Neurophysiol *92*, 2456-2467.

Rodriguez-Contreras, A., and Yamoah, E.N. (2001). Direct measurement of single-channel Ca^{2+} currents in bullfrog hair cells reveals two distinct channel subtypes. J Physiol *534*, 669-689.

Rossi, M.L., Martini, M., Pelucchi, B., and Fesce, R. (1994). Quantal nature of synaptic transmission at the cytoneural junction in the frog labyrinth. J Physiol *478*, 17-35.

Rutherford, M.A., and Roberts, W.M. (2006). Frequency selectivity of synaptic exocytosis in frog saccular hair cells. Proc Natl Acad Sci U S A *103*, 2898-2903.

Sahara, Y., and Takahashi, T. (2001). Quantal components of the excitatory postsynaptic currents at a rat central auditory synapse. J Physiol *536*, 189-197.

Saito, K. (1990). Freeze-fracture organization of hair cell synapses in the sensory epithelium of guinea pig organ of Corti. J Electron Microsc Tech *15*, 173-186.

Sakaba, T. (2006). Roles of the fast-releasing and the slowly releasing vesicles in synaptic transmission at the calyx of Held. J Neurosci *26*, 5863-5871.

Schnee, M.E., Lawton, D.M., Furness, D.N., Benke, T.A., and Ricci, A.J. (2005). Auditory hair cell-afferent fiber synapses are specialized to operate at their best frequencies. Neuron *47*, 243-254.

Schnee, M.E., and Ricci, A.J. (2003). Biophysical and pharmacological characterization of voltage-gated calcium currents in turtle auditory hair cells. J Physiol *549*, 697-717.

Siegel, J.H. (1992). Spontaneous synaptic potentials from afferent terminals in the guinea pig cochlea. Hear Res *59*, 85-92.

Simmons, D.D., Bertolotto, C., and Leong, M. (1995). Synaptic ultrastructure within the

amphibian papilla of Rana pipiens pipiens: Rostrocaudal differences. Aud Neurosci *1*: 183-193.

Singer, J.H., and Diamond, J.S. (2006). Vesicle depletion and synaptic depression at a mammalian ribbon synapse. J. Neurophysiol. *95*, 3191-3198.

Singer, J.H., Lassova, L., Vardi, N., and Diamond, J.S. (2004). Coordinated multivesicular release at a mammalian ribbon synapse. Nat Neurosci *7*, 826-833.

Smotherman, M.S., and Narins, P.M. (2000). Hair cells, hearing and hopping: a field guide to hair cell physiology in the frog. J Exp Biol *203*, 2237-2246.

Spassova, M.A., Avissar, M., Furman, A.C., Crumling, M.A., Saunders, J.C., and Parsons, T.D. (2004). Evidence that rapid vesicle replenishment of the synaptic ribbon mediates recovery from short-term adaptation at the hair cell afferent synapse. J Assoc Res Otolaryngol *5*, 376-390.

Sterling, P., and Matthews, G. (2005). Structure and function of ribbon synapses. Trends Neurosci *28*, 20-29.

Sun, J.Y., and Wu, L.G. (2001). Fast kinetics of exocytosis revealed by simultaneous measurements of presynaptic capacitance and postsynaptic currents at a central synapse. Neuron *30*, 171-182.

Takamori, S., Holt, M., Stenius, K., Lemke, E.A., Gronborg, M., Riedel, D., Urlaub, H., Schenck, S., Brugger, B., Ringler, P., *et al*. (2006). Molecular anatomy of a trafficking organelle. Cell *127*, 831-846.

Tatsuoka, H., and Reese, T.S. (1989). New structural features of synapses in the anteroventral cochlear nucleus prepared by direct freezing and freeze-substitution. J. Comp. Neurol. *290*, 343-357.

Tong, G., and Jahr, C.E. (1994). Multivesicular release from excitatory synapses of cultured

hippocampal neurons. Neuron *12*, 51-59.

von Gersdorff, H., and Matthews, G. (1994). Dynamics of synaptic vesicle fusion and membrane retrieval in synaptic terminals. Nature *367*, 735-739.

von Gersdorff, H., Sakaba, T., Berglund, K., and Tachibana, M. (1998). Submillisecond kinetics of glutamate release from a sensory synapse. Neuron *21*, 1177-1188.

Wadiche, J.I., and Jahr, C.E. (2001). Multivesicular release at climbing fiber-Purkinje cell synapses. Neuron *32*, 301-313.

Wall, M.J., and Usowicz, M.M. (1998). Development of the quantal properties of evoked and spontaneous synaptic currents at a brain synapse. Nature Neurosci. *1*, 675-682.

Wen, H., and Brehm, P. (2005). Paired motor neuron-muscle recordings in zebrafish test the receptor blockade model for shaping synaptic current. J Neurosci *25*, 8104-8111.

Zenisek, D., Davila, V., Wan, L., and Almers, W. (2003). Imaging calcium entry sites and ribbon structures in two presynaptic cells. J Neurosci *23*, 2538-2548.

FIGURE LEGENDS

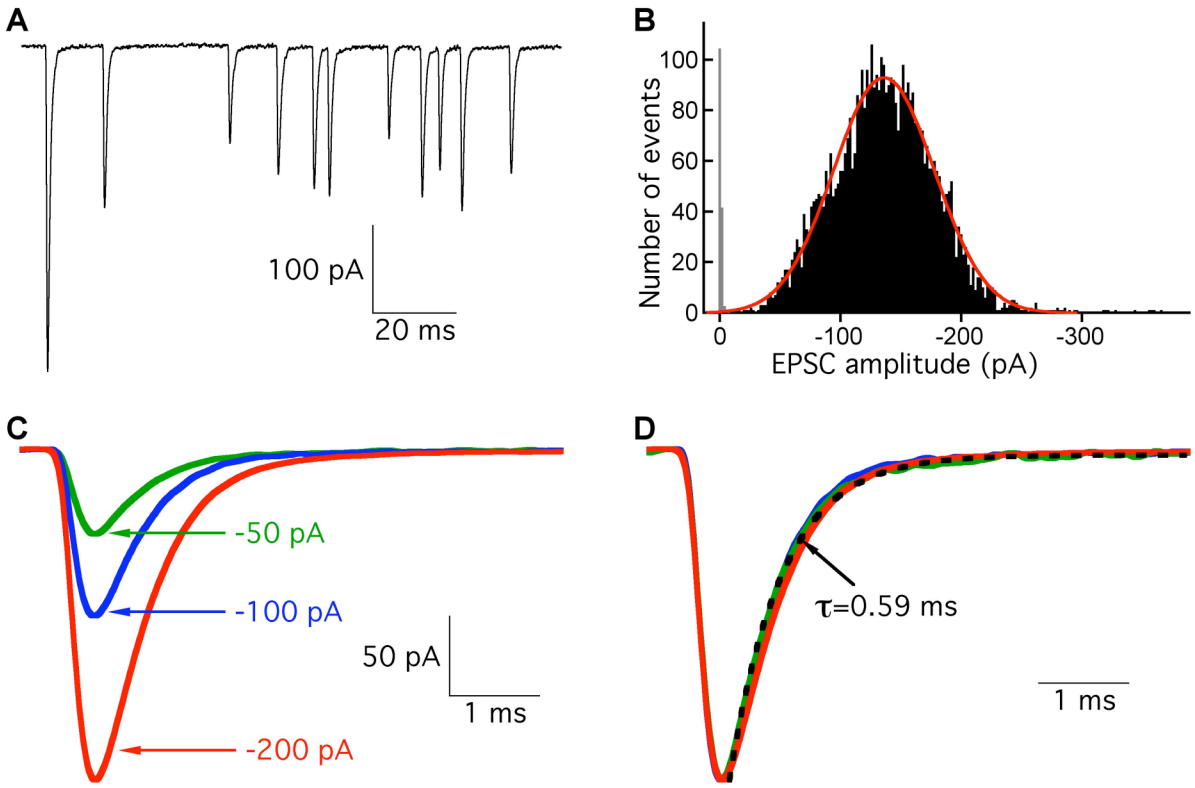

Figure 1, Li et al.

Figure 1. Spontaneous EPSCs.

A) Spontaneous EPSCs recorded from an afferent fiber exhibit a broad range of amplitudes. **B)** The amplitude distribution of 4,884 spontaneous EPSCs is fit well with a Gaussian function (blue). The average EPSC amplitude is -137 pA. The noise-amplitude distribution is shown in gray. **C)** Averages of 10-20 EPSCs with amplitudes of -50 ± 2 pA (green), -100 ± 2 pA (blue), and -200 ± 2 pA (red) show that events of these different size classes possess smooth rise and decay phases. **D)** Normalization of the three groups of EPSCs in **C** reveals that they have similar kinetics. The dashed black line is a single-exponential fit to the decay phase of the -50 pA group. Traces in panels **A**, **B**, and **C** are all from the same afferent fiber recording.

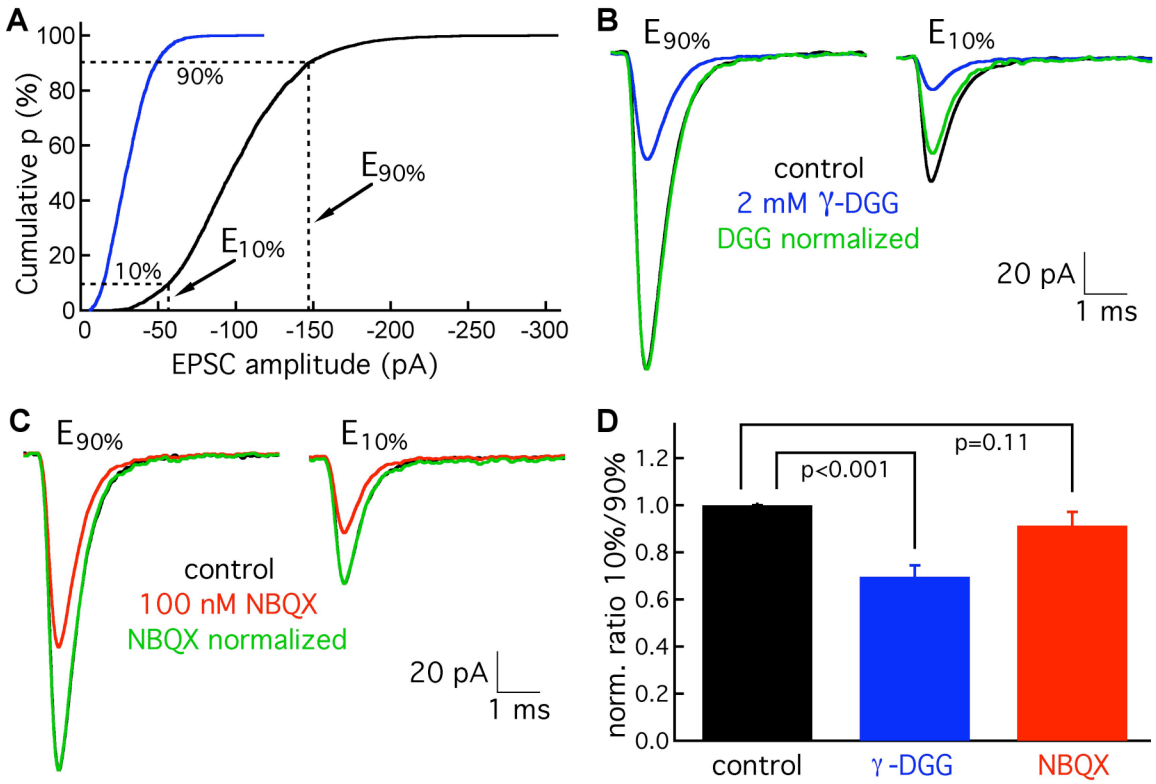

Figure 2, Li et al.

Figure 2. Differential block of EPSCs by γ-DGG.

A) The cumulative amplitude distribution of EPSCs allows the selection of events in the smallest decile ($E_{10\%}$) and those in the largest decile ($E_{90\%}$). The blue trace shows that 2 mM γ-DGG, a low affinity AMPA receptor antagonist, reduces the amplitudes of both small and large events. **B)** After averaging 10 to 20 events each from the $E_{90\%}$ and $E_{10\%}$ classes, events within ± 2 pA, under control circumstances (black) or in the presence of 2 mM γ-DGG (blue), the result for the $E_{90\%}$ class in γ-DGG is normalized to that in control solution (green). When the same normalization factor is applied to the $E_{10\%}$ results, that for γ-DGG (green) is substantially smaller than that in control solution (black), indicating that γ-DGG blocks smaller EPSCs more efficaciously. **C)** In a comparison of EPSCs in control solution (black) with those in 100 nM NBQX (red), normalization shows that events in the $E_{90\%}$ and $E_{10\%}$ classes are blocked to a similar extent (green). **D)** When the ratios ($E_{10\%}/E_{90\%}$) for results in γ-DGG (blue) and NBQX

(red) are normalized to their corresponding controls. The normalized ratio was significantly reduced by γ-DGG (n = 6), but not by NBQX (n = 5).

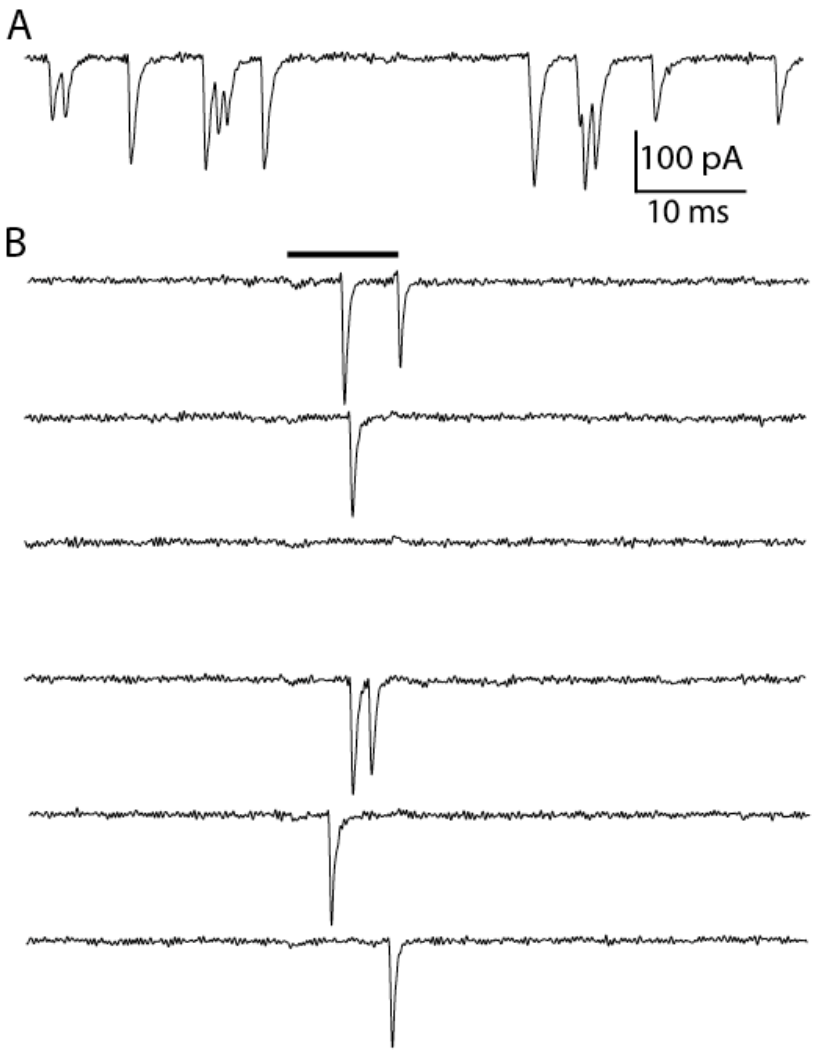

Figure 3, Li et al.

Figure 3. Ca^{2+} iontophoresis permits exocytosis from a single active zone.

A) Under control recording conditions, spontaneous EPSCs in an afferent fiber recording display a wide range of amplitudes. **B)** When the preparation is bathed in a zero-Ca^{2+} solution the spontaneous events are suppressed. A 10 ms local iontophoresis of Ca^{2+} (black bar) onto a putative single synapse evokes EPSCs as large as those recorded from the same fiber in control solution. Failures to evoke EPSCs occurred for 37% of the iontophoretic applications at this site.

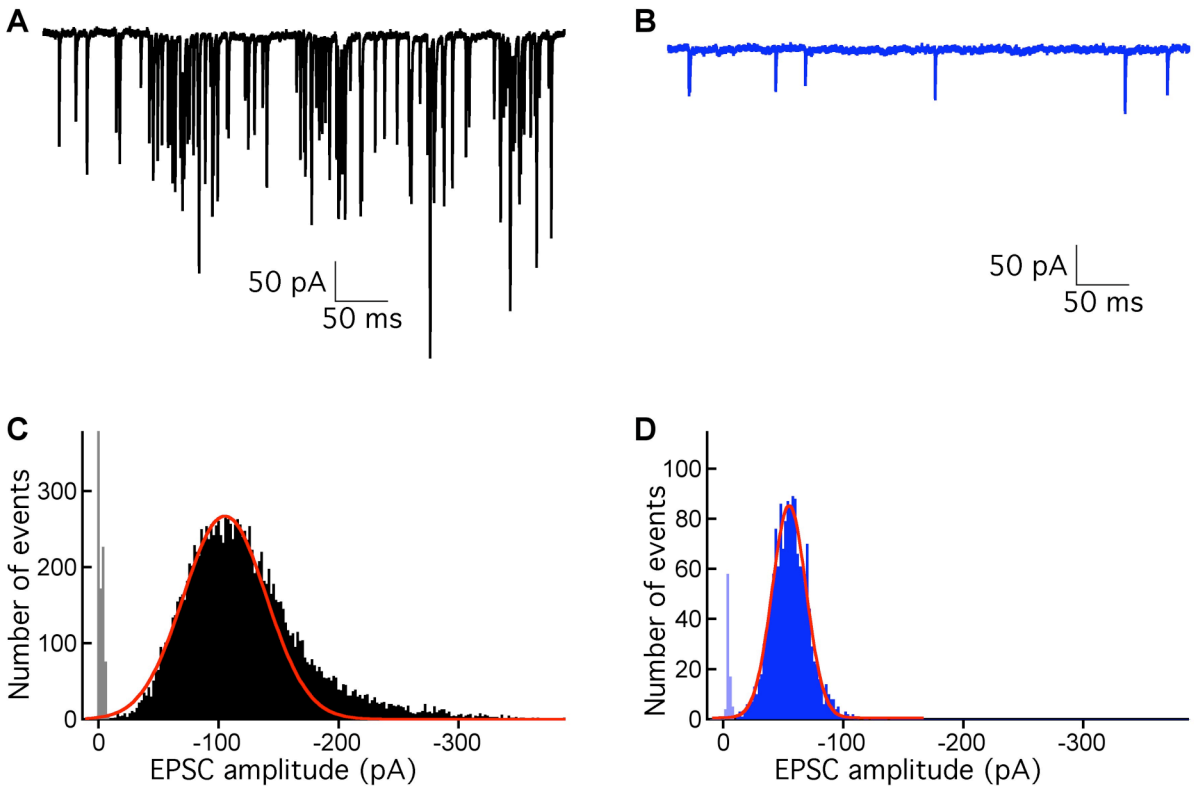

Figure 4, Li et al.

Figure 4. Presynaptic hyperpolarization during paired recordings.

A) Spontaneous EPSC events originating from an unclamped hair cell display a large range of amplitudes. **B**) Voltage-clamping the presynaptic hair cell to -90 mV eliminates all large events recorded from the same afferent fiber and reduces the frequency of the events. **C)** The rising phase of the amplitude distribution of EPSCs from panel A (n=13,791) was fit with a Gaussian function. Skewing of the distribution by large events occurred in a minority of recordings. The Gaussian fit yields a mean value of -105 pA, smaller than the value of -125 pA obtained from the average of all the events. **D)** Holding the hair cell at -90 mV shifted the amplitude distribution to an average of -57 pA (n = 1,542). The distribution is well fit by a Gaussian function with a mean value of -55 pA.

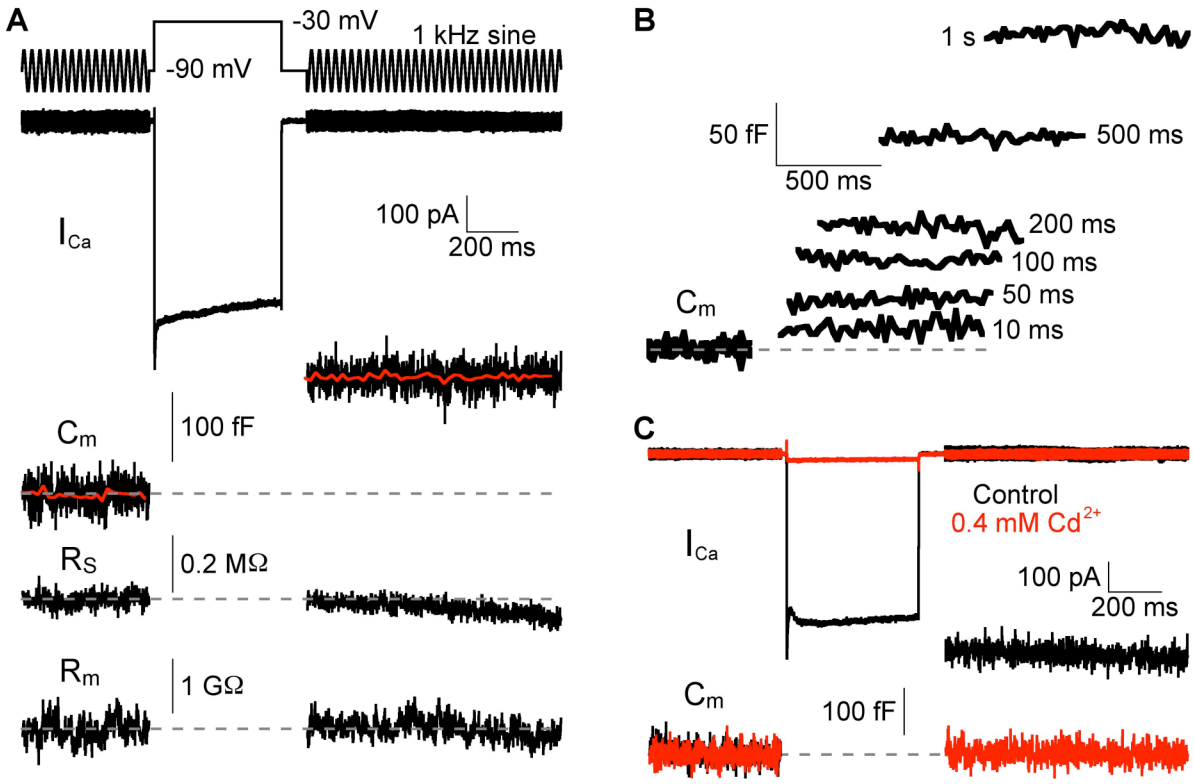

Figure 5. Presynaptic capacitance measurements.

A) A voltage-clamped hair cell was depolarized from a holding potential of -90 mV to -30 mV to evoke exocytosis. During the depolarizing stimulus, a presynaptic Ca^{2+} current (I_{Ca}) was recorded. To measure the presynaptic membrane capacitance, a sinusoid (1 kHz, 50 mV peak-to-peak) was superposed on the holding potential before and after the depolarization. From the measured current response to the sinusoid, membrane capacitance (C_m), series resistance (R_s), and membrane resistance (R_m) were calculated. The increase in C_m reflects a rise in membrane surface area due to synaptic vesicle fusion events. The red trace is the averaged value of the C_m data points. Note that R_s and R_m remain constant. **B)** C_m increases with the duration of the depolarizing stimulus. The traces shown are responses to single depolarizing pulses presented to the cell of panel A. **C)** Cd^{2+} (0.4 mM) blocks both the Ca^{2+} current and the C_m increase.

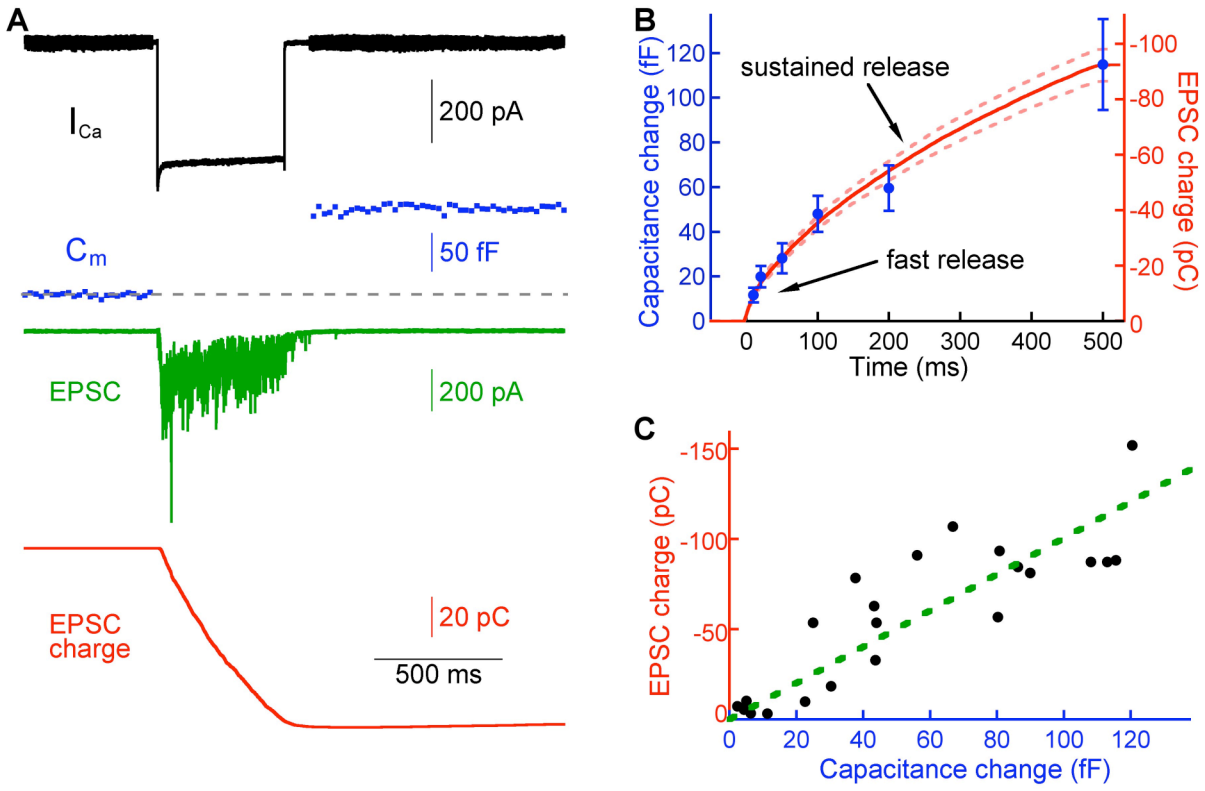

Figure 6. Paired recordings with capacitance measurements.

A) In a representative hair cell-afferent fiber paired recording, depolarization of the hair cell from -90 mV to -30 mV elicits a presynaptic Ca^{2+} current (black) and capacitance increase (blue) and a postsynaptic EPSC (green). The total charge transferred (red) is the integral of the evoked EPSC. **B)** The postsynaptic charge transferred (red, n = 11; dashed lines indicate standard error range) is well correlated with the increase in capacitance of the presynaptic membrane (blue; n = 6) induced by depolarizing pulses of different durations. This agreement suggests that AMPA receptors are not significantly saturated or desensitized during exocytosis. **C)** For each paired recording, the total postsynaptic charge transferred was plotted against the presynaptic membrane capacitance increase. The data were fit with a straight line through the origin with a slope of 1.01 $kC \cdot F^{-1}$ (correlation coefficient: 0.86).

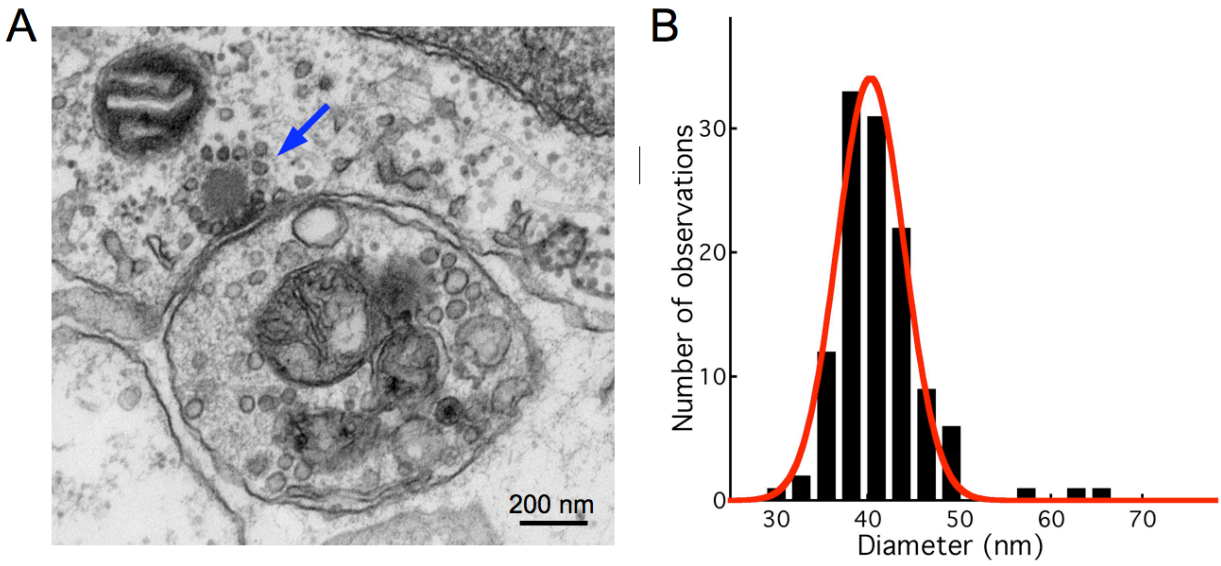

Figure 7. Electron microscopic analysis of synaptic vesicle diameters.

A) An electron-microscopic image of a hair-cell synapse shows a presynaptic active zone demarcated by its vesicle-endowed synaptic ribbon (blue arrow). The single postsynaptic afferent fiber branch shown in cross-section contains mitochondria and several organelles. **B)** The amplitude distribution of synaptic vesicle diameters is fit well by a Gaussian function (red) with a mean value of 40.3 nm.

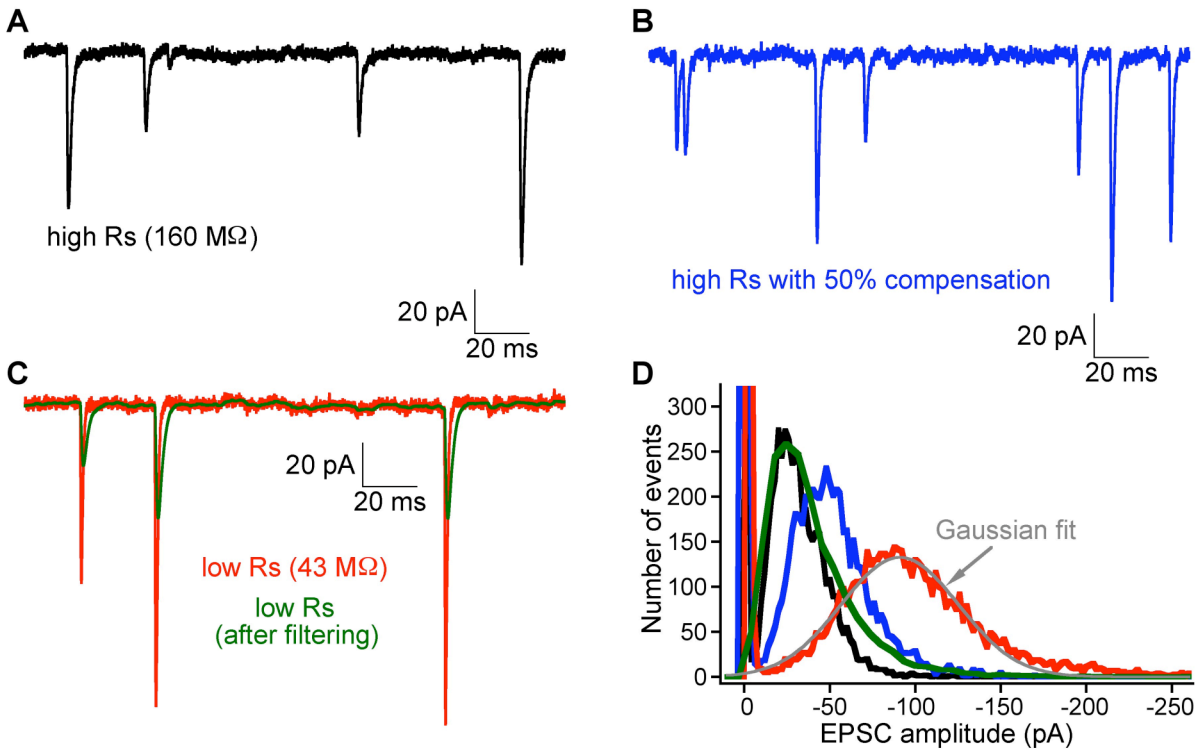

Figure S1, Li et al.

Supplementary Figure 1. Effect of series resistance on the skewness of EPSC amplitude distribution. Spontaneous EPSCs were recorded from the same afferent fiber with a high series resistance (R_s) (**A**, in black), a high series resistance after 50% electronic compensation (**B**, in blue), and a low series resistance (**C**, in red) obtained by applying several brief, sharp pulses of negative pressure to the recording pipette. We simulated the recording with a high series resistance by filtering the low-series-resistance events (in **C**) with an RC filter (**C**, green trace). **D**) The EPSC amplitude distribution for events from panels **A**, **B**, and **C** shows that compensation for half of the series resistance reduced the skewness of high-series-resistance events, but did not produce a Gaussian distribution. However, the distribution was more nearly Gaussian (grey trace) with low-series-resistance recordings (red). Furthermore, filtering of the low-series-resistance events to simulate events with a high series resistance (green) caused skewness comparable to recordings with a high series resistance. We conclude that a series

resistance of less than 40 MΩ is critical for producing Gaussian distributions of EPSC amplitudes.

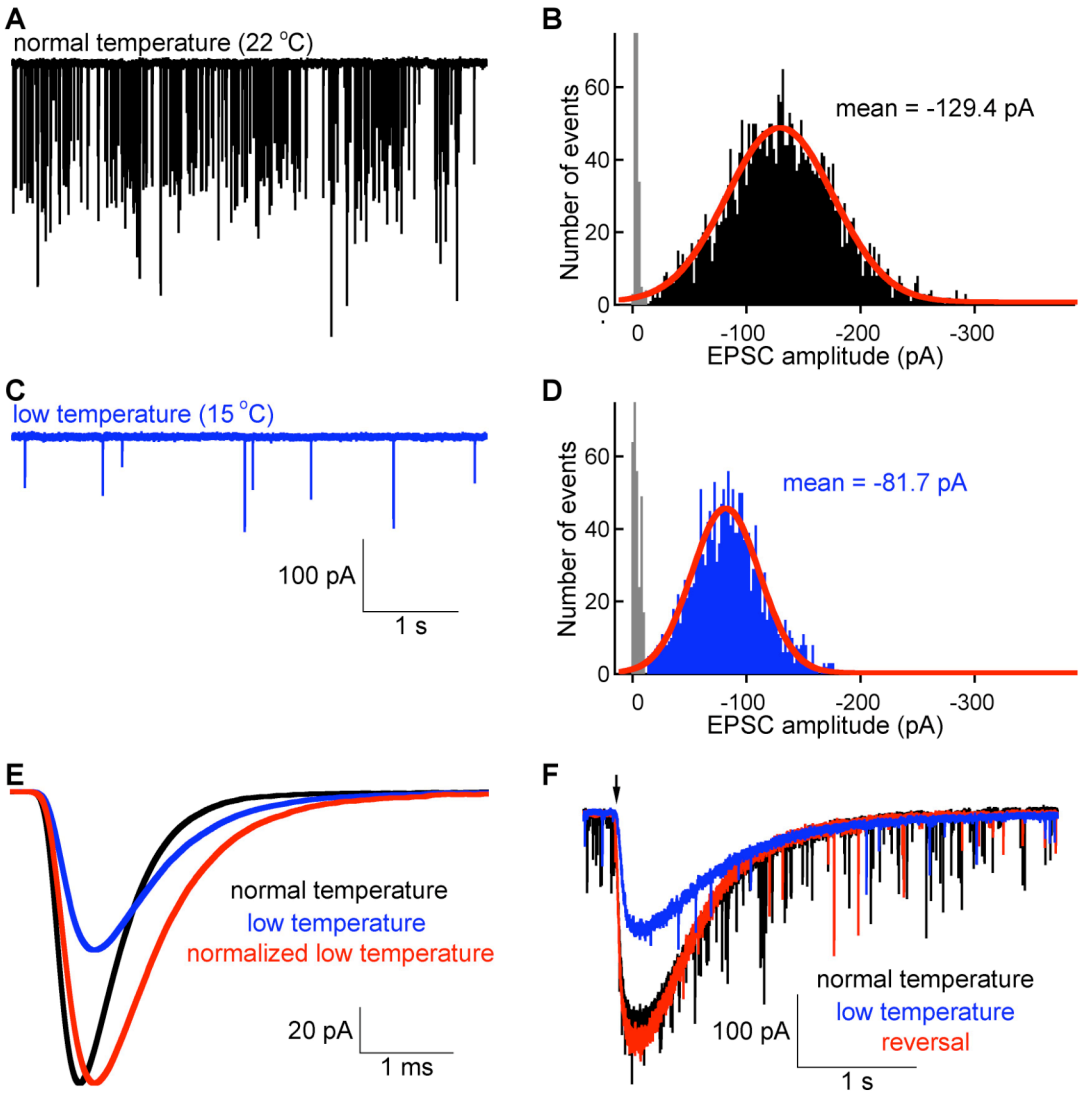

Figure S2, Li et al.

Supplementary Figure 2. Spontaneous EPSCs at low temperature.

A and **B** show a sample of spontaneous EPSCs and their amplitude distribution from an afferent fiber at room temperature. **C** and **D** show EPSCs and their amplitude distribution at a low temperature from the same fiber as in **A** and **B**. The number of EPSC events was 2,950 for **B** and 1,732 for **D**. To lower the temperature the saline solution was passed through a coil immersed in ice bath before reaching the recording chamber and the temperature was continuously monitored with a sensor within the recording chamber. In **B** and **D**, the distributions were fit to a Gaussian function (in red). **E**) Ten to twenty

EPSC events with amplitudes around the mean value (±1 pA) were averaged from **A** (black) or **C** (blue), showing that low temperature diminishes and slows EPSCs (normalization to peak amplitude shown in red). **F**) In another afferent fiber, low temperature reduced the current response induced by pressure application of 10 mM glutamate onto the afferent fiber by an amount similar to that in panel **E**, suggesting that the effect of low temperature reflects postsynaptic changes in AMPA-receptor properties. Similar results were obtained in three additional recordings.

REFERENCES

Abbott LF, Regehr WG (2004) Synaptic computation. Nature 431:796-803.

Adamson CL, Reid MA, Mo ZL, Bowne-English J, Davis RL (2002) Firing features and potassium channel content of murine spiral ganglion neurons vary with cochlear location. J Comp Neurol 447:331-350.

Auger C, Kondo S, Marty A (1998) Multivesicular release at single functional synaptic sites in cerebellar stellate and basket cells. J Neurosci 18:4532-4547.

Augustine GJ (2001) How does calcium trigger neurotransmitter release? Curr Opin Neurobiol 11:320-326.

Ault B, Evans RH, Francis AA, Oakes DJ, Watkins JC (1980) Selective depression of excitatory amino acid induced depolarizations by magnesium ions in isolated spinal cord preparations. J Physiol 307:413-428.

Bee MA, Gerhardt HC (2002) Individual voice recognition in a territorial frog (Rana catesbeiana). Proc Biol Sci 269:1443-1448.

Beurg M, Hafidi A, Skinner LJ, Ruel J, Nouvian R, Henaff M, Puel JL, Aran JM, Dulon D (2005) Ryanodine receptors and BK channels act as a presynaptic depressor of neurotransmission in cochlear inner hair cells. Eur J Neurosci 22:1109-1119.

Beutner D, Moser T (2001) The presynaptic function of mouse cochlear inner hair cells during development of hearing. J Neurosci 21:4593-4599.

Beutner D, Voets T, Neher E, Moser T (2001) Calcium dependence of exocytosis and endocytosis at the cochlear inner hair cell afferent synapse. Neuron 29:681-690.

Borst JG, Sakmann B (1999) Effect of changes in action potential shape on calcium currents and transmitter release in a calyx-type synapse of the rat auditory brainstem. Philos Trans R Soc Lond B Biol Sci 354:347-355.

Brandt A, Striessnig J, Moser T (2003) CaV1.3 channels are essential for development and presynaptic activity of cochlear inner hair cells. J Neurosci 23:10832-10840.

Brandt A, Khimich D, Moser T (2005) Few CaV1.3 channels regulate the exocytosis of a synaptic vesicle at the hair cell ribbon synapse. J Neurosci 25:11577-11585.

Burger PM, Mehl E, Cameron PL, Maycox PR, Baumert M, Lottspeich F, De Camilli P, Jahn R (1989) Synaptic vesicles immunoisolated from rat cerebral cortex contain high levels of glutamate. Neuron 3:715-720.

Burnashev N, Monyer H, Seeburg PH, Sakmann B (1992) Divalent ion permeability of AMPA receptor channels is dominated by the edited form of a single subunit. Neuron 8:189-198.

Christie JM, Jahr CE (2006) Multivesicular release at Schaffer collateral-CA1 hippocampal synapses. J Neurosci 26:210-216.

Clements JD, Lester RA, Tong G, Jahr CE, Westbrook GL (1992) The time course of glutamate in the synaptic cleft. Science 258:1498-1501.

Clements JD (1996) Transmitter timecourse in the synaptic cleft: its role in central synaptic function. Trends Neurosci 19:163-171.

Cochilla AJ, Angleson JK, Betz WJ (2000) Differential regulation of granule-to-granule and granule-to-plasma membrane fusion during secretion from rat pituitary lactotrophs. J Cell Biol 150:839-848.

Cochran SL (1995) Cationic influences upon synaptic transmission at the hair cell-afferent fiber synapse of the frog. Neuroscience 68:1147-1165.

Coggins MR, Grabner CP, Almers W, Zenisek D (2007) Stimulated exocytosis of endosomes in goldfish retinal bipolar neurons. J Physiol 584:853-865.

Deguchi-Tawarada M, Inoue E, Takao-Rikitsu E, Inoue M, Kitajima I, Ohtsuka T, Takai Y (2006) Active zone protein CAST is a component of conventional and ribbon synapses in mouse retina. J Comp Neurol 495:480-496.

Del Castillo J, Engbaek L (1954) The nature of the neuromuscular block produced by magnesium. J Physiol 124:370-384.

Del Castillo J, Katz B (1954a) The effect of magnesium on the activity of motor nerve endings. J Physiol 124:53-559.

Del Castillo J, Katz B (1954b) Quantal components of the end-plate potential. J Physiol 124:560-573.

Dou H, Vazquez AE, Namkung Y, Chu H, Cardell EL, Nie L, Parson S, Shin HS, Yamoah EN (2004) Null mutation of alpha1D Ca^{2+} channel gene results in deafness but no vestibular defect in mice. J Assoc Res Otolaryngol 5:215-226.

Dodge FA, Jr., Rahamimoff R (1967) Co-operative action a calcium ions in transmitter release at the neuromuscular junction. J Physiol 193:419-432.

Eccles JC, Jaeger JC (1958) The relationship between the mode of operation and the dimensions of the junctional regions at synapses and motor end-organs. Proc R Soc Lond B Biol Sci 148:38-56.

Edmonds B, Reyes R, Schwaller B, Roberts WM (2000) Calretinin modifies presynaptic calcium signaling in frog saccular hair cells. Nat Neurosci 3:786-790.

Edmonds BW, Gregory FD, Schweizer FE (2004) Evidence that fast exocytosis can be predominantly mediated by vesicles not docked at active zones in frog saccular hair cells. J Physiol 560:439-450.

Edwards RH (2007) The neurotransmitter cycle and quantal size. Neuron 55:835-858.

Ehret G, Moffat AJ, Capranica RR (1983) Two-tone suppression in auditory nerve fibers of the green treefrog (Hyla cinerea). J Acoust Soc Am 73:2093-2095.

Eybalin M, Caicedo A, Renard N, Ruel J, Puel JL (2004) Transient Ca^{2+}-permeable AMPA receptors in postnatal rat primary auditory neurons. Eur J Neurosci 20:2981-2989.

Favre D, Scarfone E, Di Gioia G, De Camilli P, Dememes D (1986) Presence of synapsin I in afferent and efferent nerve endings of vestibular sensory epithelia. Brain Res 384:379-382.

Fatt P, Katz B (1952) Spontaneous subthreshold activity at motor nerve endings. J Physiol 117:109-128.

Feng AS, Narins PM, Capranica RR (1975) Three populations of primary auditory fibers in the bullfrog (Rana catesbeiana): Their peripheral origins and frequency sensitivities. J Comp Physiol A 221-229.

Fleck MW, Bahring R, Patneau DK, Mayer ML (1996) AMPA receptor heterogeneity in rat hippocampal neurons revealed by differential sensitivity to cyclothiazide. J Neurophysiol 75:2322-2333.

Flock A, Flock B (1966) Ultrastructure of the amphibian papilla in the bullfrog. JASA 40:1262.

Furukawa T, Matsuura S (1978) Adaptive rundown of excitatory post-synaptic potentials at synapses between hair cells and eight nerve fibres in the goldfish. J Physiol 276:193-209.

Furukawa T, Hayashida Y, Matsuura S (1978) Quantal analysis of the size of excitatory post-synaptic potentials at synapses between hair cells and afferent nerve fibres in goldfish. J Physiol 276:211-226.

Glowatzki E, Fuchs PA (2002) Transmitter release at the hair cell ribbon synapse. Nat Neurosci 5:147-154.

Goutman JD, Glowatzki E (2007) Time course and calcium dependence of transmitter release at a single ribbon synapse. Proc Natl Acad Sci U S A 104:16341-16346.

Hackney CM, Mahendrasingam S, Jones EM, Fettiplace R (2003) The distribution of calcium buffering proteins in the turtle cochlea. J Neurosci 23:4577-4589.

Hafez I, Stolpe A, Lindau M (2003) Compound exocytosis and cumulative fusion in eosinophils. J Biol Chem 278:44921-44928.

Hartmann J, Scepek S, Hafez I, Lindau M (2003) Differential regulation of exocytotic fusion and granule-granule fusion in eosinophils by Ca^{2+} and GTP analogs. J Biol Chem 278:44929-44934.

Heller S, Bell AM, Denis CS, Choe Y, Hudspeth AJ (2002) Parvalbumin 3 is an abundant Ca^{2+} buffer in hair cells. J Assoc Res Otolaryngol 3:488-498.

Henze DA, McMahon DB, Harris KM, Barrionuevo G (2002) Giant miniature EPSCs at the hippocampal mossy fiber to CA3 pyramidal cell synapse are monoquantal. J Neurophysiol 87:15-29.

Hossain WA, Antic SD, Yang Y, Rasband MN, Morest DK (2005) Where is the spike generator of the cochlear nerve? Voltage-gated sodium channels in the mouse cochlea. J Neurosci 25:6857-6868.

Hudspeth AJ, Lewis RS (1988) Kinetic analysis of voltage- and ion-dependent conductances in saccular hair cells of the bull-frog, Rana catesbeiana. J Physiol 400:237-274.

Issa NP, Hudspeth AJ (1994) Clustering of Ca^{2+} channels and $Ca(^{2+})$-activated K+ channels at fluorescently labeled presynaptic active zones of hair cells. Proc Natl Acad Sci U S A 91:7578-7582.

Issa NP, Hudspeth AJ (1996) The entry and clearance of Ca^{2+} at individual presynaptic active zones of hair cells from the bullfrog's sacculus. Proc Natl Acad Sci U S A 93:9527-9532.

Jacobs, R.A., and Hudspeth, A.J. (1990). Ultrastructural correlates of mechanoelectrical transduction in hair cells of the bullfrog's internal ear. Cold Spring Harb Symp Quant Biol *55*, 547-561.

Jockusch WJ, Praefcke GJ, McMahon HT, Lagnado L (2005) Clathrin-dependent and clathrin-independent retrieval of synaptic vesicles in retinal bipolar cells. Neuron 46:869-878.

Johnson SL, Marcotti W, Kros CJ (2005) Increase in efficiency and reduction in Ca^{2+} dependence of exocytosis during development of mouse inner hair cells. J Physiol 563:177-191.

Johnson SL, Forge A, Knipper M, Munkner S, Marcotti W (2008) Tonotopic variation in the calcium dependence of neurotransmitter release and vesicle pool replenishment at mammalian auditory ribbon synapses. J Neurosci 28:7670-7678.

Katz B, Miledi R (1963) A study of spontaneous miniature potentials in spinal motoneurones. J Physiol 168:389-422.

Katz B, Miledi R (1969) Spontaneous and evoked activity of motor nerve endings in calcium Ringer. J Physiol 203:689-706.

Keen EC, Hudspeth AJ (2006) Transfer characteristics of the hair cell's afferent synapse. Proc Natl Acad Sci U S A 103:5537-5542.

Keenan AG, McLeod HG, Gordon AR (1945) The variation of the transference numbers for calcium chloride in aqueous solution with temperature. III. J Chem Phys 13:466-469.

Kennedy HJ, Meech RW (2002) Fast Ca^{2+} signals at mouse inner hair cell synapse: a role for Ca^{2+}-induced Ca^{2+} release. J Physiol 539:15-23.

Khimich D, Nouvian R, Pujol R, Tom Dieck S, Egner A, Gundelfinger ED, Moser T (2005) Hair cell synaptic ribbons are essential for synchronous auditory signalling. Nature 434:889-894.

Kiang NY, Pfeiffer RR, Warr WB, Backus AS (1965) Stimulus Coding in the Cochlear Nucleus. Ann Otol Rhinol Laryngol 74:463-485.

Kim TD, Eddlestone GT, Mahmoud SF, Kuchtey J, Fewtrell C (1997) Correlating Ca^{2+} responses and secretion in individual RBL-2H3 mucosal mast cells. J Biol Chem 272:31225-31229.

Klenchin VA, Martin TF (2000) Priming in exocytosis: attaining fusion-competence after vesicle docking. Biochimie 82:399-407.

Koenig JH, Yamaoka K, Ikeda K (1993) Calcium-induced translocation of synaptic vesicles to the active site. J Neurosci 13:2313-2322.

Kollmar R, Fak J, Montgomery LG, Hudspeth AJ (1997) Hair cell-specific splicing of mRNA for the alpha1D subunit of voltage-gated Ca^{2+} channels in the chicken's cochlea. Proc Natl Acad Sci U S A 94:14889-14893.

Kollmar R, Montgomery LG, Fak J, Henry LJ, Hudspeth AJ (1997) Predominance of the alpha1D subunit in L-type voltage-gated Ca^{2+} channels of hair cells in the chicken's cochlea. Proc Natl Acad Sci U S A 94:14883-14888.

Konishi M (2003) Coding of auditory space. Annu Rev Neurosci 26:31-55.

Koppl C (1997) Phase locking to high frequencies in the auditory nerve and cochlear nucleus magnocellularis of the barn owl, Tyto alba. J Neurosci 17:3312-3321.

Korn H, Sur C, Charpier S, Legendre P, Faber DS (1994) The one-vesicle hypothesis and multivesicular release. Adv Sec Mess Phosphoprot Res 29:301-22.

Koschak A, Reimer D, Huber I, Grabner M, Glossmann H, Engel J, Striessnig J (2001) alpha 1D (Cav1.3) subunits can form l-type Ca2+ channels activating at negative voltages. J Biol Chem 276:22100-22106.

Krizaj D, Bao JX, Schmitz Y, Witkovsky P, Copenhagen DR (1999) Caffeine-sensitive calcium stores regulate synaptic transmission from retinal rod photoreceptors. J Neurosci 19:7249-7261.

Kros CJ, Ruppersberg JP, Rusch A (1998) Expression of a potassium current in inner hair cells during development of hearing in mice. Nature 394:281-284.

Lenzi D, Crum J, Ellisman MH, Roberts WM (2002) Depolarization redistributes synaptic membrane and creates a gradient of vesicles on the synaptic body at a ribbon synapse. Neuron 36:649-659.

Lewis ER, Leverenze EL, Koyama H (1982) The tonotopic organization of the bullfrog amphibian papilla, an auditory organ lacking a basilar membrane. J Comp Physiol 145:437:445.

Lewis ER, Baird RA, Leverenz EL, Koyama H (1982) Inner ear: dye injection reveals peripheral origins of specific sensitivities. Science 215:1641-1643.

Lewis ER, Leverenz EL (1983) Morphological basis for tonotopy in the anuran amphibian papilla. Scan Electron Microsc:189-200.

Liberman MC (1980) Morphological differences among radial afferent fibers in the cat cochlea: an electron-microscopic study of serial sections. Hear Res 3:45-63.

Liberman MC (1982) Single-neuron labeling in the cat auditory nerve. Science 216:1239-1241.

Liu G, Choi S, Tsien RW (1999) Variability of neurotransmitter concentration and nonsaturation of postsynaptic AMPA receptors at synapses in hippocampal cultures and slices. Neuron 22:395-409.

Llano I, Gonzalez J, Caputo C, Lai FA, Blayney LM, Tan YP, Marty A (2000) Presynaptic calcium stores underlie large-amplitude miniature IPSCs and spontaneous calcium transients. Nat Neurosci 3:1256-1265.

LoGiudice L, Sterling P, Matthews G (2008) Mobility and turnover of vesicles at the synaptic ribbon. J Neurosci 28:3150-3158.

Lumpkin EA, Hudspeth AJ (1995) Detection of Ca^{2+} entry through mechanosensitive channels localizes the site of mechanoelectrical transduction in hair cells. Proc Natl Acad Sci U S A 92:10297-10301.

Mahmoud SF, Fewtrell C (2001) Microdomains of high calcium are not required for exocytosis in RBL-2H3 mucosal mast cells. J Cell Biol 153:339-349.

Martin AR. Junctional transmission. II: Presynaptic mechanisms. In: Kandel ER. , editor. *Handbook of Physiology section 1, The Nervous System, Cellular Biology of Neurons*. I. Bethesda, MD, USA: Amer Physiol Soc; 1977. pp. 329–355.

Marx SO, Gaburjakova J, Gaburjakova M, Henrikson C, Ondrias K, Marks AR (2001) Coupled gating between cardiac calcium release channels (ryanodine receptors). Circ Res 88:1151-1158.

Marx SO, Ondrias K, Marks AR (1998) Coupled gating between individual skeletal muscle Ca2+ release channels (ryanodine receptors). Science 281:818-821.

Matsubara A, Laake JH, Davanger S, Usami S, Ottersen OP (1996) Organization of AMPA receptor subunits at a glutamate synapse: a quantitative immunogold analysis of hair cell synapses in the rat organ of Corti. J Neurosci 16:4457-4467.

Matthews G, Sterling P (2008) Evidence that vesicles undergo compound fusion on the synaptic ribbon. J Neurosci 28:5403-5411.

McAllister AK, Stevens CF (2000) Nonsaturation of AMPA and NMDA receptors at hippocampal synapses. Proc Natl Acad Sci U S A 97:6173-6178.

McLaghlan EM (1978) The statistics of transmitter release at chemical synapses. Int Rev Physiol 17:49-117.

Meenderink SW, Narins PM, van Dijk P (2005) Detailed f1, f2 area study of distortion product otoacoustic emissions in the frog. J Assoc Res Otolaryngol 6:37-47.

Megela AL, Capranica RR (1981) Response patterns to tone bursts in peripheral auditory system of anurans. J Neurophysiol 46:465-478.

Megela AL (1984) Diversity of adaptation patterns in responses of eighth nerve fibers in the bullfrog, Rana catesbeiana. J Acoust Soc Am 75:1155-1162.

Mintz IM, Sabatini BL, Regehr WG (1995) Calcium control of transmitter release at a cerebellar synapse. Neuron 15:675-688.

Moser T, Beutner D (2000) Kinetics of exocytosis and endocytosis at the cochlear inner hair cell afferent synapse of the mouse. Proc Natl Acad Sci U S A 97:883-888.

Muresan V, Lyass A, Schnapp BJ (1999) The kinesin motor KIF3A is a component of the presynaptic ribbon in vertebrate photoreceptors. J Neurosci 19:1027-1037.

Murnick JG, Dube G, Krupa B, Liu G (2002) High-resolution iontophoresis for single-synapse stimulation. J Neurosci Methods 116:65-75.

Neef A, Khimich D, Pirih P, Riedel D, Wolf F, Moser T (2007) Probing the mechanism of exocytosis at the hair cell ribbon synapse. J Neurosci 27:12933-12944.

Nemoto T, Kimura R, Ito K, Tachikawa A, Miyashita Y, Iino M, Kasai H (2001) Sequential-replenishment mechanism of exocytosis in pancreatic acini. Nat Cell Biol 3:253-258.

Obholzer N, Wolfson S, Trapani JG, Mo W, Nechiporuk A, Busch-Nentwich E, Seiler C, Sidi S, Sollner C, Duncan RN, Boehland A, Nicolson T (2008) Vesicular glutamate transporter 3 is required for synaptic transmission in zebrafish hair cells. J Neurosci 28:2110-2118.

Ottersen OP, Landsend AS (1997) Organization of glutamate receptors at the synapse. Eur J Neurosci 9:2219-2224.

Ottersen OP, Takumi Y, Matsubara A, Landsend AS, Laake JH, Usami S (1998) Molecular organization of a type of peripheral glutamate synapse: the afferent synapses of hair cells in the inner ear. Prog Neurobiol 54:127-148.

Parks TN (2000) The AMPA receptors of auditory neurons. Hear Res 147:77-91.

Parsons TD, Lenzi D, Almers W, Roberts WM (1994) Calcium-triggered exocytosis and endocytosis in an isolated presynaptic cell: capacitance measurements in saccular hair cells. Neuron 13:875-883.

Partin KM, Patneau DK, Mayer ML (1994) Cyclothiazide differentially modulates desensitization of alpha-amino-3-hydroxy-5-methyl-4-isoxazolepropionic acid receptor splice variants. Mol Pharmacol 46:129-138.

Patneau DK, Mayer ML (1990) Structure-activity relationships for amino acid transmitter candidates acting at N-methyl-D-aspartate and quisqualate receptors. J Neurosci 10:2385-2399.

Pawlu C, DiAntonio A, Heckmann M (2004) Postfusional control of quantal current shape. Neuron 42:607-618.

Platzer J, Engel J, Schrott-Fischer A, Stephan K, Bova S, Chen H, Zheng H, Striessnig J (2000) Congenital deafness and sinoatrial node dysfunction in mice lacking class D L-type Ca^{2+} channels. Cell 102:89-97.

Prescott ED, Zenisek D (2005) Recent progress towards understanding the synaptic ribbon. Curr Opin Neurobiol 15:431-436.

Raghavachari S, Lisman JE (2004) Properties of quantal transmission at CA1 synapses. J Neurophysiol 92:2456-2467.

Reng D, Hack I, Muller M, Smolders JW (1999) AMPA-type glutamate receptor subunits are expressed in the avian cochlear hair cells and ganglion cells. Neuroreport 10:2137-2141.

Ricci AJ, Crawford AC, Fettiplace R (2003) Tonotopic variation in the conductance of the hair cell mechanotransducer channel. Neuron 40:983-990.

Ricci AJ, Fettiplace R (1997) The effects of calcium buffering and cyclic AMP on mechano-electrical transduction in turtle auditory hair cells. J Physiol 501 (Pt 1):111-124.

Ricci AJ, Gray-Keller M, Fettiplace R (2000) Tonotopic variations of calcium signalling in turtle auditory hair cells. J Physiol 524 Pt 2:423-436.

Roberts WM, Jacobs RA, Hudspeth AJ (1990) Colocalization of ion channels involved in frequency selectivity and synaptic transmission at presynaptic active zones of hair cells. J Neurosci 10:3664-3684.

Roberts WM (1993) Spatial calcium buffering in saccular hair cells. Nature 363:74-76.

Roberts WM (1994) Localization of calcium signals by a mobile calcium buffer in frog saccular hair cells. J Neurosci 14:3246-3262.

Robertson D, Paki B (2002) Role of L-type Ca^{2+} channels in transmitter release from mammalian inner hair cells. II. Single-neuron activity. J Neurophysiol 87:2734-2740.

Rodriguez-Contreras, A., and Yamoah, E.N. (2001). Direct measurement of single-channel Ca^{2+} currents in bullfrog hair cells reveals two distinct channel subtypes. J Physiol *534*, 669-689.

Rose JE, Brugge JF, Anderson DJ, Hind JE (1967) Phase-locked response to low-frequency tones in single auditory nerve fibers of the squirrel monkey. J Neurophysiol 30:769-793.

Roux I, Safieddine S, Nouvian R, Grati M, Simmler MC, Bahloul A, Perfettini I, Le Gall M, Rostaing P, Hamard G, Triller A, Avan P, Moser T, Petit C (2006) Otoferlin, defective in a human deafness form, is essential for exocytosis at the auditory ribbon synapse. Cell 127:277-289.

Ruel J, Bobbin RP, Vidal D, Pujol R, Puel JL (2000) The selective AMPA receptor antagonist GYKI 53784 blocks action potential generation and excitotoxicity in the guinea pig cochlea. Neuropharmacology 39:1959-1973.

Russell IJ, Sellick PM (1978) Intracellular studies of hair cells in the mammalian cochlea. J Physiol 284:261-290.

Rutherford MA, Roberts WM (2006) Frequency selectivity of synaptic exocytosis in frog saccular hair cells. Proc Natl Acad Sci U S A 103:2898-2903.

Sabatini BL, Regehr WG (1996) Timing of neurotransmission at fast synapses in the mammalian brain. Nature 384:170-172.

Sabatini BL, Regehr WG (1999) Timing of synaptic transmission. Annu Rev Physiol 61:521-542.

Safieddine S, Wenthold RJ (1999) SNARE complex at the ribbon synapses of cochlear hair cells: analysis of synaptic vesicle- and synaptic membrane-associated proteins. Eur J Neurosci 11:803-812.

Sahara, Y., and Takahashi, T. (2001). Quantal components of the excitatory postsynaptic currents at a rat central auditory synapse. J Physiol *536*, 189-197.

Saito, K. (1990). Freeze-fracture organization of hair cell synapses in the sensory epithelium of guinea pig organ of Corti. J Electron Microsc Tech *15*, 173-186.

Scepek S, Lindau M (1993) Focal exocytosis by eosinophils--compound exocytosis and cumulative fusion. Embo J 12:1811-1817.

Scepek S, Coorssen JR, Lindau M (1998) Fusion pore expansion in horse eosinophils is modulated by Ca^{2+} and protein kinase C via distinct mechanisms. Embo J 17:4340-4345.

Schmitz B, White TD, Narins PM (1992) Directionality of phase locking in auditory nerve fibers of the leopard frog Rana pipiens pipiens. J Comp Physiol [A] 170:589-604.

Schmitz F, Konigstorfer A, Sudhof TC (2000) RIBEYE, a component of synaptic ribbons: a protein's journey through evolution provides insight into synaptic ribbon function. Neuron 28:857-872.

Schnee, M.E., and Ricci, A.J. (2003). Biophysical and pharmacological characterization of voltage-gated calcium currents in turtle auditory hair cells. J Physiol *549*, 697-717.

Schnee ME, Lawton DM, Furness DN, Benke TA, Ricci AJ (2005) Auditory hair cell-afferent fiber synapses are specialized to operate at their best frequencies. Neuron 47:243-254.

Sewell WF (1984) The relation between the endocochlear potential and spontaneous activity in auditory nerve fibres of the cat. J Physiol 347:685-696.

Sharma G, Grybko M, Vijayaraghavan S (2008) Action potential-independent and nicotinic receptor-mediated concerted release of multiple quanta at hippocampal CA3-mossy fiber synapses. J Neurosci 28:2563-2575.

Shimozono M, Tono T, Morimitsu T, Nakagawa T, Komune S (1995) Measurement of intracellular free Ca^{2+} concentration in guinea pig spiral ganglion cells. Neuroreport 6:421-424.

Simmons DD, Bertolotto C, Narins PM (1992) Innervation of the amphibian and basilar papillae in the leopard frog: reconstructions of single labeled fibers. J Comp Neurol 322:191-200.

Simmons DD, Bertolotto C, Leong M (1995) Synaptic ultrastructure within the amphibian papilla of *Rana pipiens pipiens*: rostrocaudal differences. Audit Neurosci. 1:183-193.

Singer JH, Lassova L, Vardi N, Diamond JS (2004) Coordinated multivesicular release at a mammalian ribbon synapse. Nat Neurosci 7:826-833.

Sivian, L. J., and White, S. D. (1933) On minimum audible sound fields. J. Acoust. Soc. Amer., 1933, 4, 288-321.

Smotherman MS, Narins PM (1999) The electrical properties of auditory hair cells in the frog amphibian papilla. J Neurosci 19:5275-5292.

Smotherman MS, Narins PM (2000) Hair cells, hearing and hopping: a field guide to hair cell physiology in the frog. J Exp Biol 203:2237-2246.

Sobkowicz HM, Rose JE, Scott GE, Slapnick SM (1982) Ribbon synapses in the developing intact and cultured organ of Corti in the mouse. J Neurosci 2:942-957.

Sobkowicz HM, Rose JE, Scott GL, Levenick CV (1986) Distribution of synaptic ribbons in the developing organ of Corti. J Neurocytol 15:693-714.

Sommer B, Keinanen K, Verdoorn TA, Wisden W, Burnashev N, Herb A, Kohler M, Takagi T, Sakmann B, Seeburg PH (1990) Flip and flop: a cell-specific functional switch in glutamate-operated channels of the CNS. Science 249:1580-1585.

Spassova M, Eisen MD, Saunders JC, Parsons TD (2001) Chick cochlear hair cell exocytosis mediated by dihydropyridine-sensitive calcium channels. J Physiol 535:689-696.

Spassova MA, Avissar M, Furman AC, Crumling MA, Saunders JC, Parsons TD (2004) Evidence that rapid vesicle replenishment of the synaptic ribbon mediates recovery from short-term adaptation at the hair cell afferent synapse. J Assoc Res Otolaryngol 5:376-390.

Su ZL, Jiang SC, Gu R, Yang WP (1995) Two types of calcium channels in bullfrog saccular hair cells. Hear Res 87:62-68.

Sullivan WE, Konishi M (1984) Segregation of stimulus phase and intensity coding in the cochlear nucleus of the barn owl. J Neurosci 4:1787-1799.

Suryanarayanan A, Slaughter MM (2006) Synaptic transmission mediated by internal calcium stores in rod photoreceptors. J Neurosci 26:1759-1766.

Taberner AM, Liberman MC (2005) Response properties of single auditory nerve fibers in the mouse. J Neurophysiol 93:557-569.

Tatsuoka H, Reese TS (1989) New structural features of synapses in the anteroventral cochlear nucleus prepared by direct freezing and freeze-substitution. J Comp Neurol 290:343-357.

Thoreson WB, Rabl K, Townes-Anderson E, Heidelberger R (2004) A highly Ca^{2+}-sensitive pool of vesicles contributes to linearity at the rod photoreceptor ribbon synapse. Neuron 42:595-605.

Tinevez JY, Julicher F, Martin P (2007) Unifying the various incarnations of active hair-bundle motility by the vertebrate hair cell. Biophys J 93:4053-4067.

tom Dieck S, Altrock WD, Kessels MM, Qualmann B, Regus H, Brauner D, Fejtova A, Bracko O, Gundelfinger ED, Brandstatter JH (2005) Molecular dissection of the

photoreceptor ribbon synapse: physical interaction of Bassoon and RIBEYE is essential for the assembly of the ribbon complex. J Cell Biol 168:825-836.

Trussell LO (1997) Cellular mechanisms for preservation of timing in central auditory pathways. Curr Opin Neurobiol 7:487-492.

Trussell LO (2002) Transmission at the hair cell synapse. Nat Neurosci 5:85-86.

Vogel SS, Zimmerberg J (1992) Proteins on exocytic vesicles mediate calcium-triggered fusion. Proc Natl Acad Sci U S A 89:4749-4753.

von Gersdorff H, Vardi E, Matthews G, Sterling P (1996) Evidence that vesicles on the synaptic ribbon of retinal bipolar neurons can be rapidly released. Neuron 16:1221-1227.

von Gersdorff H (2001) Synaptic ribbons: versatile signal transducers. Neuron 29:7-10.

Wadiche JI, Jahr CE (2001) Multivesicular release at climbing fiber-Purkinje cell synapses. Neuron 32:301-313.

Walch-Solimena C, Blasi J, Edelmann L, Chapman ER, von Mollard GF, Jahn R (1995) The t-SNAREs syntaxin 1 and SNAP-25 are present on organelles that participate in synaptic vesicle recycling. J Cell Biol 128:637-645.

Wall MJ, Usowicz MM (1998) Development of the quantal properties of evoked and spontaneous synaptic currents at a brain synapse. Nat Neurosci 1:675-682.

Wang Y, Okamoto M, Schmitz F, Hofmann K, Sudhof TC (1997) Rim is a putative Rab3 effector in regulating synaptic-vesicle fusion. Nature 388:593-598.

Wu XS, Xue L, Mohan R, Paradiso K, Gillis KD, Wu LG (2007) The origin of quantal size variation: vesicular glutamate concentration plays a significant role. J Neurosci 27:3046-3056.

Yoshida S, Plant S (1992) Mechanism of release of Ca^{2+} from intracellular stores in response to ionomycin in oocytes of the frog Xenopus laevis. J Physiol 458:307-318.

Zampini V, Valli P, Zucca G, Masetto S (2006) Single-channel L-type Ca^{2+} currents in chicken embryo semicircular canal type I and type II hair cells. J Neurophysiol 96:602-612.

Zenisek D, Steyer JA, Almers W (2000) Transport, capture and exocytosis of single synaptic vesicles at active zones. Nature 406:849-854.

Zenisek D, Steyer JA, Feldman ME, Almers W (2002) A membrane marker leaves synaptic vesicles in milliseconds after exocytosis in retinal bipolar cells. Neuron 35:1085-1097.

Zenisek D, Davila V, Wan L, Almers W (2003) Imaging calcium entry sites and ribbon structures in two presynaptic cells. J Neurosci 23:2538-2548.

Zenisek D, Horst NK, Merrifield C, Sterling P, Matthews G (2004) Visualizing synaptic ribbons in the living cell. J Neurosci 24:9752-9759.

Zenisek D (2008) Vesicle association and exocytosis at ribbon and extraribbon sites in retinal bipolar cell presynaptic terminals. Proc Natl Acad Sci U S A 105:4922-4927.

Zhai RG, Bellen HJ (2004) The architecture of the active zone in the presynaptic nerve terminal. Physiology (Bethesda) 19:262-270.